

國立交通大學  
電機與控制工程學系

博士論文

智慧車側影像駕駛人輔助安全系統

Smart Lateral Imaging for Driving Safety  
Supporting System



研究生：范剛維

指導教授：林進燈

中華民國九十六年九月

智慧車側影像駕駛人輔助安全系統  
Smart Lateral Imaging for Driving Safety  
Supporting System

研究生：范剛維      Student: Kang-Wei Fan

指導教授：林進燈      Advisor: Chin-Teng Lin

國立交通大學

電機與控制工程學系



A Dissertation

Submitted to Department of Electrical and Control Engineering  
College of Electrical Engineering and Computer Science  
National Chiao Tung University  
in Partial Fulfillment of the Requirements  
for the Degree of  
Doctor of Philosophy  
In  
Electrical and Control Engineering

September 2007

Hsinchu, Taiwan, Republic of China

中華民國九十六年九月

# 智慧車側影像駕駛人輔助安全系統

研究生：范剛維

指導教授：林進燈

國立交通大學電機與控制工程研究所

## 摘要

最近幾年，車輛安全是個非常重要的社會、經濟問題。一般來說，很多交通意外都來自於駕駛者精神狀態不佳、注意力不集中、未保持安全距離或甚至打瞌睡，在很多情形是駕駛者打瞌睡偏離車道而造成交通意外。而高速公路上，也很多意外是車輛側邊或是後方的直接碰撞。因為這些原因造成許多的意外，所以車道偵測與車側碰撞預防系統在智慧型交通傳輸計畫內扮演著相當重要的地位。以價格與效果為考量，本論文以裝置於車輛照後鏡的車側攝影機為感應器，且此攝影機搭配魚眼鏡頭，廣角的鏡頭，可能得到更多車輛附近的相關資訊。

因為攝影機位於車輛上，所以在車輛行進中，攝影機所取得的影像是晃動的，故在進行分析之前，必須先做影像穩定的修正，雖然只是前處理，但是可以簡化後續之演算法。本論文提出了車道偏移與車側碰撞警告系統，此系統不僅可以提醒駕駛人在偏移車道的時候是否會發生危險，透過車側碰撞警告系統更幫助駕駛者監看盲點區域是否有車輛進入，此外，我們亦借助交大腦科學中心對駕駛者的分析資料來推測駕駛者是否有打瞌睡或其他異常狀態。因為本論文只用車側攝影機，所以比較容易整合車道偵測與車側碰撞警告系統，一般拍攝車前的影像式車道偵測系統，主要目的是提醒駕駛者不要偏離目前車道。而車側碰撞警告為了當有車輛進入盲點區而發出警告，但其整合比較麻煩且必須要兩套系統。故本論文的架構能更有效的提供駕駛者在變換車道時，是否會發生危險，且這個架構是非常特別且有用的，進而達到輔助駕駛人安全的目的。

# Smart Lateral Imaging for Driving Safety Supporting System

Student: Kang-Wei Fan

Advisor: Chin-Teng Lin

Department of Electrical and Control Engineering  
National Chiao-Tung University

## ABSTRACT

In recent years, an important social and economic problem is traffic safety. In general, a considerable fraction of these accidents is due to driver's fatigue, inattentive driving and driving without keeping proper distance. In many cases, the driver falls asleep will make the vehicle to leave its designated lane and possibly cause an accident. On the highway, the most important cause of traffic accidents is the lateral and same direction collision.

Due to the inattentive driving, the driver may deviate from the correct lane orientation, which induces the traffic accidents. As a result, the lane detection system and vehicle lateral collision warning system play a significant role in improving the driver's safety in a moving vehicle. For cost and performance consideration, a lateral fish-eye camera mounted under the rear-view mirror is chosen as our sensing device. The robust in-car DIS technique offers all major algorithms a stable image source. It is a minor pre-processing, but the following processing can be simplified massively.

We propose an integrated system for lane departure warning and lateral collision

warning. The lateral collision warning system aims at detecting the image in driver's blind spot region and exporting signal to remind driver in the realistic driving environment. In addition, driver's drowsiness will also be estimated by integrating the EEG-based analysis approach developed by the Brain Research Center, NCTU, into our lane departure warning system.

In this thesis, for the lane detection, we develop a method for automatic region of interesting extraction only by analyzing the image contents captured by the lateral fish-eye camera without knowing the related camera parameters in advance. The lane-based stable system is integrated into the blind-spot lateral collision warning system to increase the better detection rate and provide more adaptive performance. Besides, by constructing the mechanism for drowsiness estimation in the dynamic driving environments, we can collect more data to further analyze other inattentive behavior of drivers so that the safety driving system can consider all possible risks caused by the internal or external factors of drivers as much as possible.

Achieving these algorithms simultaneously by lateral camera is very novel and useful. Warning from this kind of system reflects real hazard and is really worth noticing, it does achieve the goal of "assisting in driving".

## 致謝

本論文的整個研究過程，需要感謝的人實在太多了，無論是碩士班的學弟還是博士班的同學與學長們，對於我都給予相當多的支持與鼓勵，讓我在博士班的時期能不斷地精進。

最感謝的當然是指導教授 林進燈 博士的悉心指導，在研究的方向總是給我最正確的方向與建議，儘管指導教授再忙碌，也從不忘記督促我的進度與研究內容，且老師也給我相當大的彈性，讓我能有更多的機會與時間，讓我學習到如何面對及解決問題的正確態度和方法。另外也要感謝 鄭芳炫、林道通、梁勝富 教授千里迢迢來擔任我的口試委員，教授們的建議及指教，更讓本論文的內容完整與充實。

其次要感謝超視覺實驗室的 蒲鶴章、劉得正 及 鍾仁峯 學長，在我的研究內容給我相當多的建議與糾正，並在我博士班時期遇到的所有困難與低潮，都給予最大的協助與體諒。也感謝 vision group 的博士班學弟 建霆、子貴 及 肇廷，碩士班的學弟 凱翔、宗恆、力倬，及所有學弟妹們在研究過程中給我的幫忙與鼓勵，也在這段時間和我共同度過許許多多難忘的回憶。

最後要感謝默默支持我的我的父母、老婆、以及妹妹給予我精神及物質上的一切支援，也感謝其他親朋好友的關心與鼓勵。你們的關心及支持，才是我保持研究動力的精神來源。

謹以本論文獻給我的家人及所有關心我的師長與朋友們。

# Contents

<b>Abstract in Chinese</b> .....	<b>i</b>
<b>Abstract in English</b> .....	<b>ii</b>
<b>Acknowledgements in Chinese</b> .....	<b>iv</b>
<b>Contents</b> .....	<b>v</b>
<b>List of Figures</b> .....	<b>viii</b>
<b>List of Tables</b> .....	<b>xi</b>
<b>Chapter 1 Introduction</b> .....	<b>1</b>
1.1 Thesis Overview .....	3
1.2 Contributions.....	4
<b>Chapter 2 Background</b> .....	<b>6</b>
2.1 Taxonomy for Classification of ITS Applications .....	6
2.2 Related Products and Functions .....	7
2.2.1 Lane Departure Warning .....	7
2.2.2 Lateral Collision Warning.....	11
2.3 Camera Configuration.....	13
2.4 Discussion and Summary.....	18
<b>Chapter 3 Digital Image Stabilizer</b> .....	<b>21</b>
3.1 Introduction.....	21
3.2 Previous Algorithms.....	22
3.3 System Architecture of the DIS and Motion Estimation .....	26
3.3.1 Motion Estimation .....	27
3.3.2 GMV Estimation .....	28
3.4 Motion Compensation and Evaluation.....	30
3.4 Experimental Results .....	34
3.5 Summary .....	37
<b>Chapter 4 Lateral Collision Warning System</b> .....	<b>38</b>
4.1 Introduction.....	38
4.1.1 Definition of Vehicle Blind Spot .....	38
4.1.2 Previous Work.....	42
4.1.3 Lateral Collision Warning System Structure.....	43
4.2 ROI Definition and Image Processing .....	44

4.2.1	ROI definition .....	45
4.2.2	Image Preprocessing .....	48
4.2.3	HVS-Directed Object Edge Detection .....	49
4.2.4	Angle Evaluation .....	56
4.3	Vehicle Detection and Alarm .....	59
4.3.1	Vehicle Detection .....	59
4.3.2	BLIS Alarm and Stability of System .....	60
4.4	Experimental Results .....	61
4.4.1	Simulation on Personal Computer .....	62
4.4.2	DSP-based Lateral Collision Warning System .....	63
4.5	Summary .....	66
<b>Chapter 5</b>	<b>Lane Departure Warning System.....</b>	<b>68</b>
5.1	Introduction.....	68
5.1.1	Previous Work.....	68
5.1.2	Principles of Lane Detection and Lane Departure Warning.....	69
5.2	Lane Detection.....	70
5.2.1	Preprocessing .....	71
5.2.2	Lane Boundary Detection.....	79
5.2.3	Lane-Finding Algorithm.....	84
5.3	Lane Departure Warning.....	91
5.4	Experimental Results .....	93
5.5	Summary.....	101
<b>Chapter 6</b>	<b>Driver Assistance Alarm System.....</b>	<b>104</b>
6.1	Drowsiness Estimation.....	104
6.1.1	Experimental Architecture of BRC.....	105
6.1.2	Predictive Mechanism for Drowsiness Effect.....	107
6.2	Driving in Danger Analysis .....	109
6.2.1	Construct the Stable-Driving Region with Different Driver's Habit.....	109
6.2.2	Data Collection and Adjustment for the Realistic Environment .....	112
6.3	Summary.....	115
<b>Chapter 7</b>	<b>Realization on Embedded Real-Time System .....</b>	<b>118</b>
7.1	Introduction.....	118
7.2	Cross-Platform Development Framework .....	119
7.3	Hardware Environment.....	119
7.3.1	Introduction to Black-Fin 561 Processor .....	119
7.3.2	Black-Fin 561 Hardware Structure .....	122



7.3.3	Black-Fin 561 Evaluation Board .....	123
7.4	Optimization .....	125
7.4.1	System Optimization.....	125
7.4.2	Tuning C Code for Black-Fin 561 .....	127
7.5	Summary .....	129
<b>Chapter 8</b>	<b>Conclusions and Future Work.....</b>	<b>130</b>
8.1	Conclusions.....	130
8.2	Future Work .....	131
<b>References.....</b>	<b>.....</b>	<b>132</b>
<b>Vita in Chinese .....</b>	<b>.....</b>	<b>138</b>



## List of Figures

Fig. 1: Delphi Lane Departure Warning System.....	10
Fig. 2: Volvo Blind Spot Information System.....	12
Fig. 3: Camera configuration. ....	14
Fig. 4: Vehicle and image coordinate systems. ....	15
Fig. 5: Side view of the geometric relation between the vehicle coordinate and the image coordinate system. ....	15
Fig. 6: Bird's eye view of the geometric relation between the vehicle coordinate and the image coordinate system. ....	16
Fig. 7: Motion compensation schematics. ....	23
Fig. 8: System architecture of the proposed digital image stabilization technique. ....	26
Fig. 9: Division of image for LMV estimation. ....	27
Fig. 10: Performance comparison of three different CMV generation methods applied to a video sequence with panning and hand shaking. (a) CMV generation method in (7). (b) CMV generation method in (7) with clipper in (10). (c) Proposed method in (11).....	33
Fig. 11: Block diagram of the proposed CMV generation method. ....	34
Fig. 12: The diagram of the driver's field of view.....	40
Fig. 13: The relation about field of view between the side mirror and the driver.....	41
Fig. 14: BLIS side collision warning system structure .....	44
Fig. 15: ROI definition flow chart .....	44
Fig. 16: Field of driver's view .....	46
Fig. 17: Image captured by common camera.....	46
Fig. 18: Image captured by fish-eye camera.....	47
Fig. 19: 3D ROI definition.....	48
Fig. 20: Image preprocessing flow chart.....	48
Fig. 21: A 4 x 4 sliding block in the original image.....	51
Fig. 22: Visibility thresholds corresponding to different back- ground luminance. ....	51
Fig. 23: An illustration of the relation between SD parameter and the distribution of pixels in a sliding block. ....	53
Fig. 24: Portions of (a) the sliding block including texture structure, (b) the sliding block including edge structure.....	53
Fig. 25: (a)-(d) Membership functions of fuzzy sets on input variables VD, SD, CD, and output variable Mo, respectively. ....	55
Fig. 26: Flow diagram of the angle evaluation. ....	56
Fig. 27: Portions of (a) smooth region, (b) texture region, (c) edge region, and (d) noise	

region.....	58
Fig. 28: Three areas of ROI .....	60
Fig. 29: Relation between time and alarm (rear) .....	60
Fig. 30: Relation between time and alarm (front).....	61
Fig. 31: PC-based lateral collision warning system.....	62
Fig. 32: System operates in the daytime .....	63
Fig. 33: System operates in the nighttime.....	63
Fig. 34: Daytime DSP-based lateral collision warning system.....	64
Fig. 35: Nighttime DSP-based lateral collision warning system .....	64
Fig. 36: System operates on normal traffic islands.....	65
Fig. 37: System operates in the tunnel .....	65
Fig. 38: System recognizes the vehicle on the outside lane.....	66
Fig. 39: System won't be affected by the street lamp in the nighttime.....	66
Fig. 40: The flow chart of lane detection .....	72
Fig. 41: (a) The image acquired by the camera alongside the rearview mirror. (b) The upper left point of ROI next to the boundary of the vehicle window. ....	74
Fig. 42: (a) Original image. (b) Edge detection by Gy. (c) Edge detection by Gx. (d) Edge detection by Gx+Gy.....	75
Fig. 43: (a) Day light. (b) ROI extraction of (a). (c) ROI extraction at night. (d) ROI extraction with different view-angle in the nighttime. ....	76
Fig. 44: (a) 2-D Gaussian Distribution with mean(0,0) and $\sigma=1$ . (b) Suitable 5x5 mask of Gaussian filter with $\sigma=1$ .....	78
Fig. 45: (a) Mean filter. (b) Gaussian filter. (c) Edge detection after (a). (d) Edge detection after (b).....	78
Fig. 46: Flow chart of the complete preprocessing steps.....	79
Fig. 47: (a) The original image. (b) Gaussian smoothing within the ROI of (a).(c) Result of LoG mask. (d) Result of the new combined mask. ....	80
Fig. 48: The division of ROI into seven sub-regions.....	82
Fig. 49: (a) The image is photographed in a tunnel. (b) Lane-marker extraction without considering the sub-region threshold. (c) Lane-marker extraction with considering the sub-region threshold. ....	83
Fig. 50: The diagram of relationship between the x-y and r- $\theta$ coordinate systems. ....	85
Fig. 51: (a) Seven sub-regions automatically segmented within ROI. (b) the flow chart of the piece-wise edge linking model. ....	86
Fig. 52: (a) Seven sub-regions segmented within ROI. (b) the flow chart of the piece-wise edge linking model. ....	86
Fig. 53: The flow chart for finding the line-shape in the bottom sub-region (A). ....	88
Fig. 54: The flow chart for finding the line-shape in sub-regions from (B) to (G). ....	88

Fig. 55: LSR approximation. ....	90
Fig. 56: The flow chart for TLC estimation.....	93
Fig. 57: The experimental architecture. ....	94
Fig. 58: The programming interface in the PC platform. ....	95
Fig. 59: The testing image with different mounting angles. ....	96
Fig. 60: The results of lane detection.....	98
Fig. 61: The results of lane departure caused by cutting into the inside lane. ....	99
Fig. 62: The results of lane departure in the night time. ....	100
Fig. 63: The results of lane departure caused by moving into the outside lane. ....	101
Fig. 64: Results of lane detection for the unclear lane markers.....	102
Fig. 65: Some examples of detecting error in our lane detection system. ....	102
Fig. 66: The VR-based dynamic driving simulation laboratory.....	106
Fig. 67: The details about the width information of each lane, road, and car.....	106
Fig. 68: The trials collected from the VR-based experiment are sorted according to the degree of reaction time. ....	108
Fig. 69: The flow chart for stable-state region determination. ....	110
Fig. 70: The distribution of N lateral offsets and three approximately Gaussian model (N=200 in this Figure.) ....	111
Fig. 71: The mechanism for drowsiness estimation in our LDW system. (a) The relationship between the stable-state region and the lateral deviations. (b) A drowsy-degree gauge chart. (c) A stable-driving group box, (d) The start and stop points of reaction time. ....	113
Fig. 72 : The flow chart of drowsy degree estimation by the average reaction time evaluated from BRC. ....	115
Fig. 73: Results of update for the stable-driving region. ....	116
Fig. 74: Results of the variation of drivers' drowsy degree by the reaction time.....	117
Fig. 75: Cross-platform development framework.....	118
Fig. 76: Core Architecture of each ADSP-BF561 Core.....	120
Fig. 77: ADSP-BF561 Block Diagram .....	123
Fig. 78: Black-Fin 561 Evaluation Board.....	124
Fig. 79: Blackfin processor memory hierarchy.....	126
Fig. 80: Optimizing DMA traffic over the system buses .....	127

## List of Tables

Table 1: Road traffic accidents and violations in Taiwan from 2001 to 2005. ....	2
Table 2: Related factors for drivers involved in fatal crashes.....	2
Table 3: Classification of ITS Applications .....	8
Table 4: RMSE Comparisons of RPM Fuzzy and the Proposed Method with Respect to Four Real Video Sequences .....	36
Table 5: Comparisons of Three CMV Generation Methods .....	36
Table 6: Parameters Applied to CMV Generation with Different Equations .....	36
Table 7: Causes of traffic accidents between two cars on highway. ....	39
Table 8: The relationship between the field of view and the vehicle velocity. ....	40
Table 9: The relation between speed and field of view .....	46
Table 10: Processing results of the proposed FUZZY decision system corresponding to four different structures shown in Fig. 14 .....	58
Table 11: Specification of platform information.....	94



## Chapter 1 Introduction

In recent years, the traffic accidents cause very serious social and economic problems. In 1999, about 800,000 people died globally in road related accidents, and these accidents caused losses of around US\$ 518 billion [1]. According to the United Nations, there were more than 23,000 vehicle drivers died in traffic accidents in 2004. In Taiwan, the number of traffic accidents was increasing from 64,264 in 2001 to 155,814 in 2005 as shown in Table 1[2]. In general, a considerable fraction of these accidents is due to driver's fatigue, drowsiness, inattentive driving or driving without keeping distance with frontal vehicle and leaving its proper lane. The related factors are as listed in Table 2[3]. On the highway, the most important cause of traffic accidents is the lateral and frontal collision. In order to improve the driving safety, a lot of researches about the Intelligent Transportation Systems (ITS) have been proposed in recent years. For example, the Advanced Vehicle Control and Safety System (AVCSS) not only prevents the driver from danger, but controls the traffic flow efficiently.

According to Table 2, we can group those accident factors as three types: type I lane departure (factor 1), type II side vehicles collision (factor 5), and type III drivers' exceptionally driving (factors 3, 4, 6).

According to the type I, lane departure, the lateral position and velocity of the lane boundary are the key factors to predict departing action immediately. It can be very useful if there is a lane departure warning system providing the warning signal to the driver by monitoring the distance from the vehicle to the both sides of the lane markers.

For the type II, side vehicles collision, it happens a lot even the driver can get the surrounding information by wing mirrors and a rear-view mirror. The major reason to

cause type II traffic accidents is the existence of the blind spot region and driver's negligence. If there is a lateral vehicle collision warning system detecting the distance of the later vehicle, it can prevent from the side vehicle collision happening.

According the above discovery, a new system is expecting that can provide the driver real-time warning signal to prevent the traffic accidents and decrease the social and economic problems. In order to reach this goal, this thesis proposes such a new system meanwhile considering the future commercial possibility. On account of our proposed system, it can support the driver to notice about 60% factors of traffic accidents by giving the driver an actual warning signal. Within our proposed system, the abundant information collecting the real-time road images road is necessary, therefore, a lateral camera with the vision-based system is chosen as the sensing device in this thesis to capture and process it. More details of algorithms will be introduced in the following chapters.

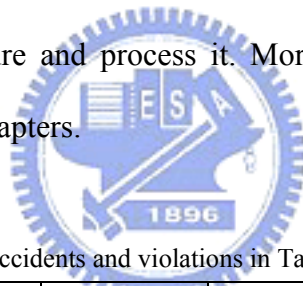


Table 1: Road traffic accidents and violations in Taiwan from 2001 to 2005.

<b>Year</b>	<b>2001</b>	<b>2002</b>	<b>2003</b>	<b>2004</b>	<b>2005</b>
<b>Numbers of Event</b>	64,264	86,259	120,223	137,221	155,814
<b>Fatalities</b>	3,344	2,861	2,718	2,634	2,894
<b>Injuries</b>	80,612	109,594	156,303	179,108	203,087

Table 2: Related factors for drivers involved in fatal crashes.

<b>Factors</b>	<b>Description</b>	<b>Percent</b>
<b>1</b>	<b>Failure to keep in proper lane or running off road</b>	24.0%
<b>2</b>	<b>Driving too fast for conditions or in excess of posted speed limit</b>	20.3%
<b>3</b>	<b>Under the influence of alcohol, drugs, or medication</b>	12.2%
<b>4</b>	<b>Inattentive (talking, eating, etc.)/ Drowsy, asleep, fatigued, or ill</b>	9.1%
<b>5</b>	<b>Failure to yield right of way</b>	7.9%
<b>6</b>	<b>Operating vehicle in erratic, reckless, careless, or negligent manner</b>	6.7%
<b>7</b>	<b>Others</b>	19.8%

## 1.1 Thesis Overview

This thesis is organized as follows. In Chapter 2, at the beginning it will be introduced the different categories of Intelligent Transportation Systems. These categories will be used to explain the relationship and problems that this thesis wants to solve. Then the following section will introduce various current techniques about Lane Departure Warning and Lateral Collision Warning. At last the advantages and disadvantages of these current techniques will be discussed by their functions.

In chapter 3, because all techniques in this thesis are based on cameras mounted a car all image information must be stabilized before further processed through Digital Image Stabilizer (DIS). Thus the following processing stages can acquire stable image source and the following algorithm can be simplified. In this chapter, current DIS techniques will be discussed and the modified PI controller for DIS will be proposed. At last there will be the related experimental results.

Lateral Collision Warning will be discussed in the forth chapter. In this chapter lateral collision is discussed and Blind Spot is defined. The rear mirror for drivers to observe cars is not enough because rear mirror has its blind spot which cars cannot be seen. This chapter also introduces the definition and processing of Region of Interest (ROI). After defining ROI, vehicles begin to be detected. If any car enters ROI, the system will issue alarm. The related computer simulation and experiments on embedded system will be explained in the later part of this chapter.

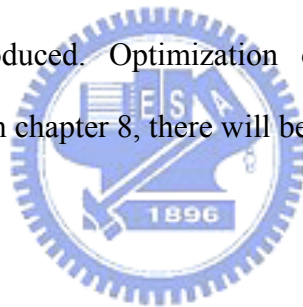
In chapter 5, Lane Departure Warning will be discussed. Here Lane Detection will be mentioned and there are some special techniques which can successfully detect lane line under different environments. By using this information about lane line detection, the relationship between a vehicle and a lane are analyzed, such as the deviating velocity, the distance measurement between a vehicle and the center of the



lane as well as the decision of changing lanes.

From the chapter 4 and 5, the lane departure warning and the lateral collision warning algorithms can come out a lot of useful information which will be used to analyze the behavior of drivers in chapter 6. In this part, data from Brain Science Center are used to determine whether a driver may doze off. Drivers' driving habits also can be analyzed and the result can be used to determine if it is safe for the driver to continue driving. After integrating Lane Departure Warning and Lateral Collision Warning, the system can give the driver warning when changing lane is dangerous. This function will increase the driver's safety.

In chapter 7, the hardware environment of this thesis will be discussed. Because all algorithms are based on embedded system, the hardware platform and its characteristics will be introduced. Optimization of the algorithm and coding notification is also included. In chapter 8, there will be conclusion and future work.



## **1.2 Contributions**

There have been a lot of researches and products in lane departure lateral collision warning, but the major function of them is to keep the driver/car in the lane without noticing the approach of the later vehicle. In addition, those lateral collision warning systems will provide the warning signal whenever the vehicle is approaching. The warning systems without considering the deviation easily cause false alarm. Once the false alarm frequently increases, the driver's attention will unconsciously decrease and the possibility of the traffic accident will rise.

Of course, these two systems can be set up and combined in a car simultaneously, but it would not be very economic: firstly it requires both frontal and lateral cameras. Secondly it needs two Engine Control Units (ECU) processing two

set data separately. Thirdly it will increase the car production cost and utility consumption. In addition, using lateral camera to deal with lane detection can reduce the problem of the ray radiation of lights.

For the drowsiness analysis utilized in the proposed system, there is not any annoying probe attached to the driver, nor an internal camera monitoring the driver's eyes. Because the latter easily misinterprets the driver's eye movement especially the driver has small eyes or wears the sun glasses. In fact, the brain signal and the lane change reaction time of the driver are two major factors to measure the driver's concentration level of the proposed system. As a result, the higher the concentration level is, the safer the driver is.

Using a single lateral camera to perform the significant functions of the lane departure warning system, the lateral collision detection system and the driver's drowsiness analysis system is very novel and useful, such as the proposed system in this thesis. This kind warning signal truly reflects real hazard and is really worth noticing and it does achieve the goal of "assisting in driving".

## **Chapter 2 Background**

In this chapter, section 2.1 will discuss the structure of Intelligent Transportation Systems (ITS) and its topics which this thesis concerns with. In section 2.2, current products in this area will be discussed, and section 2.3 will illustrate the location where we set up lateral camera. At last the advantage and disadvantage of lateral camera and frontal camera will be compared.

### **2.1 Taxonomy for Classification of ITS Applications**

Interest in ITS comes from the problems caused by traffic congestion worldwide and a synergy of new information technologies for simulation, real-time control and communications networks. Traffic congestion has been increasing world-wide as a result of increasing motorization, urbanization, population growth and changes in population density. Congestion reduces efficiency of transportation infrastructure and increases travel time, air pollution and fuel consumption.

Intelligent transportation systems have various levels based on the technologies they apply, from basic management systems such as car navigation, traffic light control systems, container management systems, variable message signs or speed cameras to monitoring applications such as security CCTV systems, and then to more advanced applications which integrate live data and feedback from a number of other sources, such as Parking Guidance, Information systems, weather information, and bridge de-icing systems.

Sensor technologies have greatly enhanced the technical capabilities and safety benefits awaiting intelligent transportation systems around the world. Sensing systems of ITS can be either infrastructure based or vehicle based systems, for example,

Intelligent vehicle technologies. Vehicle sensors are those devices installed on the road or in the vehicle.

In Table 3 a full view of ITS will be seen. From this table we can find that all ITS structure needs a huge amount of sensors in the roads of vehicles. It means that sensors play an important role in ITS. All these sensors are set up for providing more information for drivers, and in this thesis we focus on driver assistance and collision avoidance system which are the application of sensors on vehicles. In collision avoidance systems section, this thesis will deal with obstacle detection, lane change assistance and lane departure warning. In driver assistance systems section, the problem of lane keeping assistance and drowsy driver warning will be solved by lateral cameras as the only sensor.

## **2.2 Related Products and Functions**

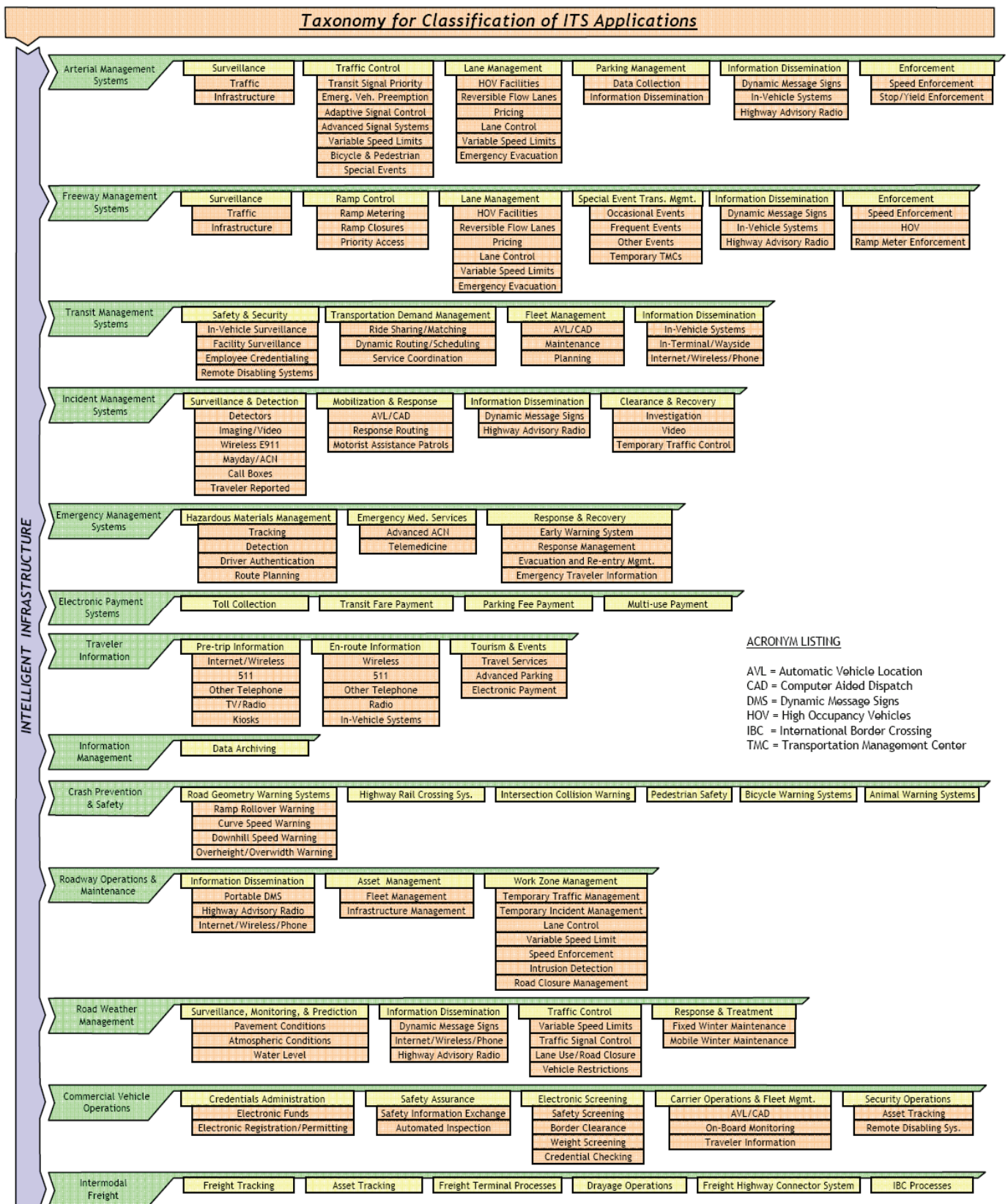
### **2.2.1 Lane Departure Warning**

LDW technology is currently divided into 2 categories: one of them is using camera as its sensor and the other is using laser as its sensor. The previous one will be discussed first.

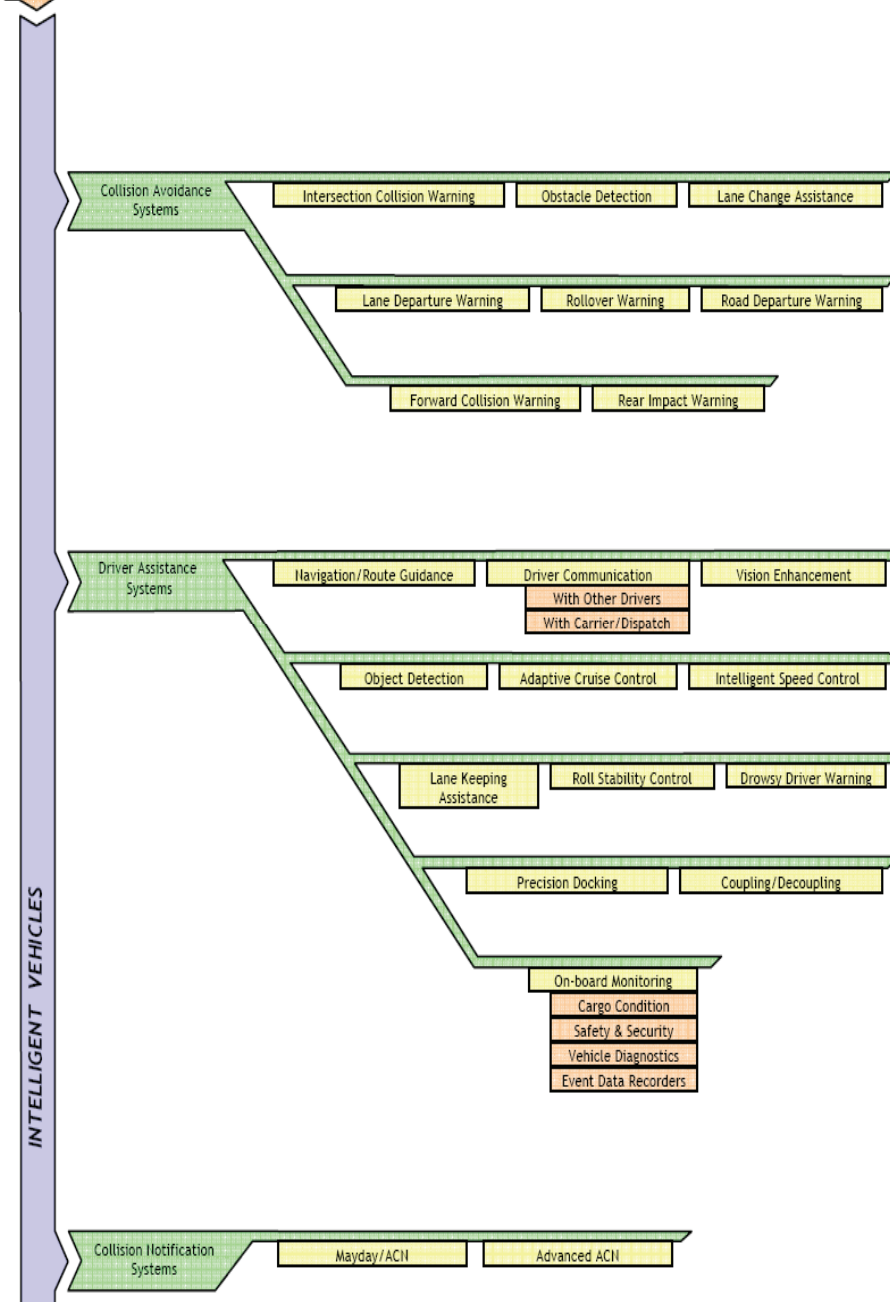
#### **Delphi: [11]**

The Delphi Lane Departure Warning system is a lane tracking system that helps alert drivers when they unintentionally drift out of their intended lane. Using a camera and image processing to detect painted lane markers up to 25 meters ahead of the equipped vehicle, the system determines the vehicle's heading and lateral position in the lane to provide the appropriate warning. Helps drivers become aware of lane drifting quickly. This system would not report stopped objects along the roadside,

Table 3: Classification of ITS Applications



## Taxonomy for Classification of ITS Applications



reducing false alarms. Flexible alert configuration is based upon OEM requirements, including audible, tactile and/or visual driver warnings. Camera mounted behind the wiped area of the windshield allows driver to maintain a clear line of sight. Camera can be shared with Delphi Active Night Vision system.



Fig. 1: Delphi Lane Departure Warning System

**Siemens:** [12]

Lane Departure Warning makes driving more relaxed by protecting from unintentional lane changes through warning messages and discrete steering corrections. A good song on the radio, a stimulating conversation with a passenger or the sun, which suddenly blinds the driver – there are many reasons to drift off the lane. Especially longer highway trips with little traffic or drives on monotonous country roads present the danger of briefly drifting off the lane unintentionally. In most of these cases of inattentiveness can be corrected through counter steering and the drive can be continued.

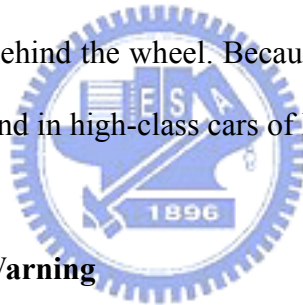
**ITRI:** [14]

For drive safety, it is necessary for a vehicle to perform the ability to detect the environmental condition. The lane departure warning system is to detect the lane marks accurately, robustly, and reliable and warn the driver according to the decision-marking algorithm processed by vehicle computer.

Systems that based on image sensor have some characteristics: 1.Active safety warning system which is integrated in the main rear mirror. 2. By using technologies such as computer vision and pattern recognition algorithm, real vehicle integration

and safety warning, these systems can accurately and real-time detect lane and give alarm if the vehicle deviates the safe lane. This system has been tested on shuttles which run on the highway. This system also integrate itinerary recorder which can monitor long term driving behavior to prevent drivers form changing lane improperly. This system is mainly applied in public transportation industry to decrease severe car accidents.

Another sensor which is based on laser is ibeo, the laser scanner detects the lane markings and carriageway limits in front of the vehicle, as well as potential obstacles. The position of the vehicle on the road is calculated at the same time. If the car is about to stray from its lane, a pre-emptive warning is issued immediately in the form of a seat or steering wheel vibration. This system provides an effective weapon against any lack of attention behind the wheel. Because of the high price of ibeo, this kind of sensor only can be found in high-class cars of BMW.



### **2.2.2 Lateral Collision Warning**

Lateral Collision Warning is called Blind Spot Information System (BLIS) or Blind Spot Detection System in market. Most of these systems are based on camera because laser or IR sensor may sensitive to irrelative objects such as traffic islands and wire poles. However, sensors based on image information can filter out irrelative objects by image processing.

#### **Volvo:**

Volvo is first to offer car drivers a high-tech solution to help avoid the risk of accidents caused by blind spots with its new safety system – BLIS. Volvo's latest safety innovation uses an intelligent digital camera system incorporated into both door mirrors that constantly monitor the area alongside the car for cars or motorbikes, then alerts the driver via an orange light housed in the car's A-pillar by the door mirror.



BLIS also works after dark when it will react to the headlamps of any surrounding vehicles.

As Britain's roads get ever busier, Volvo believes the additional visual information BLIS relays to the driver before changing lanes or overtaking in busy urban environments or on multi-lane highways, will prove particularly useful.

The BLIS system does not relieve the driver of his or her obligation and responsibility to do the usual visual checks before attempting any maneuvering, but does afford frequent motorway users or city drivers an added level of protection against vehicles hovering in the periphery of the driver's field of vision.

While a dash mounted button can be used to temporarily switch the safety aid off, if required, BLIS is capable of making the distinction between mobile and immobile objects such as parked cars, road barriers, lampposts and other static objects, ensuring all alerts are limited to potentially hazardous moving obstacles.



Fig. 2: Volvo Blind Spot Information System

## Siemens:

Blind Spot Detection helps to expand the rear viewing angle and thus relieve the driver. If there is a car in the blind spot, the Blind Spot Detection informs early on using a visual warning.

A passing maneuver on the highway: looking in the side mirror confirmed that the lane is free – but a car comes into the visual field from behind, just when the driver is about to change lanes. Critical situations, such as these can arise in urban traffic if vehicles in the blind spot are overlooked. Blind Spot Detection provides information on whether there are any vehicles in this area that are not visible to the driver.

## 2.3 Camera Configuration

In this section, the geometric relationship and transformation between the image coordinate and the realistic vehicle coordinate are explained in detail.

To extract the image information of road plane on the side of the vehicle, a single camera is mounted near the rearview mirror. In the vision-based configuration, each objects captured by the image sensor in the camera coordinate system can be projected onto the image pane in the image coordinate system. This geometric relationship can be described as the perspective projection, and the camera configuration for the proposed system is shown in Fig. 3 with the height of the camera  $H$  and the tilt angle  $\alpha$ .

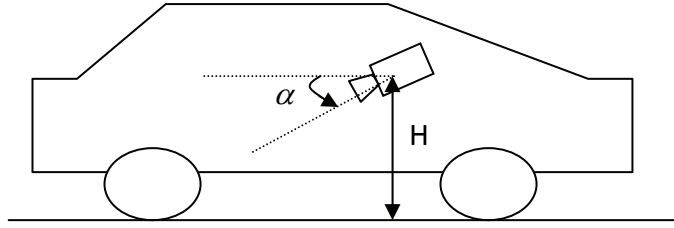


Fig. 3: Camera configuration.

Before computing the transformation between the image coordinate and the vehicle coordinate, some assumption must be established. At first, the condition in this section is only considered that the ground plane is almost flat. In general, we ignore the specific environment when the vehicle drives on the mountain road or other rugged surface. Second, the optical distortion of the camera lens can not be considered in this deduced process of the geometric transformation.

The spatial relationship between the vehicle coordinate and image coordinate system are shown in Fig. 4. For practicality, the pan and tilt angle of the camera must be taken into account for this systematic configuration. The tilt angle  $\alpha$  is an included angle from road plane to the optical axis. On the other hand, the pan angle  $\beta$  is an included angle from the moving direction of the vehicle (Y-axis) to the projection of the optical axis onto the road plane. In general, the camera can be modeled as the pin-hole model. The distance between the optical center (OC) and the central point of the image plane  $(u_0, v_0)$  can be used to the focal length. Moreover, according to the known camera height H and the information of pan-tilt angle, we can deduce where the object is contained by projecting road surface onto the image plane from the perspective geometry.

For further analysis, we discuss the spatial relation between the vehicle

coordinate and the image coordinate system through two different points of view. Fig. 5 and Fig. 6 are the side view and bird's eye view of the geometric chart between the vehicle coordinate and the image coordinate system.

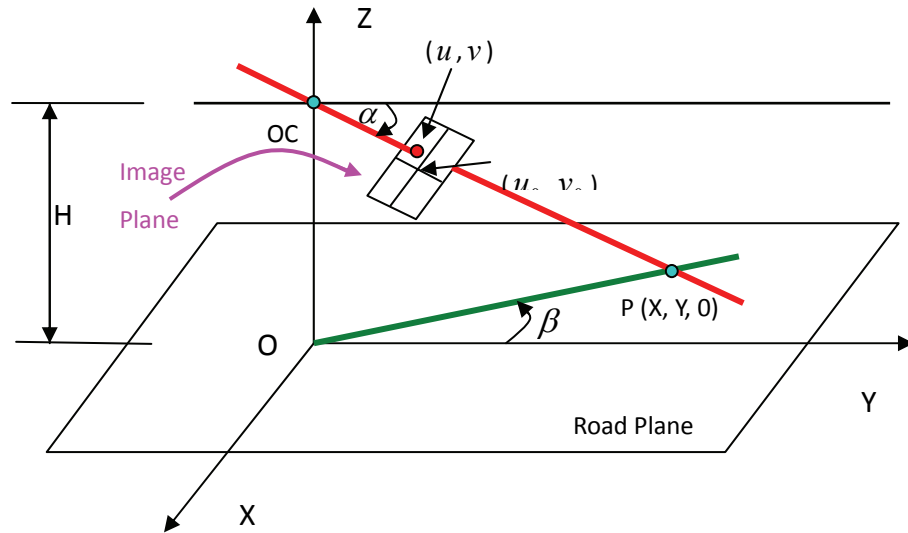


Fig. 4: Vehicle and image coordinate systems.

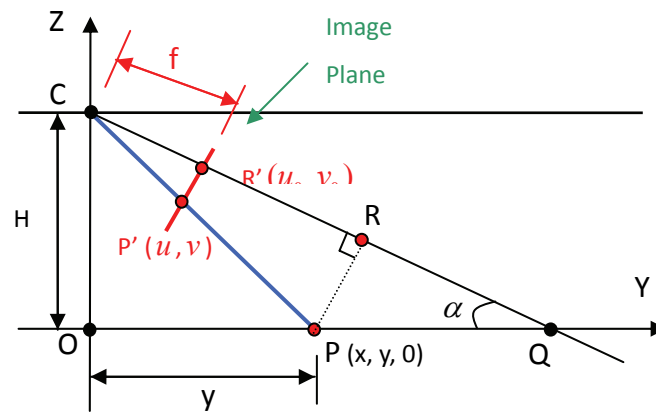


Fig. 5: Side view of the geometric relation between the vehicle coordinate and the image coordinate system.

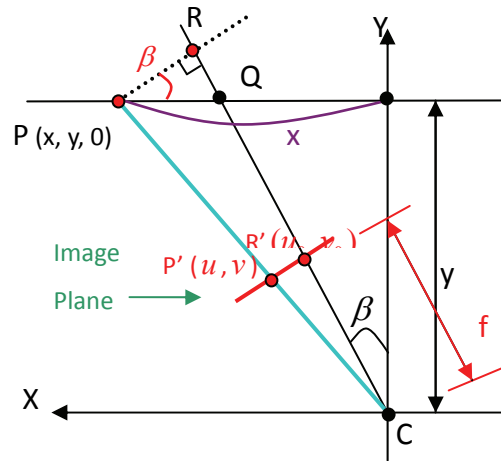


Fig. 6: Bird's eye view of the geometric relation between the vehicle coordinate and the image coordinate system.

Before explaining the formulation of the transformation between the two coordinate systems, some annotations about Fig. 5 and Fig. 6 must be introduced in advance.

$f$ : Focal length of the camera

$f_u, f_v$  : The scaling factors of the image plane in the horizontal and vertical axis

$H$ : The distance from the road plane to the camera

$\alpha$  : Tilt angle of the camera

$\beta$ : Pan angle of the camera

$(u, v)$ : The corresponding point in the image plane is projected from the road surface

$(u_0, v_0)$  : The central point of the image plane

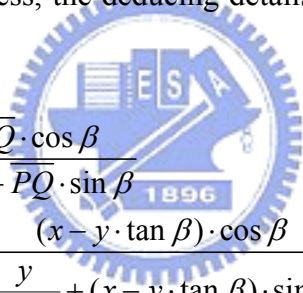
In Fig. 5,  $\triangle CPR$  and  $\triangle CP'R'$  are similar triangles. With this property, the spatial relation between two coordinate systems can be derived as follows.

$$\begin{aligned} \frac{\overline{PR'}}{\overline{CR'}} &= \frac{\overline{PR}}{\overline{CR}} \\ \Rightarrow \frac{(v-v_0) \cdot f_v}{f} &= \frac{\overline{PQ} \cdot \sin \alpha}{\overline{CQ} - \overline{PQ} \cdot \cos \alpha} = \frac{\left(\frac{h}{\tan \alpha} - y\right) \cdot \sin \alpha}{\frac{h}{\sin \alpha} - \left(\frac{h}{\tan \alpha} - y\right) \cdot \cos \alpha} \\ \Rightarrow \frac{(v-v_0) \cdot f_v}{f} &= \frac{h \cdot \cos \alpha - y \cdot \sin \alpha}{\frac{h}{\sin \alpha} - \left(\frac{h \cos^2 \alpha}{\tan \alpha} - y\right) \cdot \cos \alpha} = \frac{h - y \cdot \tan \alpha}{h \cdot \tan \alpha + y} \\ \Rightarrow [f_v \cdot (v-v_0) + f \cdot \tan \alpha] \cdot y &= [\tan \alpha \cdot f_v \cdot (v-v_0) - f] \cdot h \end{aligned}$$

Assume  $S_v = \frac{f}{f_v}$  is the camera constant of the image plane in the vertical axis

$$\Rightarrow y = \frac{[(v-v_0) \cdot \tan \alpha - S_v] \cdot h}{(v-v_0) + S_v \cdot \tan \alpha} \quad (1)$$

Similar to the above process, the deducing details about Fig. 6 will be described in the following.



$$\begin{aligned} \frac{\overline{PR'}}{\overline{CR'}} &= \frac{\overline{PR}}{\overline{CR}} = \frac{\overline{PQ} \cdot \cos \beta}{\overline{CQ} + \overline{PQ} \cdot \sin \beta} \\ \Rightarrow \frac{(u-u_0) \cdot f_u}{f} &= \frac{(x-y \cdot \tan \beta) \cdot \cos \beta}{\frac{y}{\cos \beta} + (x-y \cdot \tan \beta) \cdot \sin \beta} = \frac{x \cdot \cos \beta - y \cdot \sin \beta}{y \cdot \cos \beta + x \cdot \sin \beta} \\ \Rightarrow \frac{(u-u_0) \cdot f_u}{f} &= \frac{x - y \cdot \tan \beta}{y + x \cdot \tan \beta} \end{aligned}$$

Assume  $S_u = \frac{f}{f_u}$  is the camera constant of the image plane in the horizontal axis

$$\begin{aligned} \Rightarrow \frac{u-u_0}{S_u} &= \frac{x - y \cdot \tan \beta}{y + x \cdot \tan \beta} \\ \Rightarrow x &= \frac{y \cdot [(u-u_0) + S_u \cdot \tan \beta]}{S_u - (u-u_0) \cdot \tan \beta} \quad (2) \end{aligned}$$

Equations (1) and (2) are the transformation from the point  $(u, v)$  in the image plane to that  $(x, y, 0)$  within the road surface in the vehicle coordinate system. However, parts of the parameters in this formulation are unknown. We must make use

of some probability approaches to estimate those values if the precision of the perspective phenomenon is adequate.

## 2.4 Discussion and Summary

For several years, many researchers worked on driving assistance problem by using the concept of artificial vision. Among those applications in intelligent transportation, automatic navigation has been taken seriously in recent years. For accomplishing this objective with efficient performance, most vision-based methods are to extract the road information by mounting the image sensor on the windshield of the vehicle, such as the human eye and forward-looking camera. These sensors can extract the widest field of view than other mounting position around the car body. In general, by detecting the contrast between the white lines and the road, the lane boundary in front of the vehicle can be detected. The variation of the lane's curvature also can be predicted in time without resulting in the erroneous following of the vehicle. Besides, some obstacles captured by the camera can be recognized with 2D or 3D techniques of computer vision. Other related works such as keeping the secure distance ahead of the car are based on this system configuration.

Some risks of road traffic which occur on highway during the lane-changed maneuver happen easily if another vehicle besides the own one has been overlooked. In other words, drivers have not assured accurately if there is no other vehicle alongside in the blind spot of the lateral view. During the general driving procedure, drivers must keep notifying the frontal field of view so that they forget to check the information of the lateral blind-spot at the same time. In order to overcome this kind of traffic hazard with efficiency, a camera is mounted at the driver's outside rear-view mirror to monitor the blind spot and the alongside lane. Approaching vehicles should

be detected in time and tracked until they leave the blind spot by this configuration. In addition, this system can restrain the intended lane-changed maneuver and maintain the distance from the lane boundary in the blind spot for the car body. This system can prevent vehicles from a significant amount of the potential collisions.

In addition to the distinct effect of the geometric projection onto the image plane, there are still other different factors and applications in the frontal-view and lateral-view configurations. The four reasons are listed as follows.

(1) The initial purpose has influenced on the place where the camera is mounted:

As explained above, road images extracted from the forward sight of the vehicle can yield more driving information to track the real-time road curvature by the lane-marking modeling. Furthermore, the related data of them has effectively contributed to the system with respect to the assistant navigation. On the other word, the major objective about mounting the camera on the side of the car is to adjust how much the detecting range of the blind-spot region is. This configuration only puts emphasis on judging whether the approaching car or the lane trajectory is near the vehicle, and the variation of the forward road information cannot be considered.

(2) The diverse sensation of the driver with respect to two mounting position:

In general, to extract the forward visual information as far as possible, the camera was almost fixed to the windshield. This setting location could easily reduce the eyesight of the driver, no matter how small the camera is. The disadvantage resulting from the driver's unfamiliar looking will be concerned in the research about driver analysis. Nevertheless, because of the position of the camera which is near the rear-view mirror, drivers should not be confused in this experimental environment when focusing on extracting the lateral-view content of the vehicle. In other words, the camera added to the vehicle can not affect the original driving habit of the driver,



and the data collected by driver analysis system will still be higher accuracy.

(3) The different extrinsic factors of two locations of the sensing device:

Compared with the initial purpose of two configurations, the camera mounted in front of the vehicle must have farther distance from its optical center to the specified lane portion on the road plane than that on the side of the car because of the perspective geometry. In addition, the overtaking cars which cross the lane are almost captured by the frontal-view image sequences. Therefore, the information of the lane trajectory extracted by the sideward camera can be more complete than the forward one throughout the driving experiment on highway. However, with the headlight switching in the gloomy driving situation, the video collected by the frontal camera still holds more acceptable luminance information in night vision.



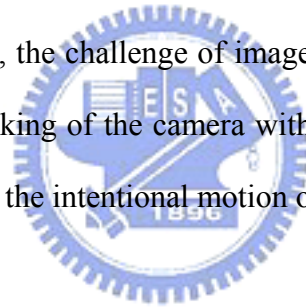
## Chapter 3 Digital Image Stabilizer

### 3.1 Introduction

Machine vision is a key technology used in any intelligent transportation system (ITS) to augment or replace human drivers' visual capabilities. ITS research involves four major issues: increasing the capacity of highways, improving safety, reducing fuel consumption, and reducing pollution. ITS can use some intelligent control strategies, such as agent-based control concepts [4], [5], to manage the transportation and traffic problems. In machine vision aspect, it can be used to detect land markings, vehicles, pedestrians, road signs, traffic conditions, traffic incidents, and even driver drowsiness or to assist the driver to get more information and reduce driving accidents. These applications are almost included in the first two issues of ITS researches. Four typical applications that involve machine vision are: 1) cruise assistance; 2) urban driving assistance; 3) driver monitoring; and 4) traffic and road monitoring. From the site of image acquisition, it can be divided into in-car or off-car applications. The former three items belong to in-car applications, and the common concern in most applications is reliability. The reliability is related to the image acquisition process and image interpretation process, i.e., the contrast and the resolution of the images, the stability of the image sequence, and the reliability of image interpretation, etc. The better image-acquisition process will increase the feasibility and reliability of the process and analysis afterward. The increase in the contrast and the resolution of images are pure hardware issues. It has been designed by a wide-dynamic-range approach to improve the success rate of lane detection under high-intensity contrast [6]. Most image interpretation processes need to detect the motion field (motion vector) in the image. In an ideal environment, the motion field is easy to interpret.

However, practical motion fields deviate from the simple description. Additional motion components are induced by disturbances like the bumpy ride of the vehicle or the steering effect. To enable the efficient image interpretation process, these disturbances have to be compensated in advance. In this thesis, a method to acquire the stable image sequence by in-car cameras which can be used for driver assistance or subsequent processes is proposed.

Digital image sequences acquired by in-car video cameras are usually affected by undesired motions produced by a bumpy ride or by steering. The unwanted positional fluctuations of the image sequence will affect the visual quality and impede the subsequent processes for various applications. Although undesired motions are usually irregular and uneven compared to intentional global motions such as car movement or camera panning, the challenge of image stabilization systems is how to compensate the unwanted shaking of the camera without the influence caused by the moving object in the image or the intentional motion of the car.



### **3.2 Previous Algorithms**

The image stabilization systems can be classified into three major types: the electronic, the optical, and the digital stabilizers. The electronic image stabilizer (EIS) stabilizes the image sequence by employing motion sensors to detect the camera movement for compensation. The optical image stabilizer (OIS) employs a prism assembly that moves opposite the shaking of camera for stabilization [7], [8]. Because both EIS and OIS are hardware dependent, the applications are restricted to device built-in online processes. Digital image stabilization (DIS) is the process of removing the undesired motion effects to generate a compensated image sequence by using digital image processing techniques without any mechanical devices such as gyro sen-

sors or a fluid prism [13]. The major advantages of DIS are: 1) machine independence and 2) suitability for miniature hardware implementation (since the mechanical device is not required for compensation) [9].

The DIS system is generally composed of two processing units: the motion estimation unit and the motion compensation unit. The purpose of the motion estimation unit is to estimate the reliable global camera movement through three processing steps on the acquired image sequence: 1) evaluation of local motion vectors (LMVs); 2) detection of unreliable motion vector components; and 3) determination of the global motion vector (GMV). Following the motion estimation, the motion compensation unit generates the compensating motion vector (CMV) and shifts the current picking window according to the CMV to obtain a smoother image sequence.

Fig. 7 shows the motion compensation schematics. The window of frame ( $t - 1$ ) is the previous compensated image. The compensating motion vector  $v$  is generated by the DIS according to the GMV between two consecutive images. The window of frame ( $t$ ) is the picking window according to the compensating motion vector  $v$  to minimize the shaking effect.

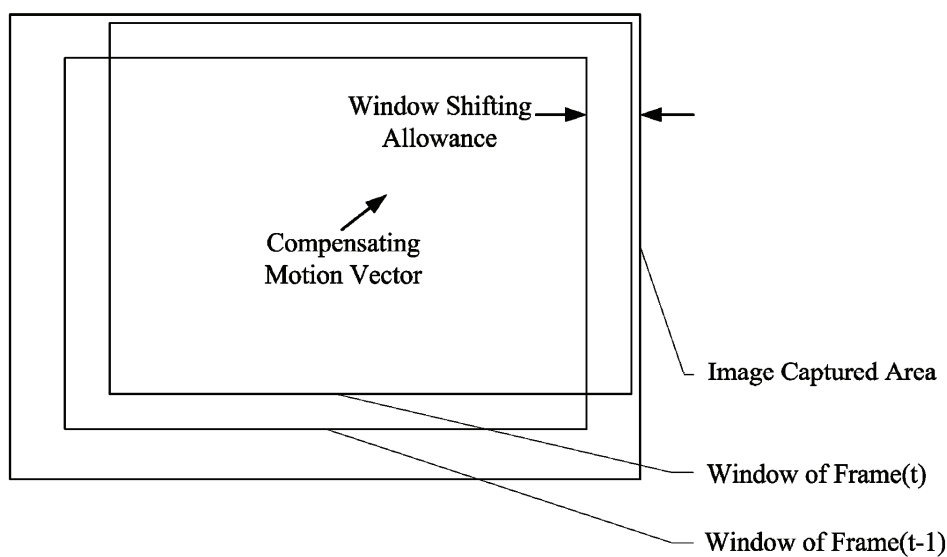


Fig. 7: Motion compensation schematics.

Various algorithms have been developed to estimate the LMVs in DIS applications such as representative point matching (RPM) [14], [15], edge pattern matching (EPM) [16], [17], bit-plane matching (BPM) [13], [18], and others [19]–[23]. It has also been demonstrated that the DIS can reduce the bit rate for video communication [24]. The major objective of these algorithms is to reduce the computational complexity, in comparison with a full-search block-matching method, without losing too much accuracy. In general, the RPM can greatly reduce the complexity of computation in comparison with the other methods. However, it is sensitive to irregular conditions such as moving objects and intentional panning, etc. [18]. Therefore, the reliability evaluation is necessary to screen the undesired motion vectors for the RPM method. In [15], a fuzzy-logic-based approach was proposed to discriminate the reliable motion vector from the LMVs. This method produced two discriminating signals based on some image information such as contrast, moving object, and scene changing to determine the GMV. However, these two signals cannot widely cover various irregular conditions such as the lack of features or containing large moving objects in the images, and it is also hard to determine an optimum threshold for discrimination in various conditions. Some researchers estimate LMV using feature-based techniques that track a small number of image features (points, lines, and contours or certain objects, etc.) to evaluate the motion vector. This makes it efficient and available for real-time implementation. But the difficulty is that, especially for outdoor applications, it cannot stably and accurately find available features in the image [25]. Based on the optical flow technique, a fundamental approach in computer vision, many methods have been proposed in the literature to solve different types of problems. The estimation of optical flow is based on the assumption that the intensity of the object (or specified pixel) in the image sequence is constant. The difficulty is that most consumer video camcorders have an auto shutter function to adjust average intensity dynamically such

that maintaining constant intensity of the object becomes impossible in real applications. In this thesis, a reliable LMV extraction method is proposed to determine the GMVs for practical applications.

In the motion compensation of DIS, accumulated motion vector estimation [16] and frame position smoothing (FPS) [26]–[28] are the two most popular approaches. The accumulated motion vector estimation needs to compromise stabilization and intentional panning (constant motion) preservation since the panning condition causes a steady-state lag in the motion trajectory [26]. The FPS accomplished the smooth reconstruction of an actual long-term camera motion by filtering out jitter components based on the concept of designing the filter with an appropriated cutoff frequency. The disadvantage of FPS is that it does not guarantee the availability of the determined CMV when the specified bound is restricted for preserving the effective image area in the DIS applications.

In this chapter, a novel robust in-car DIS technique is proposed. An adaptive background evaluation model for deriving GMV is developed to deal with irregular images that contain large moving objects or low-contrast area. The accumulated motion vector estimation combined with an integrator in the inner feedback loop is also applied to remove the shaking effect without losing the effective area of the images with constant motion. Video sequences with various irregular conditions, such as the lack of features, large low-contrast area, moving objects, or repeated patterns, etc., are used for testing, and the experimental results demonstrate that the proposed algorithm can perform very well in such conditions. A smoothness index (SI) is also proposed in this thesis to quantitatively evaluate the performances of different image stabilization methods.

### 3.3 System Architecture of the DIS and Motion Estimation

The system architecture of the proposed DIS technique is shown in Fig. 8, which includes two processing units: the motion estimation unit and the motion compensation unit. The motion estimation unit consists of two estimators: the LMVs, and the GMV estimators. The motion compensation unit consists of the CMV estimation and image compensation. The two incoming consecutive images frame ( $t-1$ ) and frame ( $t$ ) will be first divided into four regions as shown in Fig. 9. An LMV will be derived in each region by the RPM algorithm [14], [15]. The motion estimation unit also contains a reliability detection function that will generate an ill-conditioned motion vector for the irregular image conditions such as the lack of features or containing a large low-contrast area, etc. The GMV estimation determines a GMV among LMVs, another preselected motion vectors through the adaptive background-based evaluation function. Finally, the CMV is generated according to the resultant GMV, and the image sequences will be compensated based on the CMV in the motion compensation unit. The rest of this section will focus on the details of the motion estimation unit of the proposed DIS technique.

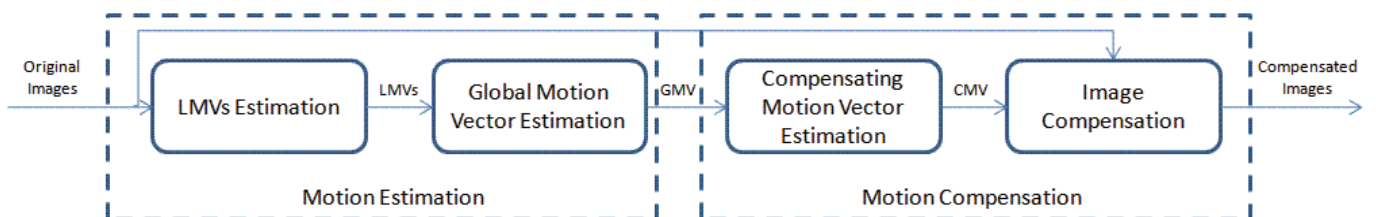


Fig. 8: System architecture of the proposed digital image stabilization technique.

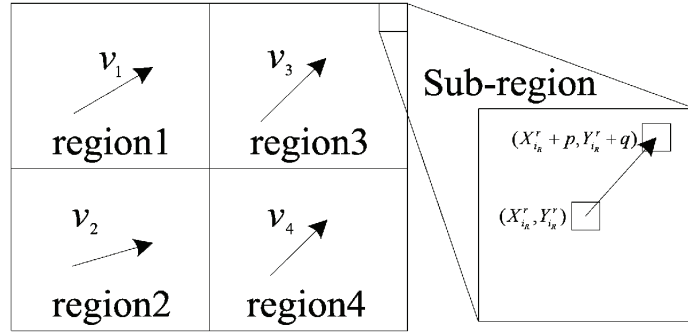


Fig. 9: Division of image for LMV estimation.

### 3.3.1 Motion Estimation

The motion estimation unit shown in Fig. 8 contains the LMV, and GMV estimators. As shown in Fig. 9, LMV estimation is to generate the LMVs for GMV estimation. The LMVs can be obtained from the correlation between two consecutive images by the RPM algorithm.

- RPM and Local Motion Estimation

It has been demonstrated that a local approach using a regional matching process is more robust and stable than a direct global matching process [29]. That means using the LMVs estimated by the divided regions to determine the GMV is more robust and stable than a direct approach. There is also a tradeoff for the size of divided region. Reducing the size of the divided region increases the robustness, but the size of the divided region should be sufficiently large to hold the average distribution [29]. If we want to divide the image such that the horizontal and vertical components have the same partitions, it should be divided into  $n^2$  regions. More divided regions will increase the computational cost to estimate the LMV for each region. Therefore, we only divide the image into four regions as shown in Fig. 9 for the RPM method, and it can cover various situations in the in-car DIS applications by combining the proposed



inverse triangle method and the adaptive background evaluation model.

Each region is further divided into 30 sub-regions (with each side of 5 rows  $\times$  6 columns), and the central pixel of each sub-region is selected as the representative point to represent the pattern of this sub-region. This layout is based on the size of images captured by the regular imaging devices such as  $640 \times 480$  or  $320 \times 240$ . In order to make the representative points equally distributed in spatial, the ratio of row and column should be maintained by as close to 0.75 as possible. It is the averaged testing result for four experimental video sequences. It can be found that if the number of the representative points is larger than 30, the cost level will go down to the threshold and almost all the motion vectors calculated by the RPM method are reliable. In other words, in this case, the cost level will be good enough as the lower cost level indicates high reliability. In order to keep low computation time complexity, 30 representative points are used in our system.

Then the correlation calculation of RPM with respect to representative point  $(X_r, Y_r)$  is performed as

$$R_i(p, q) = \sum_{r=1}^N |I(t-1, X_r, Y_r) - I(t, X_{r+p}, Y_{r+q})| \quad (3)$$

where  $N$  is the number of representative points in one region,  $I(t-1, X_r, Y_r)$  is the intensity of the representative point  $(X_r, Y_r)$  at frame  $(t-1)$ , and  $R_i(p, q)$  is the correlation measure for a shift  $(p, q)$  between the representative points in region  $i$  at frame  $(t-1)$  and the relative shifting points at frame  $(t)$ . Assuming  $R_{iMin}$  is the minimum correlation value in region  $I$ , the shift vector  $v_i$  that produces the minimum correlation value for region  $i$  represents the LMV of this region.

### 3.3.2 GMV Estimation

The objective of GMV estimation is to determine a motion vector from existing data what we have evaluated from a motion estimation process. In a practical in-car

video sequence, it always suffers from moving objects, repeated patterns, motion effects of cars, etc. The LMV in each region may represent GMV, moving-object motion vector, or even error vector, respectively. The error vector may be caused by the ill condition, repeated pattern, or the mixture of global and moving-object motion. Although the reliable GMV is essentially selected from LMVs, however, in the worst case, when the LMVs are all fault, it will induce a worse result after compensation compared with the original images. Therefore, if the evaluation includes the zero motion vector (ZMV), it can prevent the occurrence of this case. Similarly, for an image sequence with constant motion in the scene, it will induce a worse result if it is compensated by ZMV or the error motion vector rather than by the average motion vector (AMV). In the proposed DIS technique, the seven motion vectors including four LMVs, the ZMV, and the AMV, referred as preselected motion vectors (pre MV), are employed to estimate the GMV of the current frame. In general, one of the LMVs is the highly probable GMV for the regular image; the ZMV can prevent a worse compensation result caused by the unreliable MVs; and the AMV is useful for constant motion of the car. In addition, if the image sequence contains a large moving object, the determination of global motion is troublesome because the determined motion vector probably switches between the background and large moving object or is totally dominated by the large moving object. In this case, it will lead to artificial shaking and cause a major challenge in DIS.

The estimation of the GMV is calculated by the summation of absolute difference (SAD)

$$SAD_{B_i,c} = \sum_{X,Y \in B_i} |I(t-1, X, Y) - I(t, X + X_c, Y + Y_c)|, 1 \leq i \leq 5, 1 \leq c \leq 6 \quad (4)$$

where  $I(t-1, X, Y)$  is the intensity of the point  $(X, Y)$  at frame  $(t-1)$ ,  $B_i$  is the  $i$ th background region in the image,  $X_c, Y_c$  are the components of the six preselect motion

vectors ( $pre\_MV_c$ ) in  $x$  and  $y$  directions.

Different ( $pre\_MV_c$ ) will have their  $SAD_{Bi,c}$  in each region. The smaller  $SAD_{Bi,c}$  represents the higher probability of the desired motion vector among these preselected motion vectors. The score for each ( $pre\_MV_c$ ) in region  $i$  is denoted as  $S_{i,c}$ , which is the order of the  $SAD_{Bi,c}$  value, and the higher  $SAD_{Bi,c}$  indicates the higher score. The total score for each  $pre\_MV_c$  can be obtained by

$$S_c = \sum_{i=1}^5 S_{i,c} \quad (5)$$

Five-region peer-to-peer evaluation can prevent the situation that some partial high-contrast image regions dominate the evaluation result. In this algorithm, each region has an equal priority to determine the result. In (5),  $S_c$  is the index to determine the GMV. The  $pre\_MV_c$  with the smallest  $S_c$  is the desired GMV, and it can be expressed as

$$\begin{aligned} GMV &= pre\_MV_i \\ i &= \arg(\min S_c) \end{aligned} \quad (6)$$

According to these sophisticated evaluation areas, the evaluation function can detect attributed background motion vector precisely in most circumstances.

### 3.4 Motion Compensation and Evaluation

- CMV Estimation

The first step of motion compensation is to generate the CMVs for removing the undesired shaking motion and still keeping the steady motion in the image sequence. The conventional CMV estimation was given by [16], and will yield where  $t$  represents the frame number.

$$\begin{aligned} CMV(t) &= k(CMV(t-1)) + (\alpha GMV(t) + (1-\alpha)GMV(t-1)), \\ 0 < k < 1 \quad \text{and} \quad 0 \leq \alpha \leq 1 \end{aligned} \quad (7)$$

The increase in  $k$  causes the decrease in unwanted shaking effect but the increase in the value of CMV, which means the effective area of images is reduced if we want to maintain the consistent image size for the whole image sequence. To illustrate this phenomenon, the motion trajectories can be calculated to analyze the problem. The motion trajectories can be obtained by

$$MT_{raj_o}(t) = \sum_{i=1}^t GMV(i) \quad (8)$$

$$MT_{raj_c}(t) = \left( \sum_{i=1}^t GMV(i) \right) - CMV(t) \quad (9)$$

where  $MT_{raj_o}(t)$  and  $MT_{raj_c}(t)$  are the original and the compensated motion trajectories of the image sequence at frame( $t$ ). Fig. 10 shows the performance comparison of three different CMV generation methods applied to a video sequence with constant motion and jitter in the image. There are two trajectories in each subfigure; one is the original trajectory calculated by (8), and the other one is the compensated trajectory calculated by (9). The CMVs in Fig. 10(a) are generated by the conventional method shown in (7). Obviously,  $MT_{raj_c}(t)$  has tremendous lag compared to  $MT_{raj_o}(t)$  due to the constant motion effect.

The CMV probably exceeds the window shifting allowance such that the available effective image area during the compensation process is reduced. The CMVs in Fig. 10(b) are generated by (7) a with clipper function as

$$CMV(t) = clipper(CMV(t)) = \frac{1}{2} (|CMV(t) + l| - |CMV(t) - l|) \quad (10)$$

where  $l$  is boundary limitation, i.e., the maximum window shift allowance. In this case, the lag can be reduced to a certain range. However, it will also decrease the performance of shaking compensation due to the picking window operating near the boundary area.

In order to deal with the above problem, Vella *et al.* used the passive method of

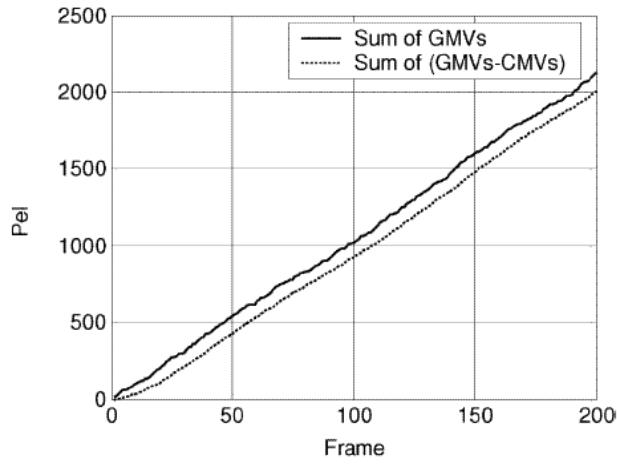
ceasing for correction in this condition [19]. That implied that the undesired shaking effect cannot be eliminated in the constant motion condition. To overcome this drawback, we combine the inner feedback-loop integrator with a clipper function to reduce the steady-state lag for steady motion as well as to keep the CMV to operate in the appropriate range. That means, by employing the integrator, shaking components of the images with constant motion effect as well as those in regular images can be stabilized. It is noted that the CMV computation procedure is applied to  $x$  and  $y$  components separately. That is, parameters corresponding to  $x$  and  $y$  directions can be set as different values. In general, the constant-motion condition usually occurs in horizontal direction such that the shaking patterns are different in both directions. The proposed CMV computation procedure is presented by

$$\begin{aligned}
 CMV(t) &= k \cdot CMV(t-1) + GMV(t) - \beta \cdot CMV\_I(t-1) \\
 CMV\_I(t) &= CMV\_I(t-1) + CMV(t) \\
 CMV(t) &= \text{clipper}(CMV(t))
 \end{aligned} \tag{11}$$

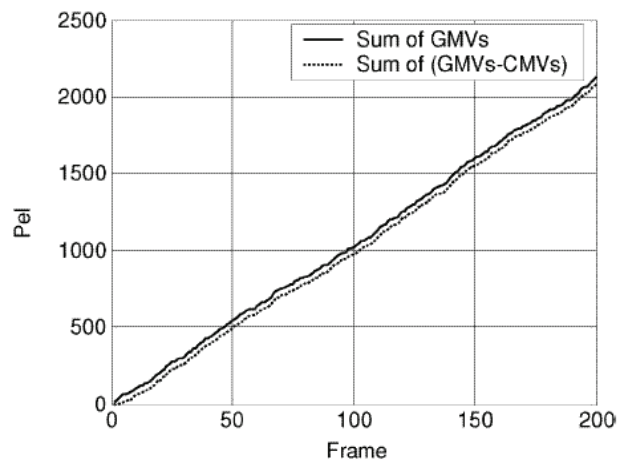
where

$$k \geq \begin{bmatrix} 0 \\ 0 \end{bmatrix} \quad \beta \leq \begin{bmatrix} 1 \\ 1 \end{bmatrix}$$

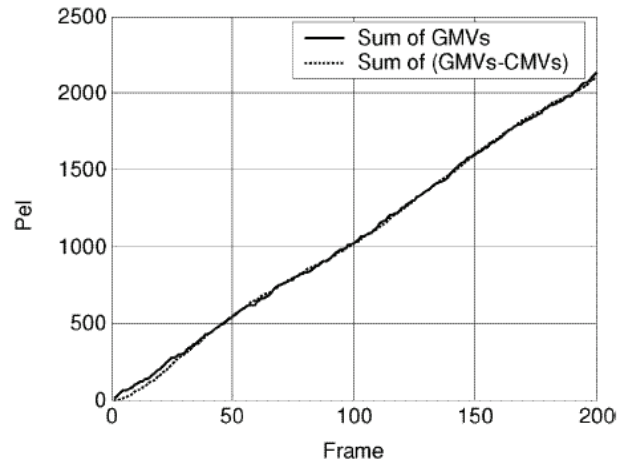
The symbol  $\cdot$  denotes array multiplication, and  $\text{clipper}(\ )$  is defined in (10). Fig. 10(c) shows the compensated motion trajectory generated by the proposed method. Compared with Fig. 10(a) and (b), the proposed method can reduce the steady-state lag of the compensated motion trajectory in the constant-motion condition and keep the CMVs in an appropriate range.



(a)



(b)



(c)

Fig. 10: Performance comparison of three different CMV generation methods applied to a video sequence with panning and hand shaking. (a) CMV generation method in (7). (b) CMV generation method in (7) with clipper in (10). (c) Proposed method in (11).

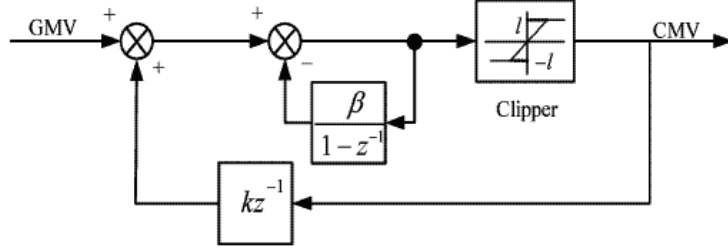


Fig. 11: Block diagram of the proposed CMV generation method.

- Quantitative Evaluation

The shaking effect of images can be evaluated by the summation of absolute differences of momentums within every two consecutive frames. The mass of an image can be set as a constant such as one for simplicity or a value from zero to one according to the degree of shaking in the images measured by human visual perception. The SI is proposed to quantitatively evaluate the performance of different DIS algorithms, and it is defined as

$$SI = \frac{1}{N-1} \sum_{t=2}^N \Delta m(t) \quad (12)$$

$$\frac{1}{N-1} \sum_{t=2}^N m \times |GMV(t) - GMV(t-1)|$$

where  $t$  is the frame number,  $N$  is the number of total frames,  $m$  is the mass of the image, and  $\Delta m(t)$  is the rate of change of the absolute value of momentum. The lower SI means less shaking components in the image sequence, and it represents the effect of better smoothness.

### 3.4 Experimental Results

In this section, the performance of the proposed DIS technique is evaluated and compared to other existing DIS methods based on the performance indices of motion estimation and motion smoothing, respectively. To do this, four real video sequences

captured by an in-car camera with various irregular conditions are used for testing. Each video sequence has resolution of  $640 \times 480$ . The VS#1 is a video of a door gate taken with constant camera motion and jitter. It lacks for features in the horizontal direction. The VS#2 is a video taken of a community road with bumpy conditions. The VS#3 is a video of highway taken with jitter. The VS#4 is a video taken of a parking lot when the car is turning. The motion estimation performance is evaluated based on the root mean square error (RMSE) between the algorithmically estimated motion vectors and the desired motion vectors evaluated by human visual perception as well as considering the background factor frame by frame. The RMSE is given by

$$RMSE = \sqrt{\frac{1}{N} \sum_{n=1}^N [(x_n - x_{dn})^2 + (y_n - y_{dn})^2]} \quad (13)$$

where  $(x_{dn}, y_{dn})$  is the desired motion vector and  $(x_n, y_n)$  is the motion vector generated from the evaluated DIS algorithms.

The proposed method is compared to a RPM approach with fuzzy set theory (RPM FUZZY) [15]. The motion estimation results of these two methods are summarized in Table 4. The proposed method applies the minimum projection approach to detect the irregular components of LMVs. This approach can sufficiently use the existing information to estimate the GMV. The testing result with respect to VS#1 shows that the RMSE reduces from 5.8348 to 2.5269 by using our method since the RPM FUZZY did not consider the condition of lack of feature. The results with respect to VS#2–4 also show that RMSEs of our method are superior to RPM FUZZY.

The motion smoothing performance is evaluated by the SI proposed in Section 3.4. Fig. 10(c) shows the original motion trajectory versus the compensated motion trajectory generated by the proposed method. Compared with Fig. 10 (a) and (b), the proposed method can reduce the steady-state lag of the compensated motion trajectory



in constant motion condition and keep the CMVs in an appropriate range.

Table 4: RMSE Comparisons of RPM Fuzzy and the Proposed Method with Respect to Four Real Video Sequences

Method	Real video sequences			
	VS#1	VS#2	VS#3	VS#4
RPMFUZZY	5.8348	0.8031	2.6618	2.2749
The proposed method	2.5269	0.3536	1.6837	0.5701

Table 5: Comparisons of Three CMV Generation Methods

Methods	SI	Max. CMV value (pels)
Eq. (7)	0.7990	134
Eq. (7) with clipper	5.6482	47
The proposed CMV generation method (Eq. (11))	0.9346	47
Note: The original SI is 7.4372. The clipper is bounded within $\pm 47$ pels.		

Table 6: Parameters Applied to CMV Generation with Different Equations

Method (Equation)	Parameters		
	k	P	Clipper Limit
18	$\begin{bmatrix} 0.95 \\ 0.95 \end{bmatrix}$	$\begin{bmatrix} 0 \\ 0 \end{bmatrix}$	$\pm 47$ pels (vertical) $\pm 53$ pels (horizontal)
22	$\begin{bmatrix} 0.95 \\ 0.95 \end{bmatrix}$	$\begin{bmatrix} 0.001 \\ 0.01 \end{bmatrix}$	

Table 5 shows the SI comparisons of three CMV generation methods presented in Fig. 10. The generation of CMV without clipper is impractical since it lost too much effective image area, i.e., the maximum of the CMVs does not guarantee to fit the practical compensation range. The proposed CMV generation method dramatically reduces the SI value from 5.6482 to 0.9346 compared with the CMV generation

without integrator. The reason is that the effect of the inner feedback-loop integrator greatly reduces the steady-state lag in the image sequence with constant motion. We also evaluate the CMV generation methods by four GMV sets generated from real video sequences (GMV sets #1–4).

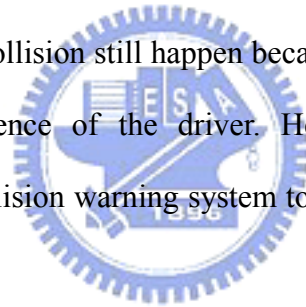
### 3.5 Summary

How to derive reliable GMVs from the video sequence captured by in-car video cameras and how to derive appropriate CMVs to smoothen the shaking effect without reducing the effective image area are two challenges for an in-car DIS system. This chapter focuses on the analysis and design of motion compensation algorithm for the real-time DIS system. It is a challenge to generate proper compensated motion vectors (CMVs) which smooth the shaking effect without reducing the effective compensated area. Hence, we take the motion compensation as a control problem and propose a modified PI controller which can both remove the unwanted jitter and preserve the deliberate, panning motion of camera. According to the experimental results, the proposed technique demonstrates the remarkable performance in both quantitative and qualitative (human vision) evaluations compared to the existing approaches. It can be implemented as software and hardware solutions for both online and offline video stabilization applications.

# Chapter 4 Lateral Collision Warning System

## 4.1 Introduction

Car electronics researches are getting more popular, drivers are not only consider comfortable car interior environment but also respect safety equipment. In our country, there are at least 80,000 traffic accidents in a year and more than 2,500 people lose their life. Most reasons are due to the driver is inattentive or neglect the driving circumstances. On the highway, the most important cause of the traffic accidents is lateral and same direction collision. Obviously, the traffic accident occurs when the driver changes the lane. Although the driver can get the information around the car by rear-view mirror, the lateral collision still happen because of the existence of the blind spot region and the negligence of the driver. Hence, we develop a real-time auto-detect vehicle lateral collision warning system to assist the driver to change lane more safely.



### 4.1.1 Definition of Vehicle Blind Spot

Blind spots, in the context of driving an automobile, are the areas of the road that cannot be seen while looking forward or through either the rear-view or side mirrors. The detection of vehicles or other objects in blind spots may also be aided by systems such as video cameras or distance sensors. Throughout the notation in this thesis, the area of blind spot is only regarded as the rear of the vehicle on both sides. The introduction in this section not only describes the causes of traffic accidents resulted from the blind spot, but discuss how to reasonably establish the region of blind spot by the inherent limitation of the human vision and rear-view mirror.

In Taiwan, the types of traffic accidents between two cars on highway are listed

in Table 7 from [34].

Table 7: Causes of traffic accidents between two cars on highway.

Year	Collision by the Backward Car	Rubbed Collision in the Same Direction	Lateral Collision	Colliding Collision	Others
2001	59.74%	28.57%	2.86%	1.56%	7.27%
2002	62.39%	28.04%	3.04%	1.74%	4.78%
2003	60.82%	27.88%	3.70%	2.34%	5.26%

As shown in foregoing statistics, we can conclude that the lateral and rubbed collisions are both the principal causes of the traffic accidents between the cars. There have been numerous topics focused on how to avoid the forward or backward collision for the vehicle, but the related research for lateral collision is little. While vehicles in the adjacent lanes of the road fall into the range of lateral blind spots, the driver will be unable to see them with only the car's mirrors. Due to the above reason, drivers must actively rotate their head to extract more information within the region of blind spot. However, the probability of car accident can be raised simultaneously. Therefore, vision-based system can be developed to assist the drivers in keeping away from the lateral danger of vehicles by the image sensor alongside the rear-view mirror.

The eyesight of people has obvious difference between the static and dynamic environment due to the variation of the vehicle velocity. In general, the view-angle of the single eyeshot is about 160 degrees when people lie in the stationary scene; the maximum view-angle of the double field of view is enlarged about 180 degrees. Flanagan [35] proposed that the people's double eyesight should reach to 320 degrees by adding the rotating motion for the head and body of human. According to the statistics from [36], the realistically clear field of view contained two eyes is only

about 70 degrees when a normal person situates in the static environment. Nevertheless, the human's eyesight could frequently vary when people are in the dynamic conditions such as the internal part of the moving vehicle thanks to the tunnel-vision effect. The relationship between the range of human eyesight and the variation of the vehicle velocity is in Table 8; the range of field of view between the static or dynamic environment is shown in Fig. 12.

Table 8: The relationship between the field of view and the vehicle velocity.

Speed (km/hr)	40	70	100
Field of View (degrees)	100°	65°	40°

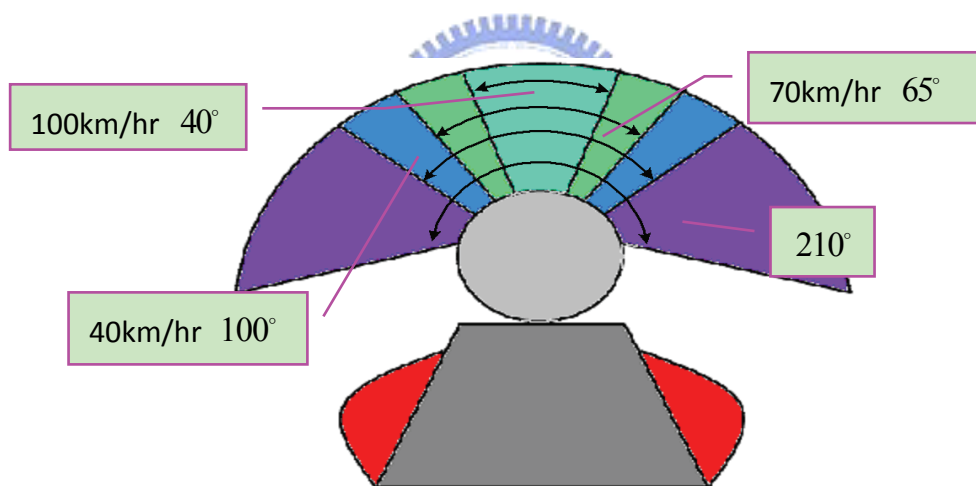


Fig. 12: The diagram of the driver's field of view.

As the information shown in Fig. 12, the eyesight becomes greatly narrow when the vehicle is driven at high speed. In other words, the driver can not judge whether there are other vehicles moving on the adjacent road surface or not only by his/her remaining eyeshot on highway as the car velocity raises to 100 km/hr. In this way, the drivers induced by the blind-spot hazard will be easily in danger.

In general, the side mirrors of the vehicle are almost used by the planar type.

Therefore, the formation of image about the normal rearview mirror is still followed by the principle which describes that the angle of incidence ( $\theta_i$ ) is the same as that of reflection ( $\theta_r$ ). In other words, the field of image produced by the rearview mirror is stretched to  $2\theta$  ( $\theta=\theta_i=\theta_r$ ) view-angle projecting into the road surface.

The relationship between the field of view of the side mirror and that of the driver is shown in Fig. 13.

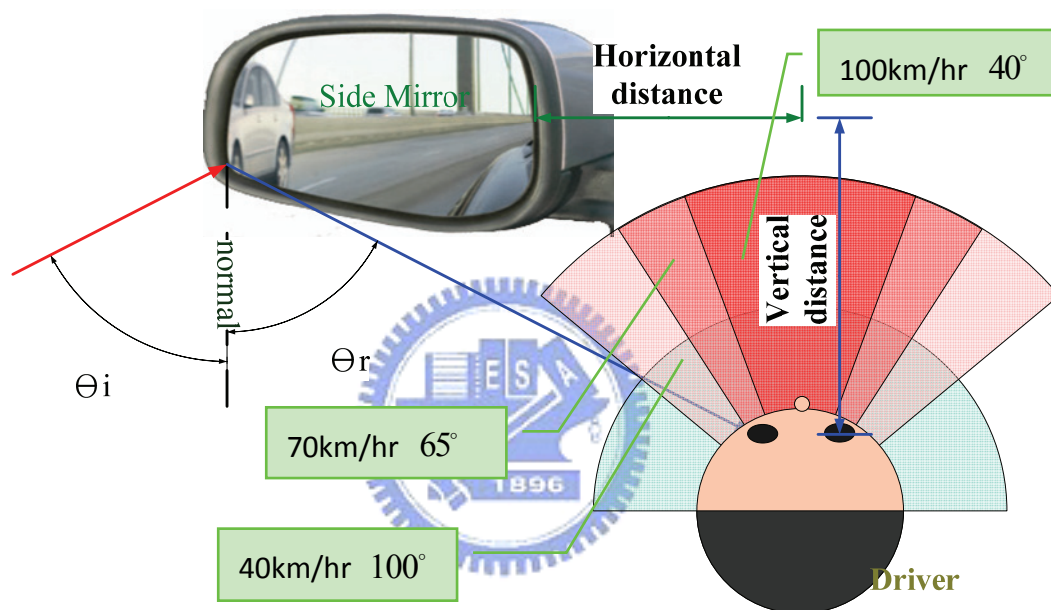


Fig. 13: The relation about field of view between the side mirror and the driver.

By the geometric relation from Fig. 13, when driving at high speed, in order to make the eyesight overlap the reflected field of the rearview mirror, the driver must rotate his/her head so as to extract the lateral information as much as possible. However, due to this unnatural motion, the driver's inattention will not keep his/her eye for the forward state of the vehicle for a long time with the occurrence of traffic accident.

There are two general approaches to extend the range of field of the rearview mirror. The first approach is to increase the distance between the side mirror and the

driver. Due to the fixed car-body, this improving effect will be restricted. The second approach is to replace the traditional planar mirror with the curved one. Nevertheless, the distortion effect of the reflected image will be serious due to the curvature of the lens. Through the above discussion, the blind-spot region between the side mirror and the driver cannot be easily resolved. For this reason, adding the camera on the side of the car with intelligent vision-based algorithm will still be regarded as the important device of the assistant system for the driver's safety.

#### **4.1.2 Previous Work**

The topics of car safety are respected during recent years and there are many studies on developing Blind Spot Information System (BLIS). But it still has some challenges need to research. For example, the accuracy of detection algorithm should be more precise and should decrease the false alarm. And the system should adapt to all kinds of the weather situation either daytime or nighttime. It can be divided into two kinds of methods to detect the objects in the blind spot area.

#### **Radar, Radio Frequency or other wireless reaction**

When object comes in the ROI, the system sends a wireless signal and gets the distance information between self and the object by the difference in time between send signal and received signal. But this method can't recognize the size, length and contour of the object. The system will be effected more easily by other not vehicle object, therefore the false alarm of this system is more than other algorithm. For this reason, some researches adopt the method including radar and vision in [37]-[39].

#### **Vision-based analysis**

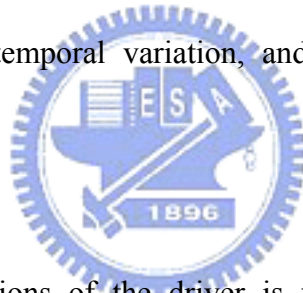
When object comes in the ROI, the system captures the images. By the way of

image processing and analysis, the system can detect the object position. There are three kinds of methods to detect the vehicle in [40].

(1) Using the single image to analysis and detect vehicle. In this method, we can establish object mode by the single image and effective decrease the computation. But it is easy to lose the depth of the environment and is also affected by the contour of the car in [41] and [42].

(2) Using optical flow method to detect vehicle. In this method, we can get the movement relation between self and object. But the operation of this method is more complex, and it's easy to false alarm when both are at low speed in [43] and [44].

(3) Using the image sequence to detect vehicle. In this method, we can rebuild the 3D position and detect vehicle with the geometric figure. Besides image processing, this method also considers temporal variation, and the computation is less than method (2) in [45].



### **Blind Spot Region Setting**

Although blind spot regions of the driver is fixed region, it still is a very important cause of the BLIS research. Lane-based Transform is a method to project the region on the vertical view, and distinguish the vehicle and shadow by the moving contour in [46]-[58]. It is an effective method to improve the BLIS result by setting the suitable blind spot region. Therefore, we will design a 3D ROI in next paragraph to improve the BLIS result precise and reduce the image process computation.

#### **4.1.3 Lateral Collision Warning System Structure**

Our system is based on the method (3).

Fig. 14 is the system structure. The system contains five parts. The first part is ROI definition. We define the driver's blind spot area and design a suitable 3D ROI.



The second part is image preprocessing. According to the first stage, we can get the information about the time of the day. Therefore, we can divide into two kinds of image preprocessing for each detection feature. The third part is vehicle detection. We design daytime and nighttime detection algorithm and export the result to the next stage. The fourth part confirms vehicle. We use the temporal static method to compute the result of the third stage. The last part is the DSP output. We will present each part in the next paragraph.

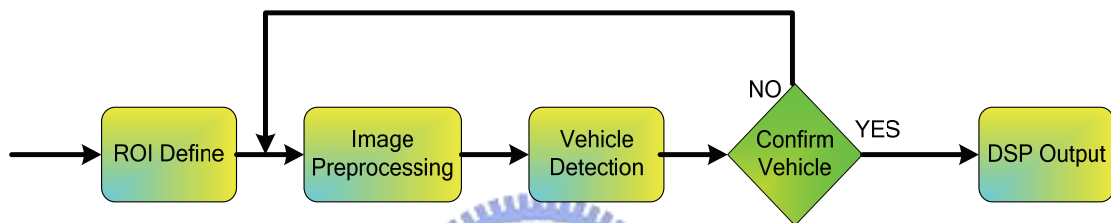


Fig. 14: BLIS side collision warning system structure

## 4.2 ROI Definition and Image Processing

Fig. 15 is the ROI definition flow chart. When we receive an image from the camera, we will convert the YUV image into gray level Y image. In order to realize on the DSP image development kit, we do down-sample and keep the pixel value inside the ROI.

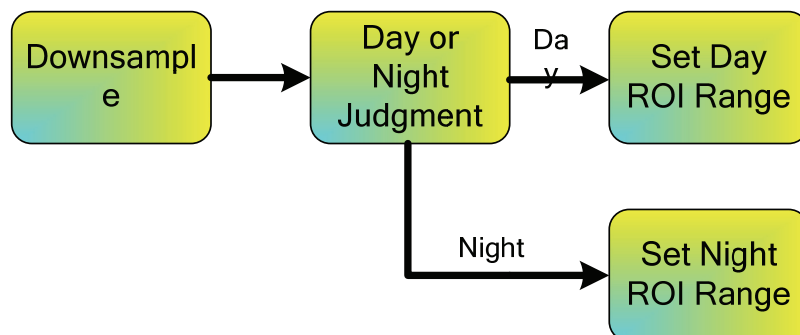


Fig. 15: ROI definition flow chart

We calculate the gray level distribution of each frame  $I(x, y, t)$ . First of all, we assume  $g_{dis}^{ROI}(t)$  is the summation of the dark pixels and  $g_{th}^{ROI}(t)$  is the threshold to separate the daytime from the nighttime. If  $g_{dis}^{ROI}(t)$  is less than  $g_{th}^{ROI}(t)$ , it means the frame maybe captured in the nighttime. Then we consider the result of continuous frames during a space  $t_1$ , we will judge the frame is in the daytime or in the nighttime and is shown in equation (14).

$$J(t) = \begin{cases} 1, & g_{dis}^{ROI}(t) \leq g_{th}^{ROI}(t) \\ 0, & g_{dis}^{ROI}(t) > g_{th}^{ROI}(t) \end{cases}$$

$$J_{result}(t) = \sum_{t_0}^{t_0+t_1} J(t)$$

$$\begin{cases} \text{Daytime}, & J_{result}(t) \geq J_{th} \\ \text{Nighttime}, & J_{result}(t) < J_{th} \end{cases} \quad (14)$$

#### 4.2.1 ROI definition

Fig. 16 is an image about the field of the driver's view. In general, the driver can see around 180° with both eyes and maybe see around 320° with rolling head. The remainder is the red region denoted blind spot region, and it will be larger when the speed of car is faster. In Table 9, we show the relation between the speed and the field of view, it is caused by the tunnel effect.

According to the Fig. 16, we know where the blind spot region is, and we can easily define a simple ROI with a common camera to cover the whole region. Hence we can get an image such as Fig. 17 captured by the common camera with traditional ROI. As the result, it is hard to differentiate cars between near and far lane because the angle of the camera lens is so quite small that makes the projection of the objects either in outside lane or in ROI on the same position in image. Hence this result will

confuse us and be difficult to make out moving vehicle.

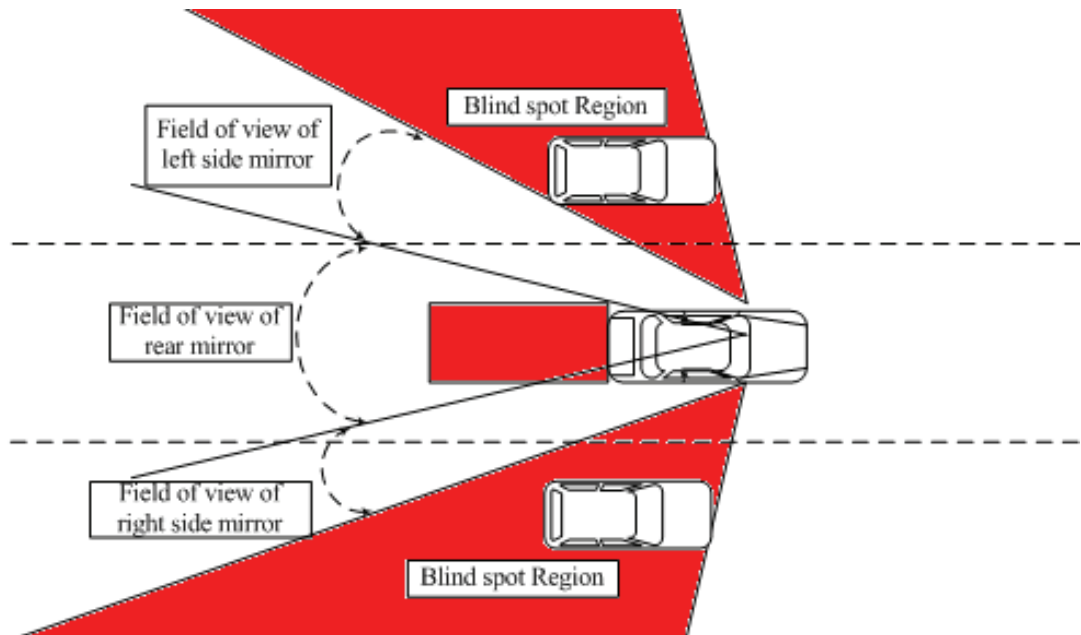


Fig. 16: Field of driver's view

Table 9: The relation between speed and field of view

Speed(km/hr)	40 km/hr	70 km/hr	100 km/hr
Field of view(degree)	100°	65°	40°

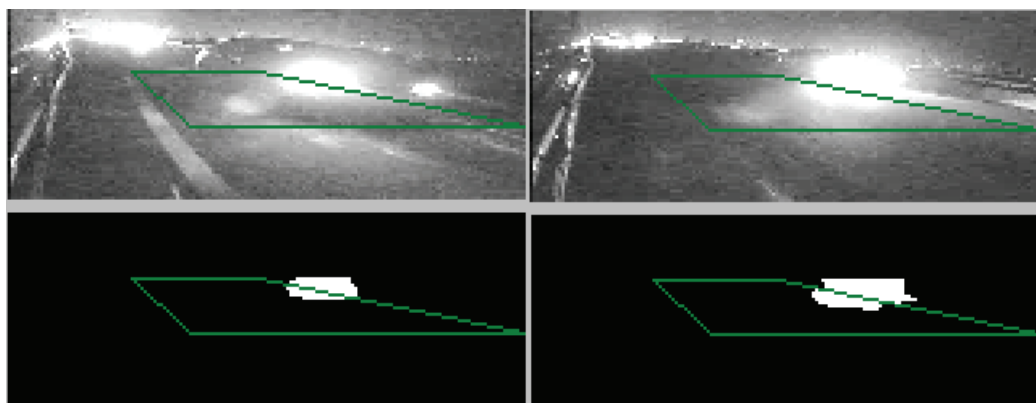


Fig. 17: Image captured by common camera

In order to deal with the upper problems, we choose the fish-eye camera to be our image input. In Fig. 18, the right image is a car approaching in the outside lane and

the left image is a car approaching in the near lane. Both head light are distorted by the fish-eye camera lens. Compare Fig. 17 and Fig. 18, when the car is in the outside lane, the image will become smaller because of the distortion turns in the direction of right. Oppositely, when the car is in the near lane, the image will become far away from the left lane because of the distortion turns in the direction of left. Hence, we can more easily compute the information from the fish-eye image to recognize the moving object inside the driver's blind spot region.

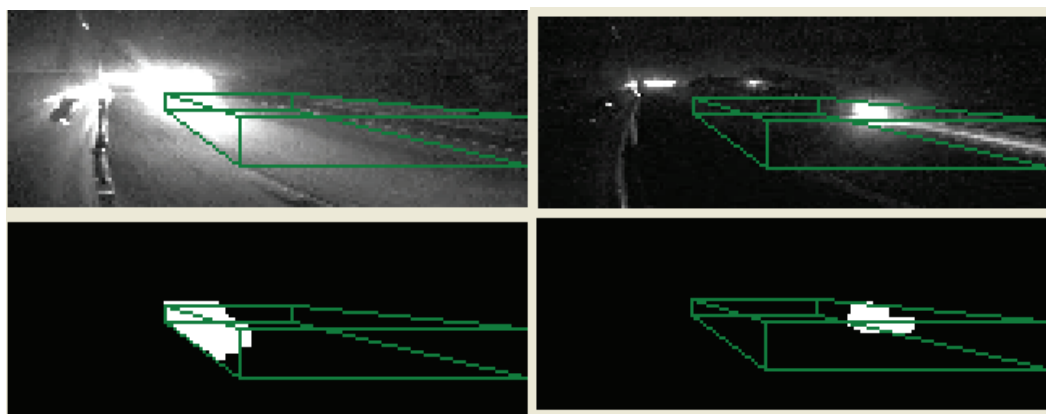


Fig. 18: Image captured by fish-eye camera

In order to exploit the information from the fish-eye image, we design a suitable 3D ROI. It is aimed at finding out the relation between moving objects and self car. First, we set up the position and angle of fish-eye camera to contain the driver's blind spot region and face it to the road surface. Second, we define the 3D ROI is a rectangular solid and we segment it into three parts. Third, we figure out the moving object distribution in the each part and eliminate the image without cars in the ROI.

Our 3D ROI design helps us to raise accuracy of detecting vehicle and decrease non-car false alarm. In this stage, 3D ROI definition only retain the image which may contain moving vehicle inside the blind spot area to get into next stage. For this reason, we effectively reduce computation and make system keep 30fps real-time

operation.

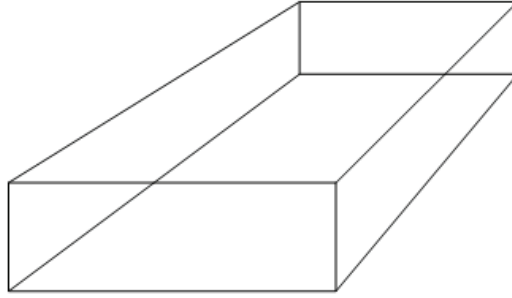


Fig. 19: 3D ROI definition

#### 4.2.2 Image Preprocessing

Image pre-processing is aimed at acquiring the feature of the vehicle in the daytime and nighttime. From Fig. 20 we can sort two categories daytime and nighttime.

In the daytime, the feature is the contour of the vehicle. First, we assume that the input image is  $I_{pre}^{Day}[n]$  and use the edge detection to obtain the edge part  $I_{pre-sobel}^{Day}[n]$  and the method of edge detection will be discussed in section 4.2.3. Second, we get moving objects by the difference frame  $I_{pre-diff}^{Day}[n]$  from  $I_{pre}^{Day}[n-1]$  and  $I_{pre}^{Day}[n]$ , then we use a low-pass filter and a high-pass filter to remove the slight variation part and enhance the strong variation part. Finally, we compare edge image

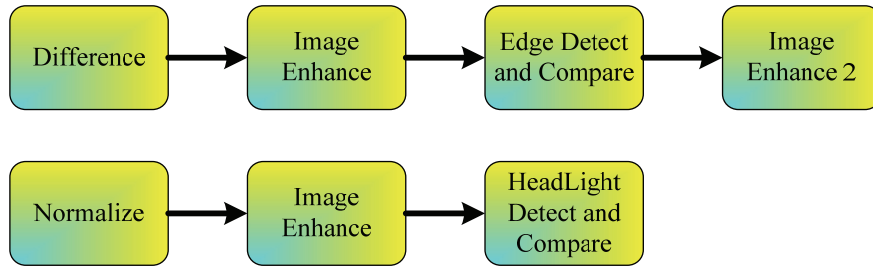


Fig. 20: Image preprocessing flow chart

$I_{pre}^{Day}[n]$  with difference image  $I_{pre-diff}^{Day}[n]$  to segment the image of objects. In order to ensure the integrity of the object image, we do twice dilation of the image. Therefore we can get an intact objects image  $I_{pre-char}^{Day}[n]$ .

In the nighttime, the feature is the head light. First, we assume that the input image is  $I_{pre}^{Night} [n]$  and normalize whole gray value to obtain an image  $I_{pre-normal}^{Night} [n]$ . This step can reduce the effect from other illuminant, such as streetlamp, light reflection and other's head lamp etc. Second, we estimate the gray level in  $I_{pre-normal}^{Night} [n]$  and get a threshold value  $g_{th}^{Night}$  and use the value to filter the high illumination object and its equation is shown in (14). Among equation (14),  $g_{avg}^{Night}$  is the average of the whole image and  $w_{th}^{Night}$  is an adaptive weight which is between 0~1. Obviously, when in the brighter environment, the value of  $g_{avg}^{Night}$  is larger and the addition is smaller. It makes the  $g_{th}^{Night}$  more effortlessly to segment the head lamp  $I_{pre-bright}^{Night} [n]$ . Third, we separately do erosion and dilation with the image  $I_{pre-bright}^{Night} [n]$  because the brighter head lamp has scattering situation and the darker or farther head lamp will be neglected more easily. Finally, we obtain the image  $I_{pre-char}^{Night} [n]$  containing head lamp by comparing the erosion and dilation image.

$$g_{th}^{Night} = g_{avg}^{Night} + (255 - g_{avg}^{Night}) * w_{th}^{Night} \quad (15)$$

### 4.2.3 HVS-Directed Object Edge Detection

Much research has been done over the years on discovering the characteristics of the human visual system (HVS). It was found that the perception of HVS is more sensitive to luminance contrast rather than uniform brightness. The ability of human eyes to tell the magnitude difference between an object and its background depends on the average value of background luminance. According to Fig. 22, we find that the visibility threshold is lower when the background luminance is within the interval 70 to 150, and the visibility threshold will increase if the background luminance becomes darker or brighter away from this interval. In addition, high visibility threshold will occur when the background luminance is in a very dark region.

In addition to the magnitude difference between an object and the background, different structures of images also cause different visual perceptions for HVS. Human eyes are more sensitive to high contrast regions such as texture or edge regions than the smooth regions. A novel fuzzy decision system inspired by HVS is proposed to classify the input image into human perception non-sensitive regions and sensitive regions.

In the proposed fuzzy decision system, there are three input variables, visibility degree (VD), structural degree (SD), complexity degree (CD), and one output variable (Mo). In order to obtain the input variables corresponding to each sliding block shown in Fig. 21, two index parameters called background luminance (BL) and difference (D) are defined and should be calculated first. Parameter BL is the average luminance of the sliding block and can be calculated by

$$BL = \frac{1}{23} \sum_{i=0}^3 \sum_{j=0}^3 O(i, j) \times B(i, j) \quad (16)$$

where

$$B(i, j) = \begin{bmatrix} 2 & 2 & 2 & 1 \\ 2 & 0 & 2 & 1 \\ 2 & 2 & 2 & 1 \\ 1 & 1 & 1 & 1 \end{bmatrix} \quad (17)$$

Parameter D is the difference between the maximum pixel value and the minimum pixel value in the sliding block and can be calculated by

$$D = \max(O(i, j)) - \min(O(i, j)) \quad (18)$$

A nonlinear function  $V(BL)$  is also designed to approximate the relation between the visibility threshold and background luminance. It is the approximation of Fig. 22 obtained by using the nonlinearly recursive approach and can be represented as

$$V(BL) = 20.66e^{-0.03BL} + e^{0.008BL} \quad (19)$$

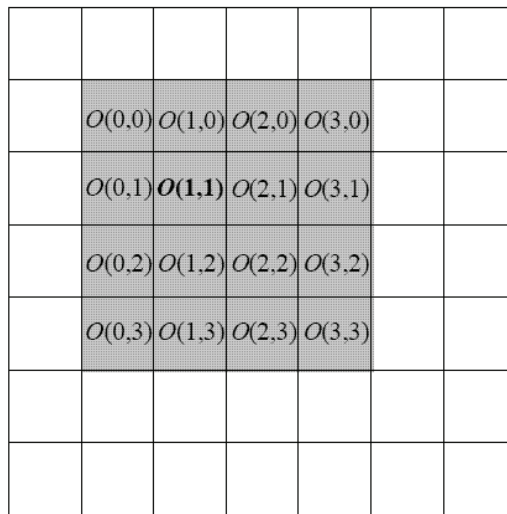


Fig. 21: A 4 x 4 sliding block in the original image

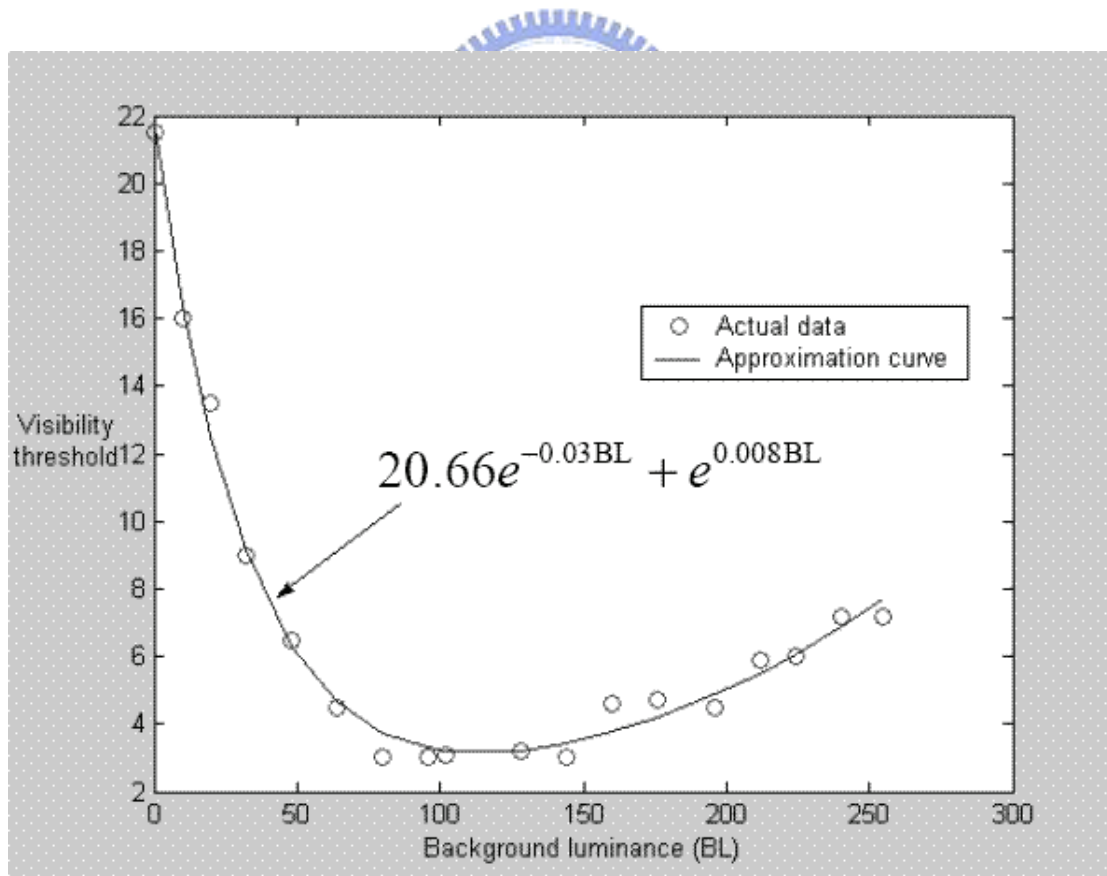


Fig. 22: Visibility thresholds corresponding to different back- ground luminance.

After BL, D and V(BL) are obtained, we can calculate the input variables (VD,



SD, and CD) of the fuzzy decision system. Parameter VD is defined as the difference between D and V(BL) and can be represented as

$$VD = D - V(BL) \quad (20)$$

In Eq. (20), ‘D’ value defined in Eq. (18) is used to approximate the magnitude difference between the object and its background. Therefore, if  $VD > 0$ , it means the magnitude difference between the object and its background exceeds the visibility threshold and the object is sensible. Otherwise, this object is not sensible. SD and CD are used to indicate whether the pixels in the sliding block perform edge structure. SD shows if the sliding block is a high contrast region and the pixels in the block can be obviously separated into two clusters. It is calculated by (21), as shown at the bottom of the page, where

$$SD = \frac{|(\max(O(i, j)) - \text{mean}(O(i, j))) - (\text{mean}(O(i, j)) - \min(O(i, j)))|}{\max(O(i, j)) - \min(O(i, j))} \quad (21)$$

$$CD = \sum_{i=0}^3 \sum_{j=0}^3 |O'(i, j) - [O'(i+1, j) + O'(i-1, j) + O'(i, j+1) + O'(i, j-1)]| \quad (22)$$

$$\text{mean}(O(i, j)) = \frac{1}{16} \sum_{i=0}^3 \sum_{j=0}^3 O(i, j) \quad (23)$$

An illustration of Eq. (21) is shown in Fig. 23. According to Fig. 23, Eq. (21) can be expressed as  $|\sigma_1 - \sigma_2| / (\sigma_1 + \sigma_2)$ . So the SD has been normalized to [0, 1] and this rule can also be applied to images with a different intensity range. If SD is small (close to 0), and  $\sigma_2$  and  $\sigma_1$  are close (see Fig. 23(a)), it means the pixels in the block can be separated into two even clusters. The block may contain edge or texture structure. On the contrary, if SD is a large value,  $|\sigma_1 - \sigma_2| \gg 0$  (Fig. 4(b)), it means the pixel number of one cluster and that of the other cluster are not even, thus, the block may contain noise or thin line edge.

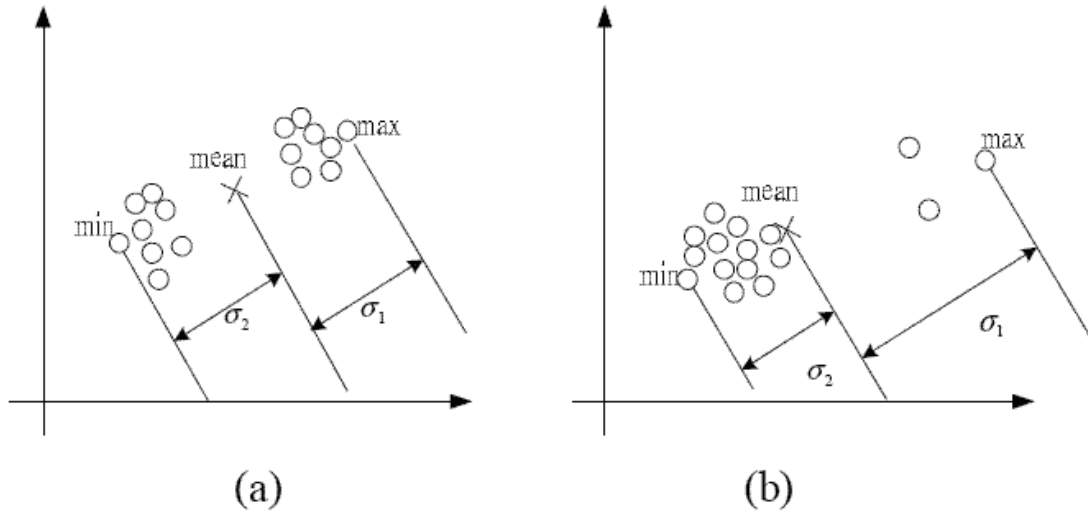


Fig. 23: An illustration of the relation between SD parameter and the distribution of pixels in a sliding block.

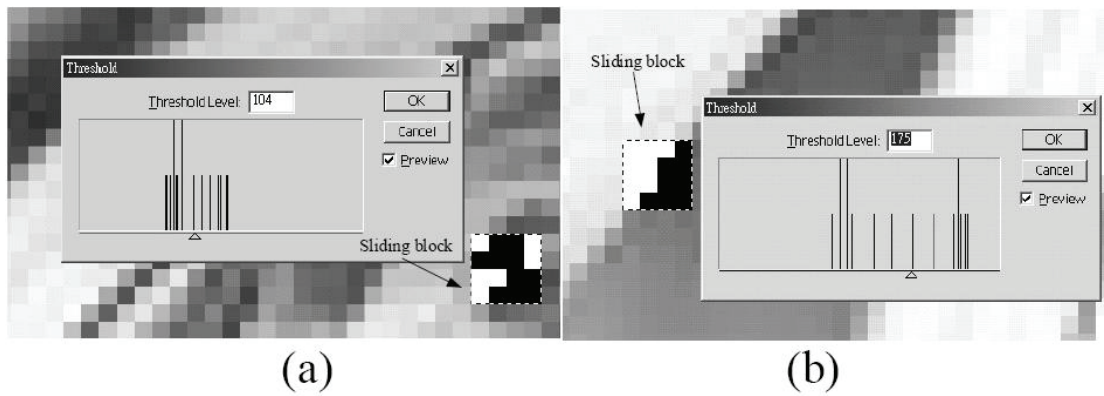


Fig. 24: Portions of (a) the sliding block including texture structure, (b) the sliding block including edge structure.

Fig. 24(a) and (b) show a texture structure and a delineated edge structure in a sliding block, respectively. In these two plots, pixel numbers of the two clusters are the same. Therefore, the SD values corresponding to these two structures are close. CD input variable based on the local gradient process is proposed to tell the delineated edge structure from texture structure. It is calculated by (22), where  $\theta(i,j)$  is the binary version of  $0(7,7)$  to eliminate the influence of image intensity. In Eq. (22), each pixel in the  $4 \times 4$  sliding block takes the 4-directional local gradient operation and the CD is the summation of the 16 local gradient values. If the CD is a large value, it means the

block may contain texture structure. On the contrary, if the CD is a small value, the block may contain delineated edge structure.

The input variable VD has two fuzzy sets, N (negative) and P (positive). The input variable SD has three fuzzy sets S (small), M (medium), and B (Big). The input variable CD has three fuzzy sets, S (small), M (medium), and B (Big). The membership functions corresponding to the VD, SD, and CD are shown in Fig. 25(a)-(c), respectively. In order to determine the fuzzy membership functions, seven nature images were used to generate the model. The images were separated into smooth, texture and edge regions by the admission of the majority (seven of ten subjects). Then the ranges of VD, SD and CD proposed in Eqs. (20), (21) and (22) corresponding to these regions were evaluated. Finally, the membership functions of the VD, SD and CD could be designed according to the distribution ranges of the parameters in four regions, respectively. The membership functions corresponding to Mo are shown in Fig. 25(d). Originally there are thirty-six fuzzy rules in the proposed fuzzy system ( $2 \times 3 \times 3 \times 2 = 36$  rules). These fuzzy rules can be combined and reduced in accordance with the following three rules:

1. The fuzzy decision rules have exactly the same consequence.
2. Some preconditions are common to all the rule nodes in this set.
3. The union of other preconditions of these rules nodes composes the whole term set of some input linguistic variables.

Therefore, we can combine these thirty-six fuzzy decision rules into seven rules as follows:

1. If VD is N then Mo is BL
2. If SD is B then Mo is BL
3. If CD is B then Mo is BL

4. If VD is P and SD is S and CD is S then Mo is NN
5. If VD is P and SD is S and CD is M then Mo is BL
6. If VD is P and SD is M and CD is S then Mo is NN
7. If VD is P and SD is M and CD is M then Mo is BL.

The numerical value of Mo after defuzzification by center of area (COA) is compared with a threshold value, Th, where Th is preferably set as the value 5 by experiments. The COA strategy generates the center of gravity of the possibility distribution for the decision action. In the case of discrete universe, assuming n is the number of quantization levels of the output,  $z_h$  is the amount of system output at the quantization level  $h$ , and  $\mu_{MO}(z_h)$  represents its membership value in the output fuzzy set, MO can be calculated by

$$MO_{COA} = \frac{\sum_{h=1}^p \mu_{MO}(z_h) z_h}{\sum_{h=1}^p \mu_{MO}(z_h)} \quad (24)$$

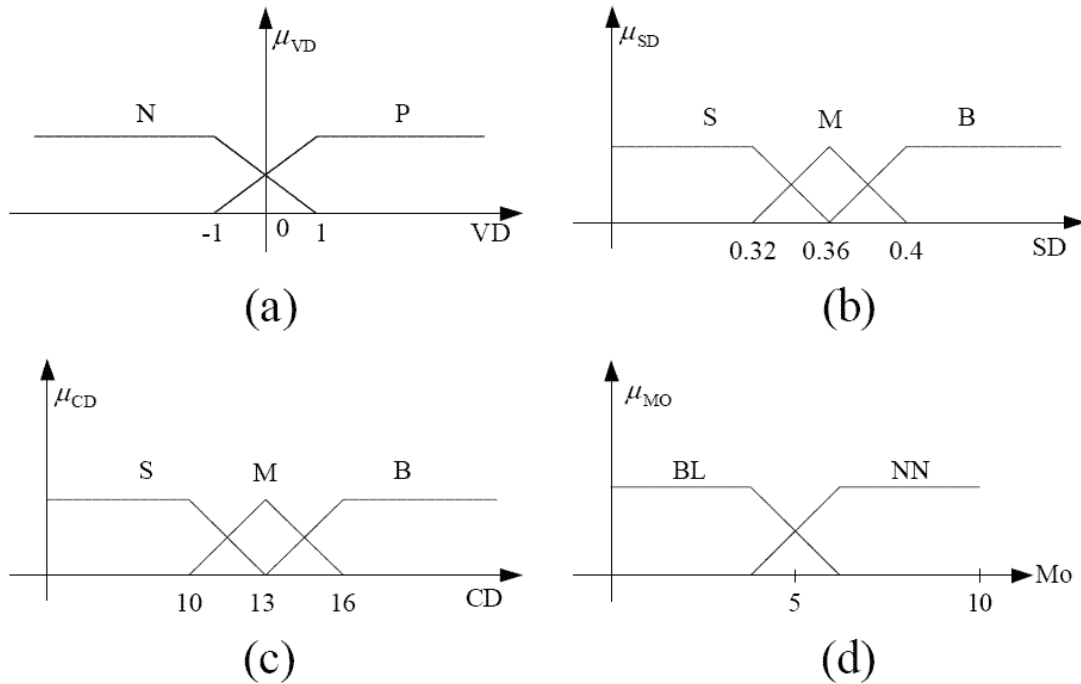


Fig. 25: (a)-(d) Membership functions of fuzzy sets on input variables VD, SD, CD, and output variable Mo, respectively.

#### 4.2.4 Angle Evaluation

When  $MO > Th$ , the angle evaluation is performed to determine the dominant orientation of the sliding block. The flow diagram of angle evaluation is shown in Fig. 26. When angle evaluation is operating, the orientation angle of each neighborhood original image pixel is computed. According to Fig. 21 when the orientation angle of  $\theta(i, j)$  denoted as  $A(i, j)$  is computed, the luminance values of the original pixels nearby  $\theta(i, j)$  are used for the following computations:

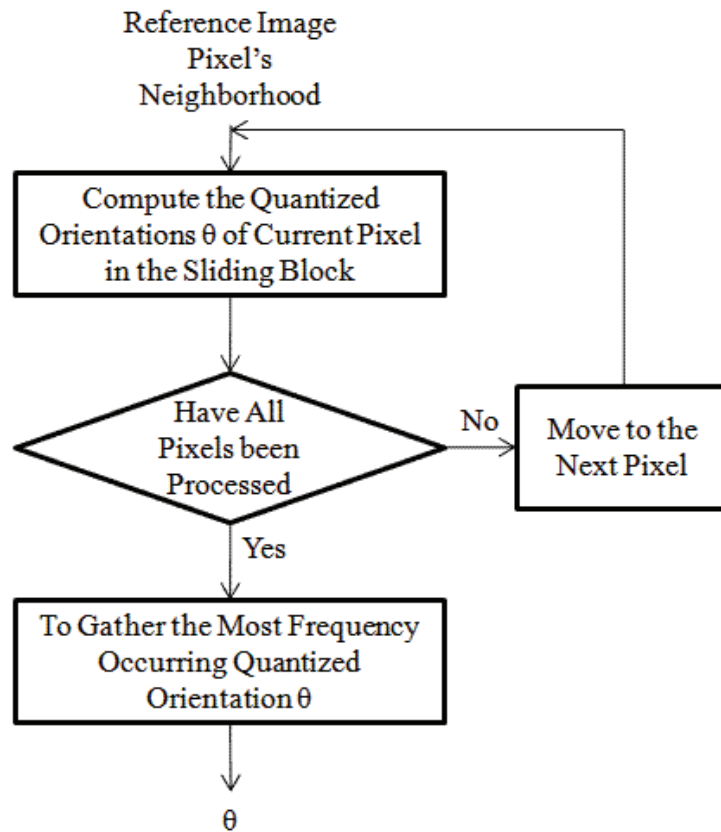


Fig. 26: Flow diagram of the angle evaluation.

$$D_x(i, j) = O(i-1, j-1) + 2O(i-1, j) + O(i-1, j+1) - (O(i+1, j-1) + 2O(i+1, j) + O(i+1, j+1)) \quad (25)$$

$$D_y(i, j) = O(i-1, j-1) + 2O(i, j-1) + O(i+1, j-1) - (O(i-1, j+1) + 2O(i, j+1) + O(i+1, j+1)) \quad (26)$$

$$A(i, j) = -\frac{180}{\pi} \left[ \tan^{-1} \left( \frac{Dy(i, j)}{Dx(i, j)} \right) \right] \quad (27)$$

where  $0 \leq i \leq 3$  and  $0 \leq j \leq 3$ .

The obtained orientation angle of each pixel in the sliding block (as shown in Fig. 21) is quantized into eight quantization sectors such as  $\theta = 22.5 * k$  degrees, where  $k = 0, 1, \dots, 7$ .  $\theta$  is the quantized angle for most pixels oriented in the sliding block, and regarded as the dominant orientation of the reference image pixel.

Fig. 27 shows four different image structures extracted from “home” to illustrate the operations of the proposed fuzzy decision system. Fig. 27 (a), (b), (c), and (d) represent smooth, texture, edge and noise regions, respectively. The VD, SD, and CD values of these regions calculated by Eqs. (20)-(22) are shown in Table 10.

According to the VD values in Table 10, only the Fig. 27 (a) (smooth region) is negative which activates fuzzy rule 1 and follows the assumption that “if  $VD > 0$ , it contains visible objects.” The SD value of Fig. 27 (d) (noise) is large (B) which activates fuzzy rule 2 and follows the assumption that “If SD is a large value, the block may contain noise.” The SD values of Fig. 27 (b) (texture region) and Fig. 27 (c) (edge region) are small (S) which follows our assumption that “if SD is small, the block may contain edge or texture structure. The CD value of Fig. 27 (b) is medium (M) which activates fuzzy rules 5 and it follows the assumption that “If CD is a large value, the block may contain texture structure.” And the CD value of Fig. 27 (c) is small (S) which activates fuzzy rule 4 and follows the assumption that “If CD is a small value, the block may contain edge structure.”

After defuzzification, their MO values are 2.2, 3.4, 7.3 and 2.2, respectively. Since the threshold value is 5, only the edge region shown in Fig. 27 (c). The threshold value can be adjusted to meet the speed and quality requirements of

different applications.

Table 10: Processing results of the proposed FUZZY decision system corresponding to four different structures shown in Fig. 14

	Smooth region	Texture region	Edge region	Noise
VD	-1.42	47	182	111.78
SD	0.42	0.11	0.24	0.6
CD	12	12	10	11
Mo	2.2	3.4	7.3	2.2

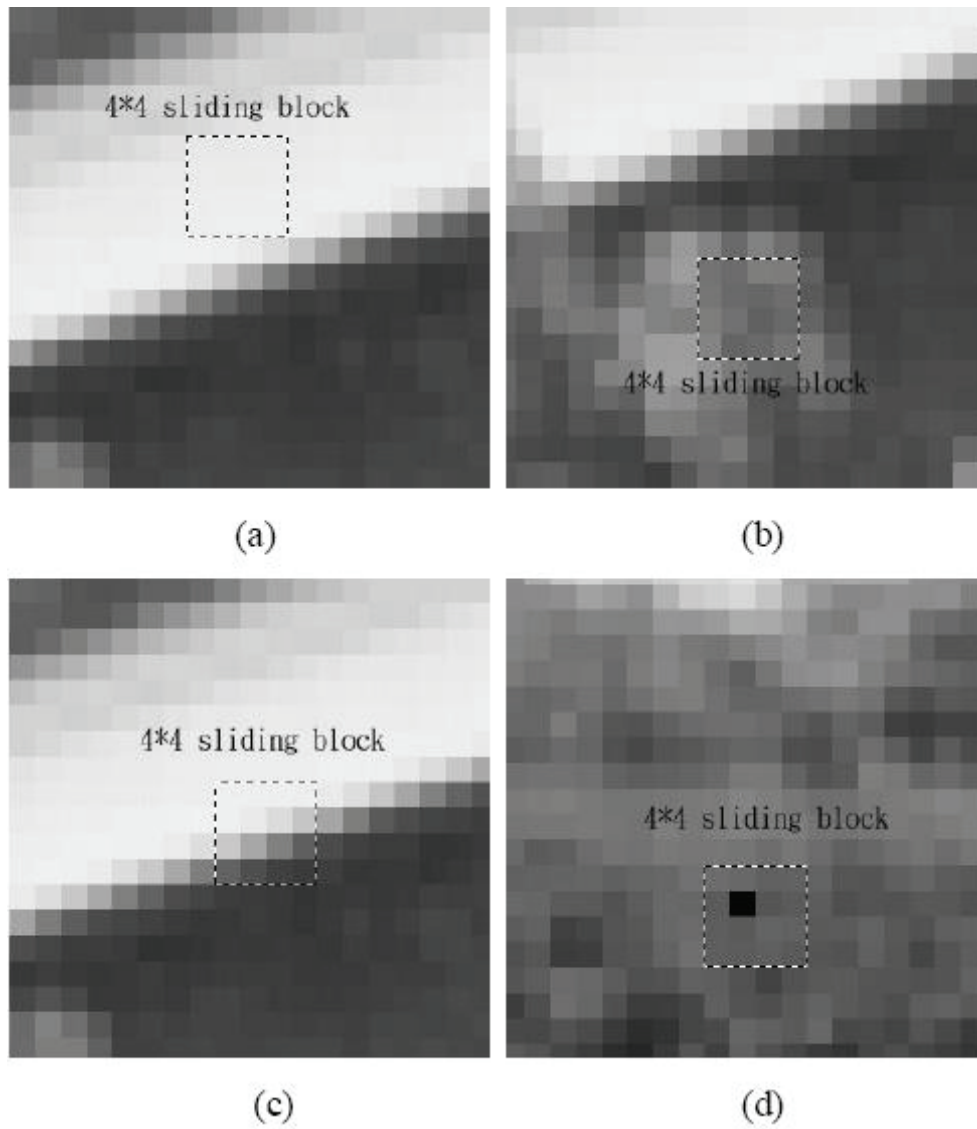


Fig. 27: Portions of (a) smooth region, (b) texture region, (c) edge region, and (d) noise region.

### 4.3 Vehicle Detection and Alarm

This paragraph will present vehicle detection, alarm and system stability. We choose the method 3 in II using the image sequence to detect vehicle and utilize the property of 3D ROI and image preprocessing to label the possible objects. According to the feature, we estimate the information given by image. If the statistics is stratified with our conditions, we will decide there is a car inside the blind spot area.

#### 4.3.1 Vehicle Detection

Similarly, we sort two categories daytime and nighttime. In the daytime, we consider the 3D ROI and divide into three areas and each of them owns its weight. In Fig. 28, the yellow area means there is an object gradually approaching the blind spot area and we set the weight  $w_{near}^{Day}$  is 0.5. The weight  $w_{outside}^{Day}$  of red area is 0.8, and we calculate the distribution  $d_{outside}^{Day}$  of red area. The blue area is the most important area on detecting vehicle on the lateral lane and we set the weight equal to 1. First, we observe the object whether it connects to in red area. Second, we estimate the length, width and height of the object with position and distribution. Third, we calculate the distribution  $d_{side}^{Day}$  of blue area and compare with  $d_{outside}^{Day}$ . In equation (28), we define two thresholds  $d_{th-side}^{Day}$  and  $d_{th-outside}^{Day}$ . According to the result of equation (28), it can assist in segregating the vehicle on outside lane and the effect from other non-car object. Finally, if statistic  $V_{statistic}^{Day}$  that we amount the result of each area is satisfied with our condition, we decide there is certainly a car inside the blind spot area. In the nighttime, we change the thresholds in the red area and the condition in the blue area to suit nighttime feature. The other steps are the same as in the daytime.



$$d_{result}^{Day} = \begin{cases} 1 & d_{side}^{Day} > d_{th-side}^{Day}, d_{outside}^{Day} > d_{outside}^{Day} \\ 0 & d_{side}^{Day} > d_{th-side}^{Day}, d_{outside}^{Day} < d_{outside}^{Day} \\ 1 & d_{side}^{Day} < d_{th-side}^{Day}, d_{outside}^{Day} > d_{outside}^{Day} \\ 0 & d_{side}^{Day} < d_{th-side}^{Day}, d_{outside}^{Day} < d_{outside}^{Day} \end{cases} \quad (28)$$

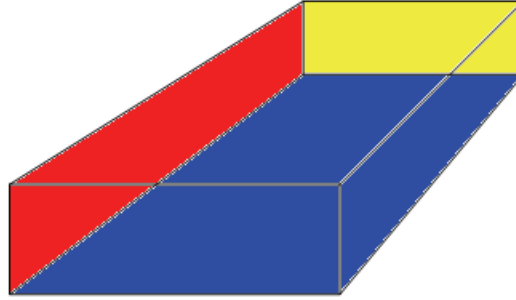


Fig. 28: Three areas of ROI

### 4.3.2 BLIS Alarm and Stability of System

When the system detects a moving car approaching, we use a temporal filter to let it more robust and improve the stability of the alarm signal more smooth. Here, we decide the vehicle comes inside the blind spot area in two ways. First, the vehicle comes from the rear area. The relation between alarm and time is close to be a trapezoid as shown in Fig. 29. We assume that the statistic is  $A_{statistic}^{BLIS}[n]$  which contains  $n$  as the result from last paragraph. When  $A_{statistic}^{BLIS}[n]$  is getting large, we determine that there is a vehicle approaching the blind spot area. Oppositely, when  $A_{statistic}^{BLIS}[n]$  is getting small, we determine that there is a vehicle leaving the blind spot area.

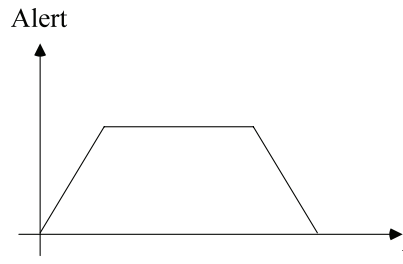


Fig. 29: Relation between time and alarm (rear)

Second, the vehicle comes from the front area. The relation between alarm and time is close to be a trapezoid with a right angle as shown in Fig. 30. When  $A_{statistic}^{BLIS}[n]$  is suddenly getting large, we determine that there is a vehicle coming into the blind spot area from the front side. Oppositely, when  $A_{statistic}^{BLIS}[n]$  is getting small, we determine that there is a vehicle leaving the blind spot area.

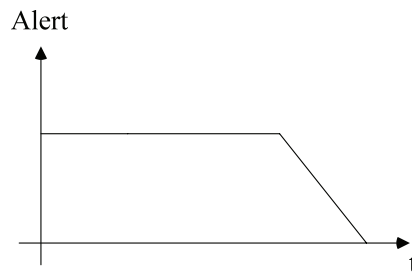


Fig. 30: Relation between time and alarm (front)

The method of dealing with the leaving blind spot area is the same. Whether it leaves from front or rear side, it will continue a while and provide the safety message to the driver. We must extend the time for the driver and it will make the driver to keep a distance with the moving vehicle along his car. It will reduce false alarm cause of the input image with noise and the inaccurate analysis of the image processing.

#### 4.4 Experimental Results

We choose the Borland C++ builder 6.0 to be the development kit and run the whole system on the Intel Centrino Duo 1.66GHz, 1.67GHz, with 1GB DDRII RAM. Finally, we realize the whole system on DSP BF561 image development kit. The Fish-eye camera is set up on the sport utility vehicle and the experiment environment is on the highway.

#### 4.4.1 Simulation on Personal Computer

Fig. 31 is the PC-based side collision warning system. We develop the functions and analyze the variable for optimizing the system. In order to narrate more particularly, we similarly show the result in the daytime and nighttime as following. The yellow region is our design 3D ROI and Fig. 32 is the system in the daytime. For porting function on DSP, we only use the field1 of the input image and use the gray level Y value of the YUV standard. The left-top shows the edge frame and the left-middle shows the difference frame. We compare these two frames to get the left-down frame and put it into our vehicle detection function as showing the right-down frame. In the image, the system will decide that there is a vehicle inside the blind spot area with the red part and the system will show the result on the top circle light. Fig. 33 is the system working in the nighttime. The left-top shows the binary frame after normalizing and the left-middle shows the dilation frame. The left-down shows the erosion frame and the right-down frame is the result decided by the vehicle detection. From upper two figures, our system operates successfully in both daytime and nighttime.



Fig. 31: PC-based lateral collision warning system

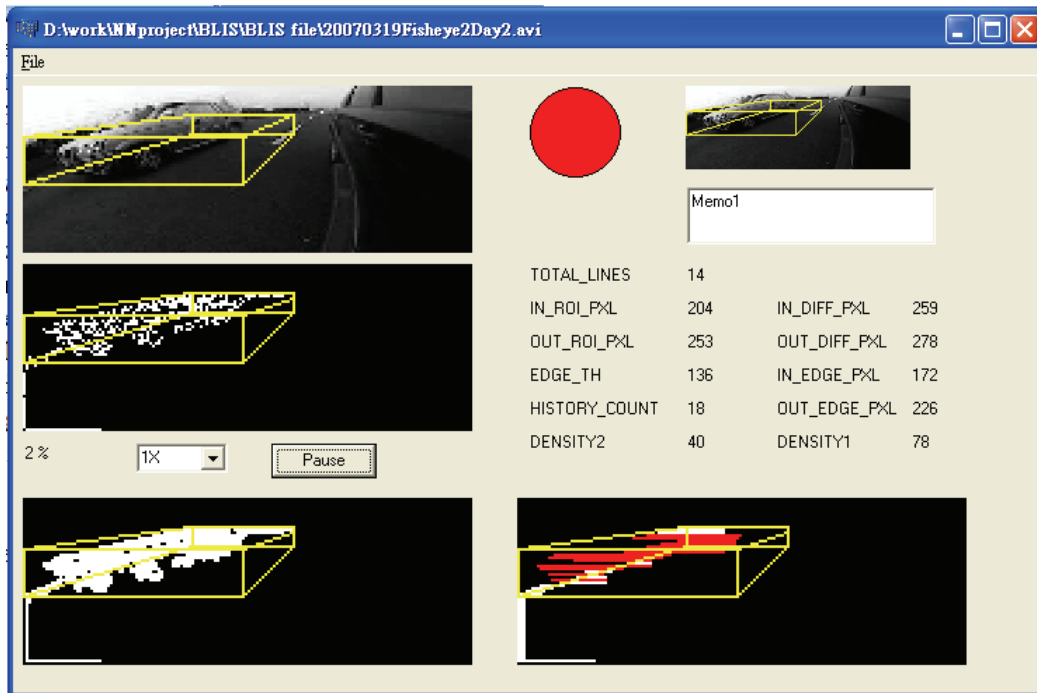


Fig. 32: System operates in the daytime



Fig. 33: System operates in the nighttime

#### 4.4.2 DSP-based Lateral Collision Warning System

Fig. 34 and Fig. 35 are the results from the DSP image output. We show the result

of the lateral collision warning system with a square on the right-top. When there is no vehicle inside the blind spot area, it becomes green light, otherwise it becomes red light to remind the driver of the vehicle approaching.

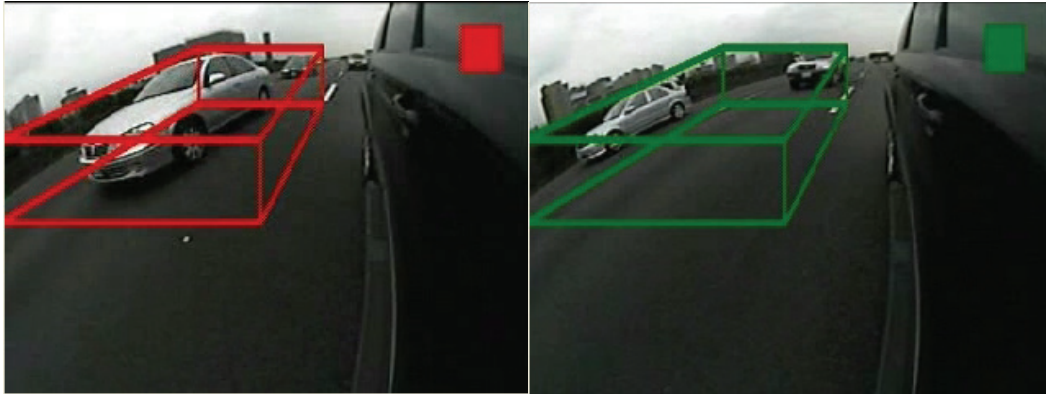


Fig. 34: Daytime DSP-based lateral collision warning system

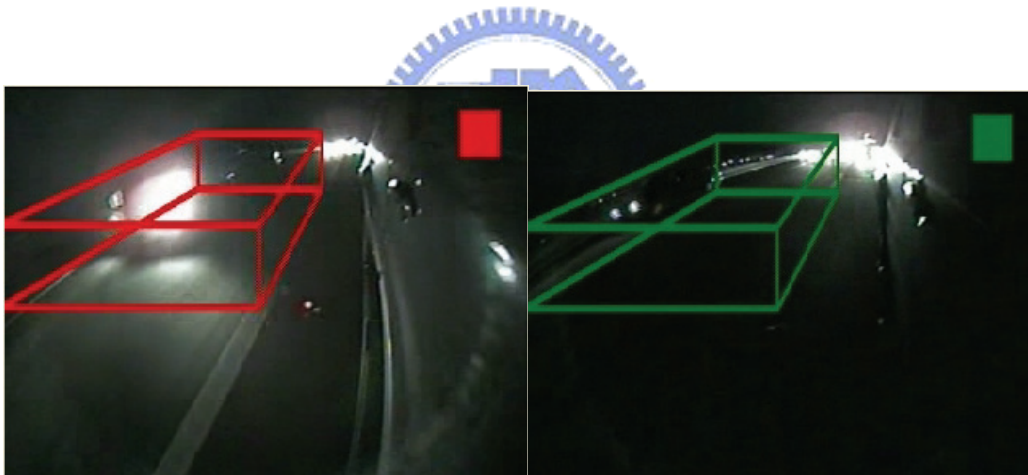


Fig. 35: Nighttime DSP-based lateral collision warning system

There are two kinds of common false alarms in the daytime listed as following, but both of them are correctly distinguished from the image in our lateral collision warning system. First, it is hardly to present all kinds of traffic islands, hence we only show two kinds of normal traffic islands in Fig. 36. Second, when the car passes through in the tunnel, the light variation is different from that of outside in Fig. 37.

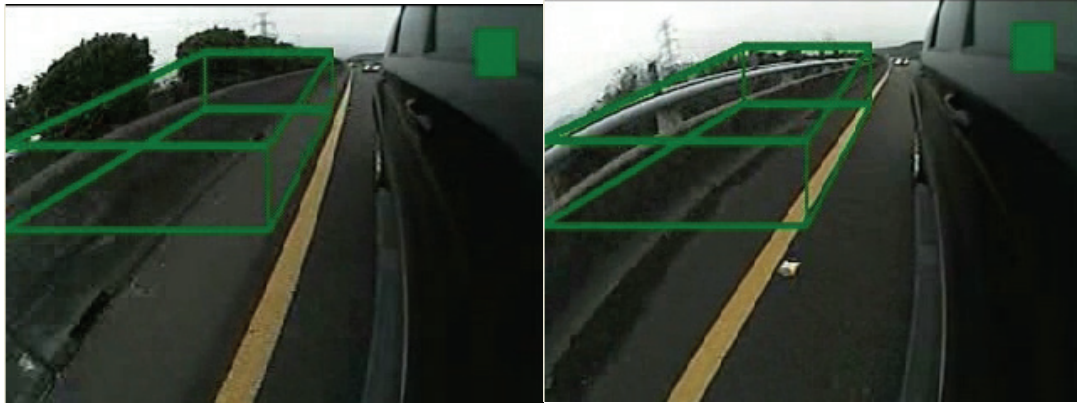


Fig. 36: System operates on normal traffic islands

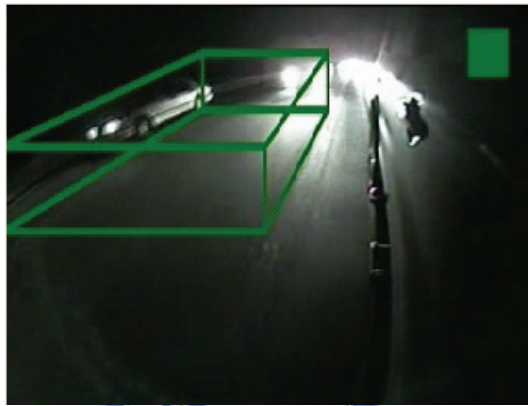


Fig. 37: System operates in the tunnel

There are also two kinds of common false alarms in the nighttime listed as following. First, the vehicle in the nighttime is difficultly to recognize the vehicle on the outside lane or on the side lane in Fig. 38. Second, when the car passes through the greatly dark road, it's hard to catch the contour of the car. When the car passes through the road with street lamps, the feature of head light will be influenced by the other illuminant. But we improve this problem with our adaptive threshold and use temporal filter to let it more smoothly in Fig. 39.

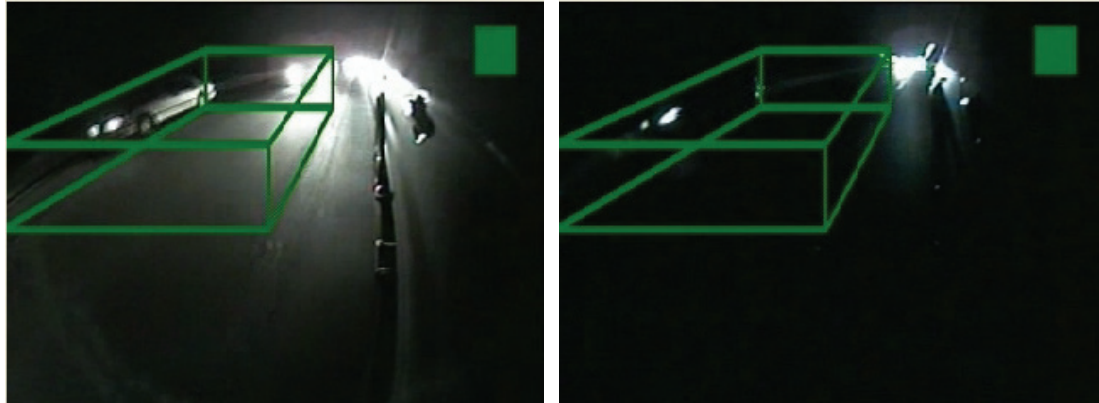


Fig. 38: System recognizes the vehicle on the outside lane.



Fig. 39: System won't be affected by the street lamp in the nighttime.

## 4.5 Summary

Our vehicle lateral collision warning system aims at detecting the image in driver's blind spot region and exporting the warning signal to remind driver. In order to deal with the vehicle in the different lane projecting on the same place, we choose the camera to be image input and the distortion image contains more information of right and left lateral.

We separate our system into two modules. The first module is 3D ROI design and auto-adjust parameters according the variation of weather. Although the measure of 3D ROI is bigger than the driver's blind spot area, but the region that needs to be computed is smaller than that of other algorithms. It also is divided into three areas to

analyze the moving objects and improve the accuracy of our algorithm result.

The second module is the vehicle detection. The features which we chose are different between daytime and nighttime. Our algorithm focus on the length, width, height, position and distribution of the moving object and each threshold are different from each other feature. As the result, our lateral collision warning system successfully operates in both daytime and nighttime.

The system operates on the highway where is filled with high-speed vehicles. We also realize a DSP-based lateral collision warning system and real time operates with 30fps.





# Chapter 5 Lane Departure Warning System

## 5.1 Introduction

In order to improve the driving safety, a lot of researches about the intelligent transportation systems (ITS) have been proposed in recent years. The Advanced vehicle control and safety system (AVCSS), one part of the ITS, contributes to prevent the driver in danger, and efficiently controls the traffic flow combining the distinct fields of technology, such as sensor, computer, and electrical engineering. Within this chapter, we focus on concerning the applications of the smart vehicles. In general, it is so necessary to acquire the information about the lane tendency while driving on the way.

Due to the inattentive driving, the driver may deviate from the correct lane orientation, which induces the traffic accidents. As a result, the lane detection system plays a significant role about improving the driver's safety in a moving vehicle. For cost and performance consideration, a camera is chosen as our sensing device for providing the abundant information. The vision-based system with cameras can be captured and processed the real-time images of road. Many approaches have been proposed about the lane detection algorithm by developing the image processing. More explanation of their techniques will be introduced in the next section.

### 5.1.1 Previous Work

The ARGO system [49] proposed at the University in Parma, Italy is aimed to develop the autonomous vehicle that could drive on highways and rural roads. In the GOLD system [50], the IPM (inverse perspective mapping) architecture is constructed to remove the perspective effect by mapping the road image into the top view.

Moreover, this algorithm can detect the lane markings depending on the feature of the contrast and lane-width with the road plane, which may fail when the assumption of a flat road is not valid. Based on the GOLD system, Jiang et al. [51] models the lane as two straight lines to estimate the inclined angle on the degree of non-flat roads. However, the road shape is not usually straight in realistic conditions. Based on the lane geometry, some geometric model-based lane detection techniques such as polynomials and splines can fit the lane trajectory more than the model of straight lines. Wang and Teoh [52] [53] have proposed the deformable road models to track the lane curvature without any camera's parameters. But the searching speed of those correlated methods is slower while finding the new control-point in each frame. Jung [54] has developed the parabolic lane boundary model to approximate the lane boundaries by the combination of the edge function. This technique only demands the low computational power but has the difficulty in porting on other platform except for the PC due to the fitting process. To extract the lane shape in the nighttime, Fu [55] used the vision-based driver assistance system to enhance the driver's safety at night with the preprocessing of camera calibration.

### **5.1.2 Principles of Lane Detection and Lane Departure Warning**

The objective of lane detection method we expected in this thesis is to extract the lane-marking without knowing the internal or external parameters of the camera alongside the vehicle in advance. Besides, the sensitivity of the image sensor easily disturbed by the light condition must be suppressed as much as possible. Therefore, developing an adaptive lane-finding system is essential to satisfy the previous demands. First, our system can automatically extract the ROI contained by the road surface only by the image content despite the unknown environmental information of camera. Second, the preprocessing tasks will be able to effectively restrain the noise

when driving in the nighttime. Through the property for the view-angle of blind spot, the improving edge operator will be added to acquire the clear lane boundary. Not depending on the distortion of the camera lens which results in the obviously curved lane trajectory even if people drive on the straight road, a piece-wise edge linking model will be developed to mark all information of lanes shown in the image sequence.

The part for lane departure warning is to provide some triggers for caution with respect to the driving-off-road behavior through the lateral information of the lane extracted by the lane detection algorithm. After measuring the lateral velocity from the consecutive frames, the warning system will determine when the departure driving occurs based on the lateral displacement and TLC (time to lane crossing.)

## 5.2 Lane Detection

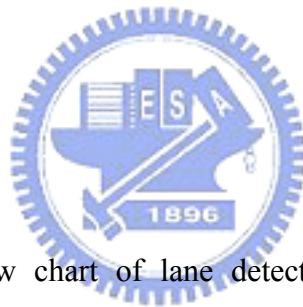


Fig. 40 shows the flow chart of lane detection. At the beginning of this architecture, because we merely aim at the monochromatic information of each frame to process, the RGB coordinate will be transformed into the YCbCr one so that the illumination component will be totally retained. Then, the automatic mechanism about searching the ROI (region of interest) of the image content and de-noising will be described in Section 5.2.1.

Next to the processing step, the flow will enter the principal detection parts. Due to the mounting position of camera on the side of the car, the image captured by that device will contain most of the lateral-view information next to the wheels. In other words, only one lane trajectory which is the most closed to the vehicle can be apparently seen. An edge detection operator will be developed to adapt to the geometry relationship of the camera based on the property of view-angle in section

5.2.2. In addition, the binarization step we proposed in this section will depend on the spatial relation with respect to the perspective effect. To eliminate the blind-spot region as much as possible, we choose the fish-eye camera for enlarging the field of view with some obvious distortion result. Therefore, the adaptive edge-linking model demonstrated in section 5.2.3 will overcome the serious problem whether the lane boundary in the image sequences is straight or not.

### 5.2.1 Preprocessing

#### Automatic ROI Extraction

Before discussing how to search for the lane-marking, the step of color transformation must be executed. In general, most of the algorithms shown in the past theses with respect to lane detection are only considered the grey-level component. This reason is that the contrast between the lane boundary and the normal road plane can be easily seen by normal people as usual even if the colors of lanes are not necessarily the same. As a result, the information of luminance for each frame must be stored in our system by the RGB-to-YCbCr transformation. On the other hand, the remaining chrominance components such as Cb and Cr are not taken seriously due to the insensitive perception about human eyes. The formulation of transformation can be described by

$$\begin{bmatrix} Y \\ Cb \\ Cr \end{bmatrix} = \begin{bmatrix} 0.257 & 0.504 & 0.098 \\ -0.148 & -0.291 & 0.439 \\ 0.439 & -0.368 & -0.071 \end{bmatrix} \cdot \begin{bmatrix} R \\ G \\ B \end{bmatrix} + \begin{bmatrix} 16 \\ 128 \\ 128 \end{bmatrix} \quad (29)$$

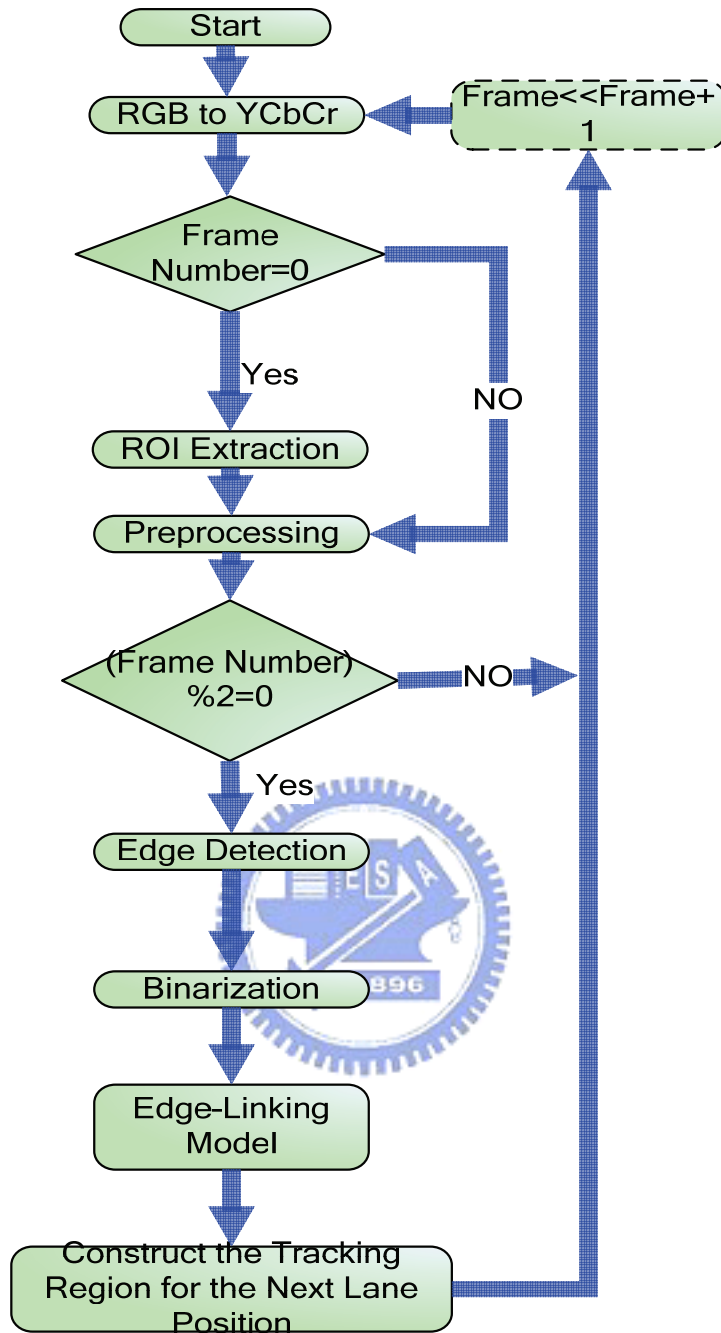
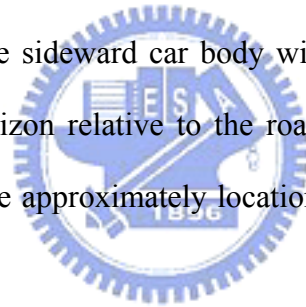


Fig. 40: The flow chart of lane detection

As shown in Section 2.3, equation (1) and (2) tell us the relationship of geometric transformation which demands the known information of camera, such as the height, pan-tilt angle, and the internal focal-length of the camera, between the image coordinate and the vehicle coordinate systems. Some methods proposed in the previous works have to compute the curvature of the realistic road plane or to estimate the lane shape effectively by these intrinsic or extrinsic parameters. However, an

adaptive system can not be sensitive to the variation of the camera mounting position for the aspect of application and commerce. For instance, the systematic performance should be not influenced by the distance between from the rear-view mirror and the road surface about various vehicles.

To take this target, we hope that our detection algorithm can automatically determine the ROI (region of interest) contained the whole lane trajectory on the road surface only by the image content with lateral view-angle. The chosen range of ROI should be unchanged by the later information of image sequences whether some new moving objects are captured or not. Fig. 41(a) demonstrates the realistic frame acquired by the camera alongside the side mirror. Through being concerned about the image content, the fixed parts within it might be regarded as the evidence for ROI extraction. In our opinion, the sideward car body with constant area throughout the image sequences and the horizon relative to the road plane both correspond to the fixed condition. Therefore, the approximately location of ROI will be determined by the edge information of them.



The definition of ROI is that a rectangle region which extends its width to the location next to wheels contains all the lane shapes in the image. In general, the height of ROI is below the vanishing point situated in the horizon closed to the border of the vehicle's window. This 2D geometry with respect to the above characteristics can not depend on the light condition or view-angle of the camera.

Fig. 41(b) shows the location of the upper left point of ROI between the boundary of the window and the vanishing point. In this figure, the portion of the green rectangle is shown as ROI, and the intersection of the marking cross stands for the key point to determine where the range of ROI has covered. In this case, the 2-D gradient operator will be used to extract the position of key point by considering the



(a)

(b)

Fig. 41: (a) The image acquired by the camera alongside the rearview mirror. (b) The upper left point of ROI next to the boundary of the vehicle window.

boundary information of the vehicle window. Hence, we use edge detection in section 4.2.3 due to the obvious edge of the window in the horizontal and vertical aspects.

Fig. 42 displays the results of edge detection with  $G_x$  and  $G_y$ . After extracting the border of the window from Fig. 42 (b) to Fig. 42(d) with the threshold, the coordinate values of the key point in the x- and y- axis will be founded to determine the range of ROI by computing which row and column retain the most edge pixels along the horizontal and vertical direction individually. This process can be expressed as:

$$I_{key}(x, y) = \begin{cases} 255 & \text{if } G_x(I(x, y)) > TH \text{ or } G_y(I(x, y)) > TH \\ 0 & \text{else} \end{cases} \quad (30)$$

where

$$TH = \frac{\sum_{y=0}^h \sum_{x=0}^w I(x, y)}{w \cdot h} \quad (31)$$

The ratio of  $w$  to the image width is closed to 0.5, and that is the same case as the ratio of  $h$  to the image height. Due to the more edge pixels naturally existed along the horizon in the horizontal axis and the perpendicular border of the vehicle in the

vertical axis, an intersection point of the car window can be found out by searching in the x-y direction respectively. The detecting results with different light conditions and view-angles are shown in Fig. 43.

Although the horizontal border of the vehicle window may be unclear in the worst conditions which the illumination from the car and street light has not adequate at night, the extracting result is still steady since the edge information of horizon can be replaced to obtain the similar position in the x-axis, as shown in Fig. 43(c) and (d).

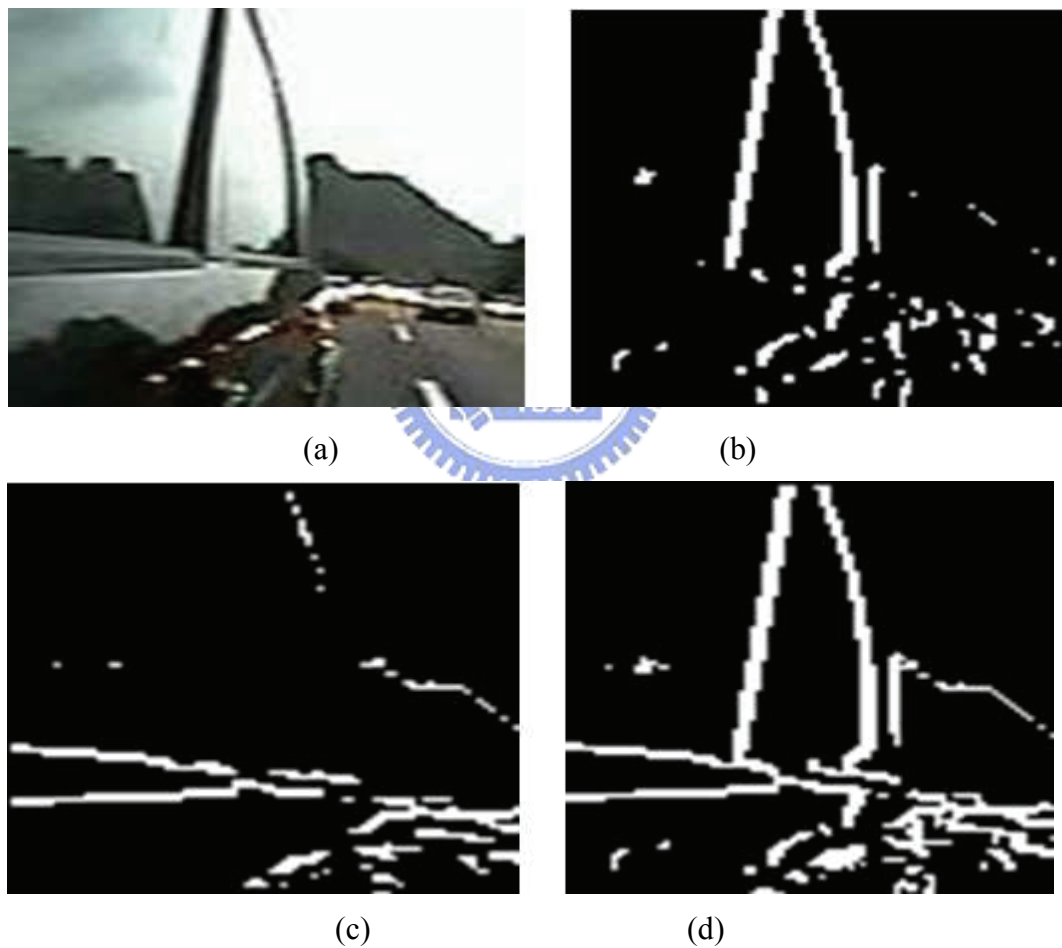


Fig. 42: (a) Original image. (b) Edge detection by  $G_y$ . (c) Edge detection by  $G_x$ . (d) Edge detection by  $G_x + G_y$ .



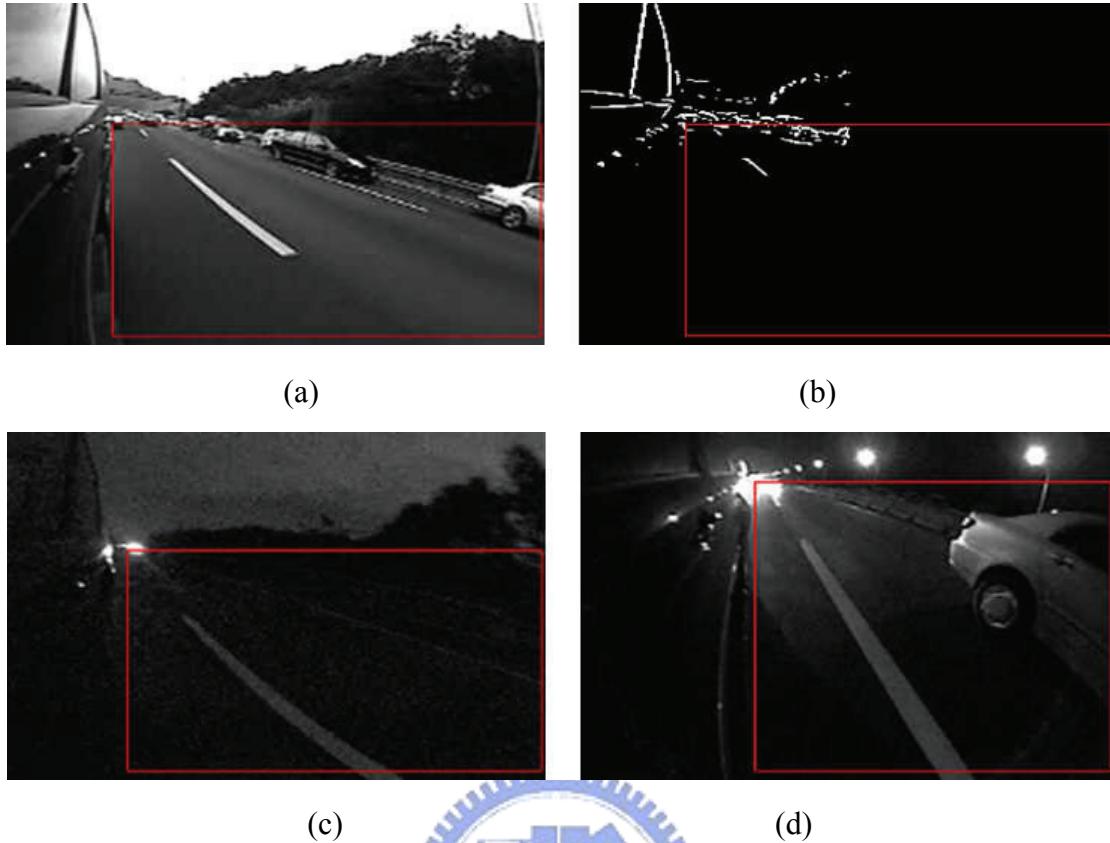


Fig. 43: (a) Day light. (b) ROI extraction of (a). (c) ROI extraction at night. (d) ROI extraction with different view-angle in the nighttime.

### De-noise Processing in Spatial and Temporal Domain

The quality of image sequences collected by the vision-based sensing device will be almost subjected to this challenge of the variance of the light conditions, such as day or night situation. Because the problems about high-frequency noise will be serious for some driving environment due to the photosensitivity of cameras, especially on night vision. Therefore, the preprocessing step for eliminating the noise effect must be considered in the detecting architecture if the system is expected to work robustly all day long.

In general, a low-pass filter can be implemented before the process which is used to extract the information about the boundary, texture, or shape of the interesting objects within the frame. Since the frame is stored as a collection of discrete pixels,

we need to produce a discrete approximation to the chosen filter-type before the convolution step. Hence, the Gaussian smoothing operator which is a 2-D point-spread function achieved by convolution is used for this de-noising task in our system. The isotropic form of Gaussian is shown as below:

$$G(x, y) = \frac{1}{2\pi\sigma^2} \exp\left(-\frac{x^2 + y^2}{2\sigma^2}\right) \quad (32)$$

where  $\sigma$  is the standard deviation of this function.

The diagram of this distribution is shown in Fig. 44(a). Moreover, this function has been assumed with a zero mean. In principle, the Gaussian distribution is non-zero everywhere, but its value is closed to zero more than about three standard deviations from the mean centered at the distribution. Therefore, we can truncate it as the mask-type at the specific pixel of each frame. Fig. 44(b) shows a suitable integer valued convolution mask of Gaussian where  $\sigma=1$ . The Gaussian filter outputs a weighted average of the neighborhood of each pixel. It can provide gentler smoothing and preserves edges better than the normal-sized mean filter due to the distinct size between 5x5 and 3x3. On the other hand, by choosing an appropriately size of Gaussian filter determined by the standard deviation, more range of spatial frequencies is still preserved in the image after filtering because its Fourier form is itself a Gaussian. However, over-wide region contained in the filter will result in the serious blur effect of the image content. Therefore, the 5x5 principal type of Gaussian mask is still adopted in this part.

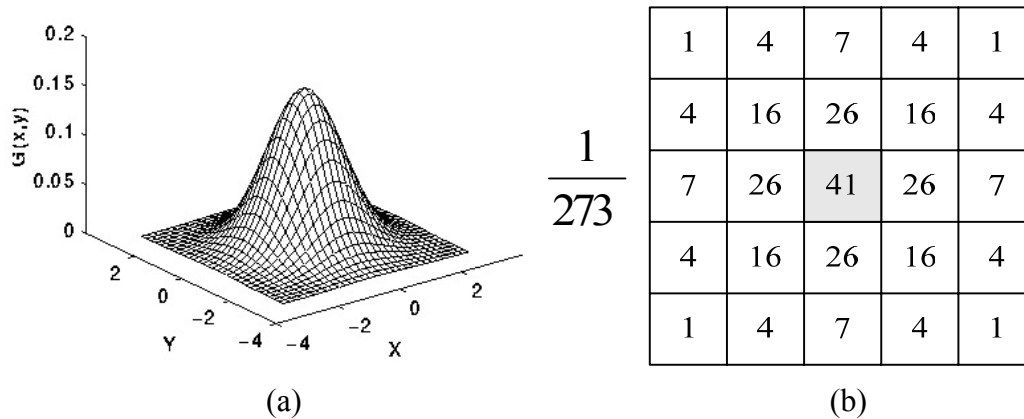


Fig. 44: (a) 2-D Gaussian Distribution with mean  $(0,0)$  and  $\sigma=1$ . (b) Suitable 5x5 mask of Gaussian filter with  $\sigma=1$ .

Some results of edge detection which describes the details in the next section is preprocessed by Gaussian and Mean filter as shown in Fig. 45. Compared with (c) and (d), the extracting method of the lane boundary will be easily disturbed by the remaining noise if the smoothing filter can not effectively remove the high-frequency perturbation.

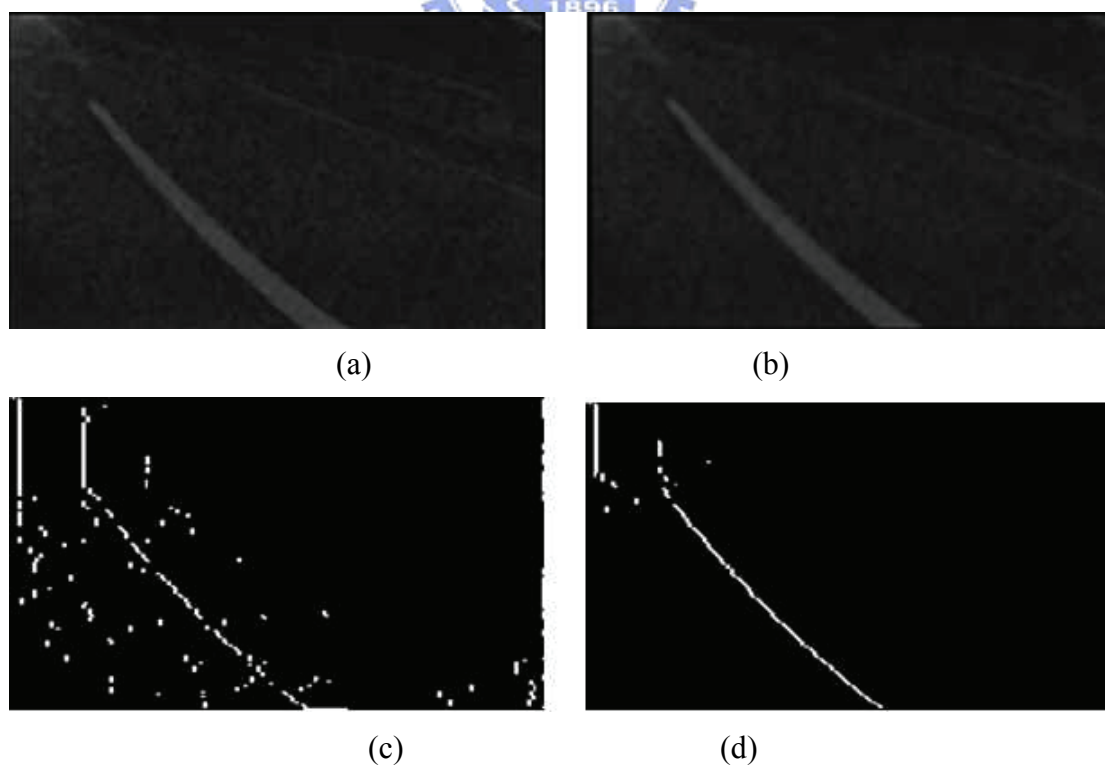


Fig. 45: (a) Mean filter. (b) Gaussian filter. (c) Edge detection after (a). (d) Edge detection after (b).

Salt and pepper noise which exist in spatial and time domain is more challenging for the preprocessing tasks, especially the night environment. To achieve the objective that the effect of the proposed lane detection method in this thesis must be independent on the variation of external light conditions, the time-averaging process focused on the current and previous frames will be added behind the Gaussian smoothing work. The integrated de-noising procedure is demonstrated in Fig. 46.

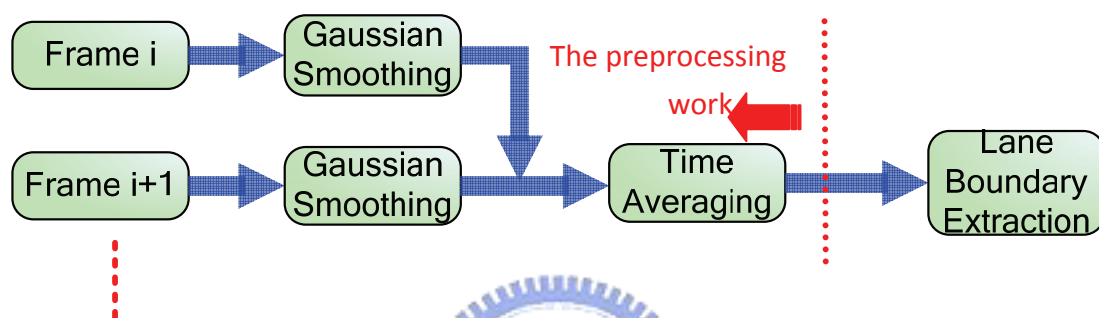


Fig. 46: Flow chart of the complete preprocessing steps.

## 5.2.2 Lane Boundary Detection

- Edge Detection

The objective in this section is to find the features of lane marker from the information of image. Through the observation, lanes must have some apparent properties about its boundary. The most obvious reason of them is that the lane markers must be brighter than the neighborhood road surface even if they are with various color information. Then, the lane shapes in the image are almost presented as slender types. In other words, extracting the lane boundary is an important step to locate the realistic lane position throughout the video by the foregoing two factors.

The determination of the edge detection operators needs to be considered the suitable and effective performance for the image contents, so we use the HVS-Directed object edge detection discussed in sector 4.2.3.

By further observing the property of blind-spot view image from the camera alongside the rear-view mirror, the included angle from the edge of lane to the vertical Y-axis of the image plane must be within the range of degree  $0^\circ$  to  $90^\circ$ , and therefore we can use the angle evaluation method in sector 4.2.4 to sort out the data wanted.

According to the result from Fig. 47(d), only the intra-boundary of the lane can be extracted, and this property will contribute to link the lane trajectory described in the later section.

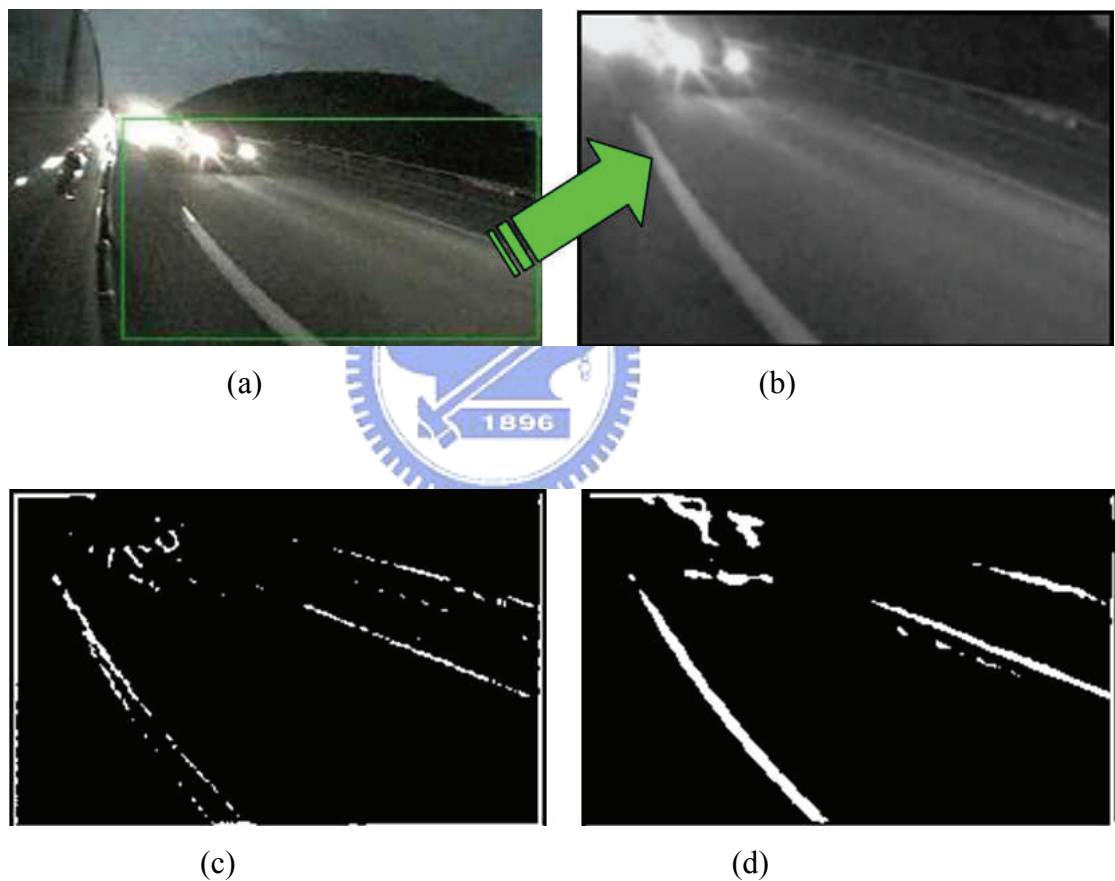


Fig. 47: (a) The original image. (b) Gaussian smoothing within the ROI of (a). (c) Result of LoG mask. (d) Result of the new combined mask.

The morphological post-procedure is to thin out the lane-marking after the edge extraction. There are two conditions determining which the pixel can be retained in the image:

if  $I(k)=255$  AND  $I(k+1)=255$   
 $\Rightarrow I(k+N)=0$  where  $N$  is a little larger than 2  
 else if  $I(k)=255$  AND  $k>P(i)$   
 $\Rightarrow I(k)=0$  where  $P(i)$  is the point corresponded to the lane boundary of the row  
 else  
 $\Rightarrow I(k)=255$

The edge-finding approach to determine the location of  $P(i)$  will be introduced in section 5.2.3.

- Adaptive Threshold Determination by Distinct Spatial Region

The pixels within the ROI can be extracted for the image processing tasks in our system. According to the perspective geometry, the length or the width of the lane markers within ROI is not the same with each different position. In other words, the lane boundary in the bottom part of ROI is always wider and longer than that in the up part. By considering the transformation effect, the adaptive mechanism is developed to adjust the threshold for different sub-regions, and the size of them depends on ROI.

After processed by edge extraction, the image needs to be decided the threshold for more obvious detecting result. Due to the evidently contrast between the lane markers and the neighborhood road surface, the gradient magnitude of lane boundary caused by the edge operator is usually larger than other locations. Therefore, in this section the values of mean and standard deviation computed by each row within the ROI will be selected as the threshold for different region.

Take the normal distribution for example, the range which contained the distance for one standard deviation from the mean will account for about 68% of the whole set. Besides, the range will account for about 95% if it contains the distance for two standard deviations from the mean. For each row within ROI in the image, the

threshold value is still selected by referencing above scattered property since the gradient magnitude of lane markers is certainly higher than that of the normal road surface. That is,

$$Threshold(j) = \underset{i \in (0, \text{width of ROI})}{\text{Mean}} |f(i, j)| + k \cdot \underset{i \in (0, \text{width of ROI})}{\text{Standard deviation}} |f(i, j)| \quad (33)$$

where

$k=2$

$j$  :  $j$ -th row of ROI

$f(i, j)$  : the value of each pixel within ROI after the edge detection

The performance of the binarizing approach may be dependent on the edge information of the adjacent moving vehicles close to the lane or the car-light of them, especially the upper part of ROI which can not contain adequate component of the magnitude of lane. Hence, the ROI will be divided into seven sub-regions when it is automatically extracted in the first frame of video, as illustrated in Fig. 48.

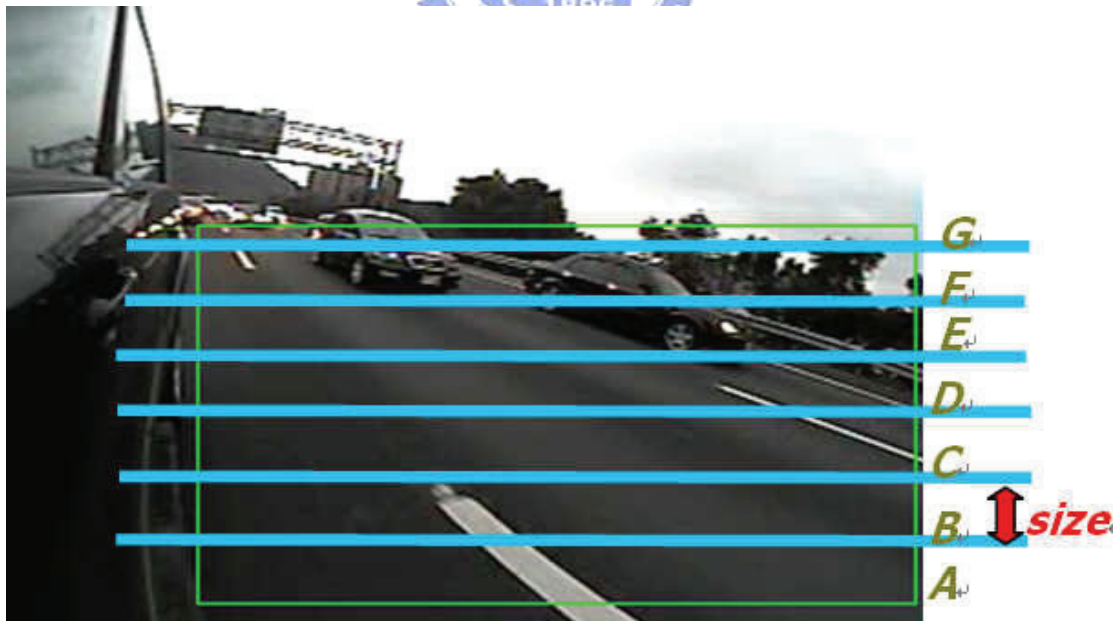


Fig. 48: The division of ROI into seven sub-regions.

Where  $size = \frac{\text{height of ROI}}{N-1}$ ,  $N$ : number of segments (we choose 7 in this system)

In this way, the values of thresholds situated in different location are selected by

tuning the mean value of each-row pixels and the arrangement of magnitude for them are from the bottom to the top sub-region, as described in the following:

$$Threshold(j) = \left( \text{Mean}_{i \in (0, \text{width of ROI})} |f(i, j)| - \alpha \right) + k \cdot \text{Standard deviation}_{i \in (0, \text{width of ROI})} |f(i, j)|$$

where

$$\alpha = 0.1 \cdot \sum_{k=0}^n (\text{Standard deviation}_{i \in (0, \text{width of ROI})} |f(i, j)|) \cdot k \quad (34)$$

$n$  :  $n$ -th sub-region of ROI

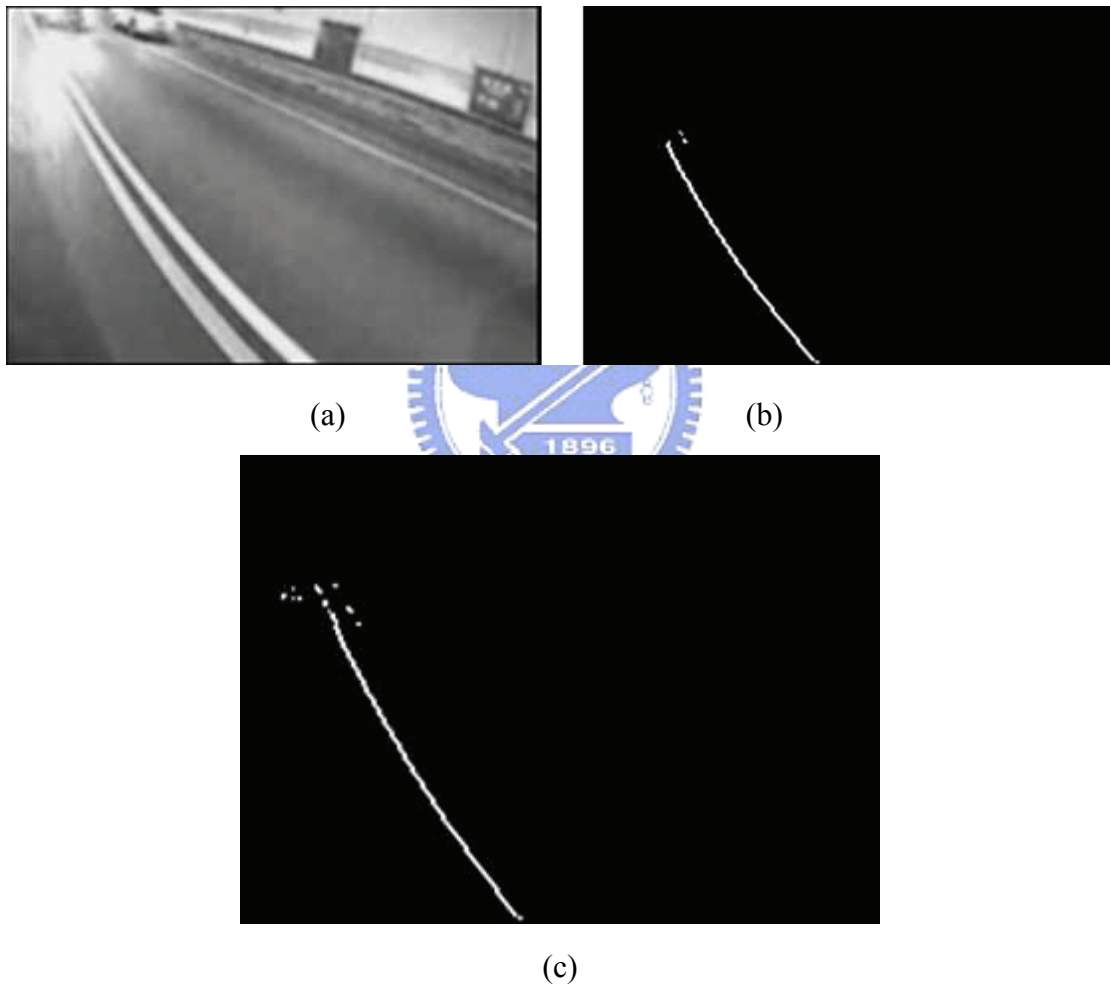


Fig. 49: (a) The image is photographed in a tunnel. (b) Lane-marker extraction without considering the sub-region threshold. (c) Lane-marker extraction with considering the sub-region threshold.

Fig. 49(a) shows an imaging environment about driving in a tunnel. The original lane boundary in the upper region is not easily seen due to the disturbance of the car-light from the backward vehicle, as shown in Fig. 49(b). This overexposure effect



will be improved by considering the tuning parameter ( $\alpha$ ) in Fig. 49(c).

### 5.2.3 Lane-Finding Algorithm

Since the edge information of lane markers has been acquired by the foregoing demonstration, marking and tracking the lane trajectory within ROI can be succeeded by such pixels lying on the sides of lane boundary in the image. There have been some researches for lane-model construction. Y. U. Yim and S. Y. Oh [57] use the starting position, direction, and saturation of the lanes regarded as the three features to initialize the lane vector and find the most probable lane trajectory by Hough Transform. Roland Chapuis [58] uses the statistical model to specify the detection ROI in order to narrow the searching area of lane markings. Different from the method merely about the image processing, the lane geometry is taken into the fitting of the lane model provided by A. Lopez [59]. D. J. Kang [60] combines the vanishing point of the road from the frontal camera with Hough Transform for lane tracking.

Based on the objectives for real-time tracking and low-cost computation, a piece-wise edge linking model we proposed in this chapter is effective for lane-shape marking whether the lens-distortion of camera is serious or not.

- **Hough Transform**

The classical type of Hough transform is to identify the edge or boundary of lines in the image. This principle is to transform the X-Y coordinate system into the r- $\theta$  parameter space, where r represents the small distance between the line and the origin of the image, and  $\theta$  is the angle of the locus vector from the origin to this closest point. The relationship of the transformation about two coordinate systems is shown in Fig. 50. According to equation (39) from this figure, they can determine if the point A and B are collinear with the same r and  $\theta$ . Besides, equation (40) is to

determine if the line segment formed by A and B is collinear with that formed by C and D by judging the condition that the parameter  $d$  is smaller than a threshold.

$$r = x_1 \cdot \cos \theta + y_1 \cdot \sin \theta = x_2 \cdot \cos \theta + y_2 \cdot \sin \theta \quad (35)$$

$$d = |r - (x \cdot \cos \theta + y \cdot \sin \theta)| \quad (36)$$

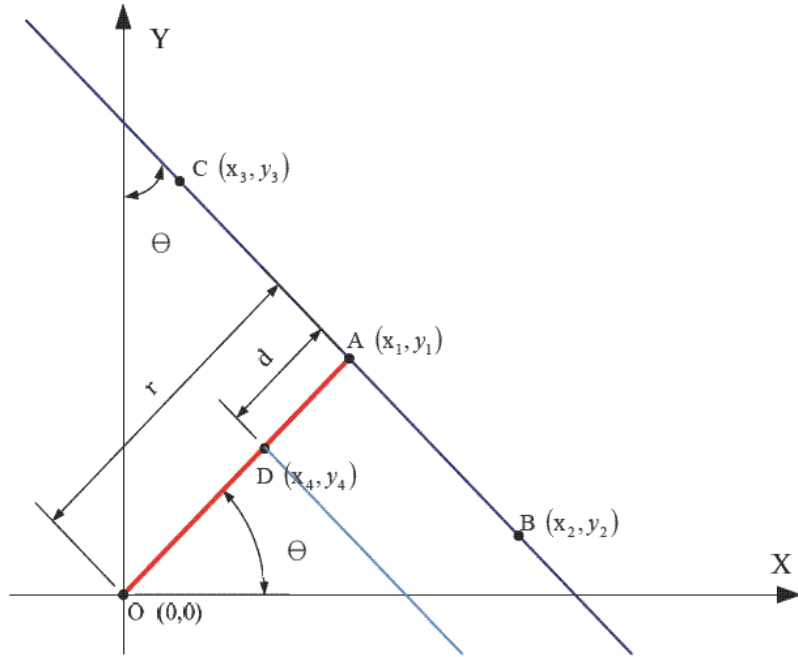


Fig. 50: The diagram of relationship between the x-y and r- $\theta$  coordinate systems.

- **Piece-Wise Edge Linking Model**

Li [61] and Yeh [62] still apply the Hough transform to track the lane markers which can not be deformed in the image captured by the normal camera. However, due to the distinct curvature with the fish-eye lens, it is impossible to take Hough transform into our system. Hence, the novel approach for lane modeling needs to be considered the geometric effect of ROI and the connectivity of the lane markers with robustness and adaptation.  $\Theta$

The flow chart of the piece-wise edge linking model is shown in Fig. 51(b).

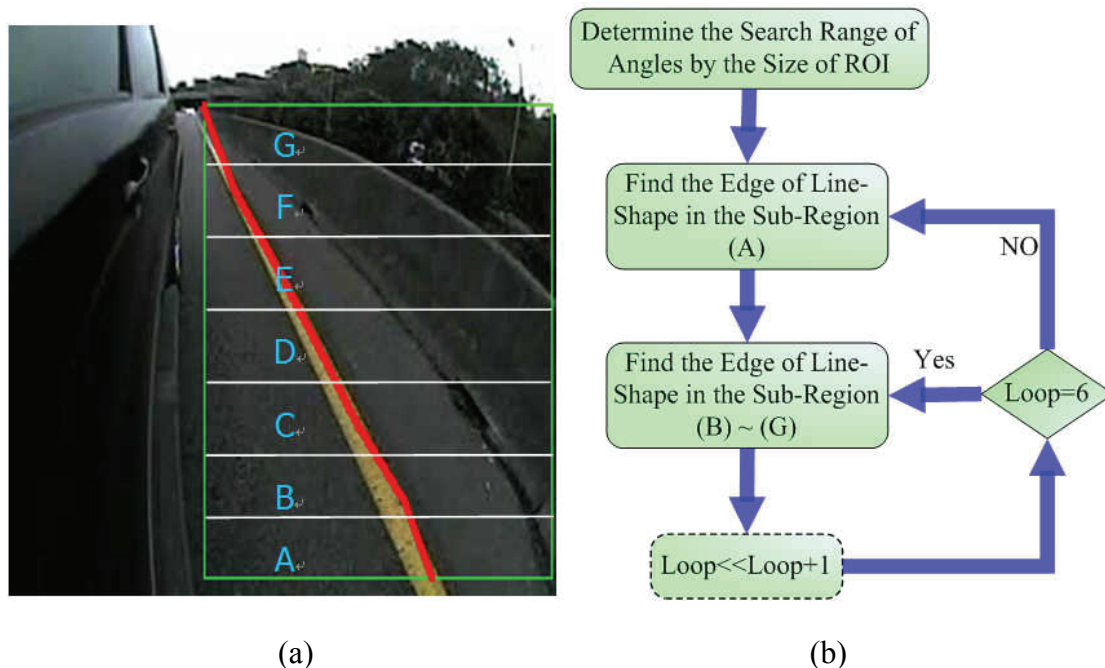


Fig. 51: (a) Seven sub-regions automatically segmented within ROI. (b) the flow chart of the piece-wise edge linking model.

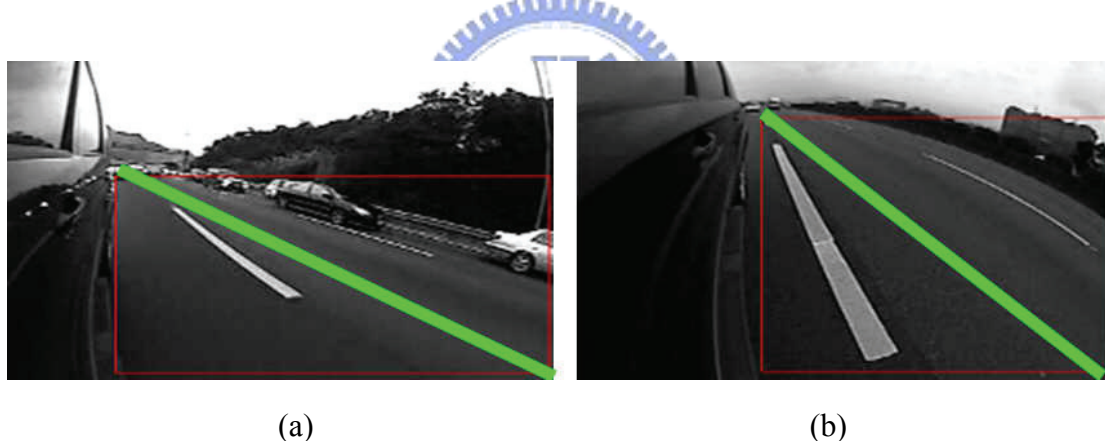


Fig. 52: (a) Seven sub-regions segmented within ROI. (b) the flow chart of the piece-wise edge linking model.

Fig. 52 shows the two different size of ROI is caused by the variation of the intrinsic and extrinsic setting of camera. In general, the width of ROI depends on the yaw angle of camera, and the height of that depends on the pitch angle or the distance from the mounting position near the rearview mirror to the road plane. Although those parameters can not be taken in our system, we still find the property that the lane boundary in the image must extend to the upper-left part of ROI even if the lateral position estimated from the lane marker is not the same through the image sequences.

By using the perspective effect that lane markers almost converge near the region of vanishing point, the included angle from the diagonal of the ROI to the vertical boundary of that can be determined the maximum searching range of angles for Hough transform. This mechanism will be regarded as the initial step in the piece-wise linking model as shown in Fig. 51(b). To overcome the irregular curvature of lane trajectory from the fish-eye lens distortion, the seven sub-regions automatically segmented in Fig. 51(a) contribute to fit the edge pixels of lane since its boundary information contained in it can be regarded as the line-shape. Therefore, the principle of Hough transform described in section 3.4.2 is directly used for the bottom sub-region (A) as demonstrated in Fig. 53. The details of parameters in Fig. 53 and Fig. 54 are explained as follows:

**St\_X, Ed\_X:**

The coordinate values of x-axis in the bottom and top border of the sub-region are determined by Hough transform. Ed\_X situated in the bottom border of the next sub-region, such as the same location as the bottom border of sub-region (B) and the top border of sub-region (A), can become the fixed point for searching the line edge pixels only by the angle  $\theta$  as the flow chart in Fig. 54.

**SkipTh:**

Its size depends on the vertical pixel-width of the sub-region (A) in Fig. 53. For some circumstances like the rapidly lane changing maneuver, the lane marker may

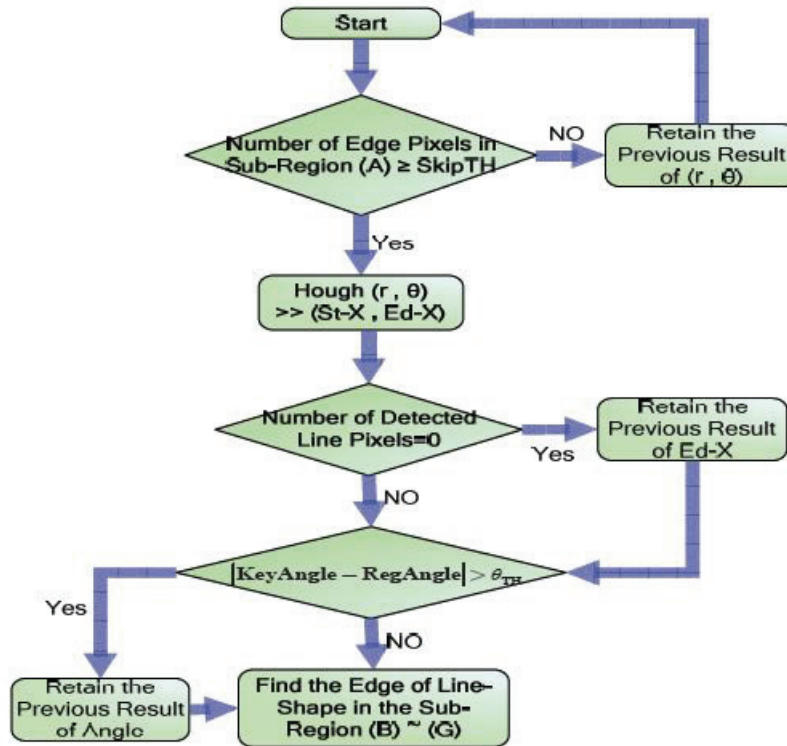


Fig. 53: The flow chart for finding the line-shape in the bottom sub-region (A).

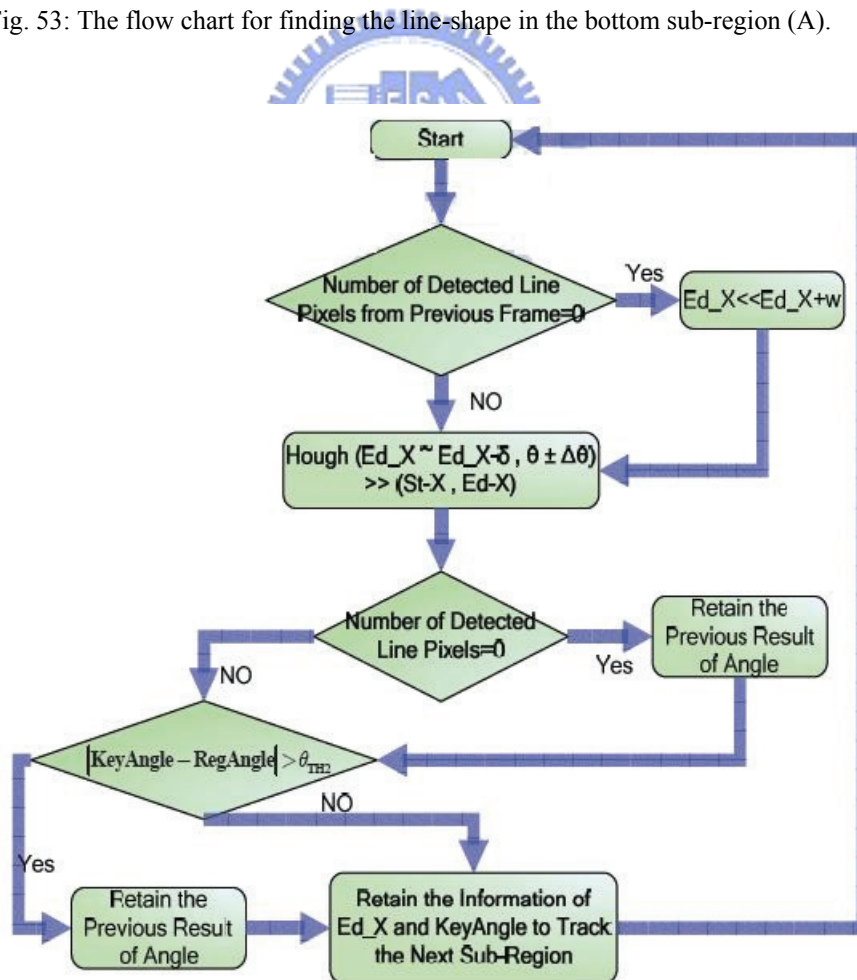


Fig. 54: The flow chart for finding the line-shape in sub-regions from (B) to (G).

be discontinuous for each sub-region in the image. The threshold is to control when the lane modeling procedure is performed and observe if the edge pixels in the bottom sub-region (A) have adequate amounts to composite the lane trajectory.

**KeyAngle, RegAngle,  $q_{TH}$ ,  $q_{TH2}$ ,  $\delta$ ,  $\Delta\theta$ , Lw:**

KeyAngle and RegAngle are the angles about appropriate orientation of line boundary in sub-regions induced by the current and previous frame. Based on the connectivity and continuity of lane markers on the road surface,  $q_{TH}$  and  $q_{TH2}$  are the thresholds to limit if the difference between KeyAngle and RegAngle is small enough. In addition,  $q_{TH2}$  must be smaller than  $q_{TH}$  since the searching angles with sub-region (B) to (G) is restricted by the previous detecting results from the bottom sub-region (A).  $\delta$  and  $\Delta\theta$  are the slight range for detection with Hough Transform from sub-region (B) to (G) where the computation power can be reduced. At last, Lw is a revised parameter to restart the seeking area in the x-axis when the number of line pixels is zero in Fig. 54.

To simply the geometric circumstance that the distance between the vehicle and lane trajectory with some curvature in the image is much different, especially the effect of fish-eye lens distortion, we use LSR (least square regression) to make the curved a lane boundary approximate a straight line. The LSR can be induced as below:

$$E = \sum_{i=1}^n e_i^2 = \sum_{i=1}^n (Y_i - a \cdot X_i - b)^2 \quad (37)$$

$$\begin{cases} \frac{\partial E}{\partial a} = \sum_{i=1}^n 2(Y_i - a \cdot X_i - b) \cdot (-X_i) = 0 \\ \frac{\partial E}{\partial b} = \sum_{i=1}^n 2(Y_i - a \cdot X_i - b) \cdot (-1) = 0 \end{cases} \quad (38)$$

Equations (37), (38) can be simplified as

$$\begin{cases} a \sum X_i^2 + b \sum X_i = \sum X_i Y_i \\ a \sum X_i + b \cdot N = \sum Y_i \end{cases} \quad (39)$$

$$\begin{cases} a = \frac{\begin{vmatrix} \sum X_i Y_i & \sum X_i \\ \sum Y_i & N \end{vmatrix}}{\begin{vmatrix} \sum X_i^2 & \sum X_i \\ \sum X_i & N \end{vmatrix}} \\ b = \frac{\begin{vmatrix} \sum X_i^2 & \sum X_i Y_i \\ \sum Y_i & N \end{vmatrix}}{\begin{vmatrix} \sum X_i^2 & \sum X_i \\ \sum X_i & N \end{vmatrix}} \end{cases}, \quad (40)$$

where  $N = (\text{Numbers of sun - regions in ROI}) + 1$

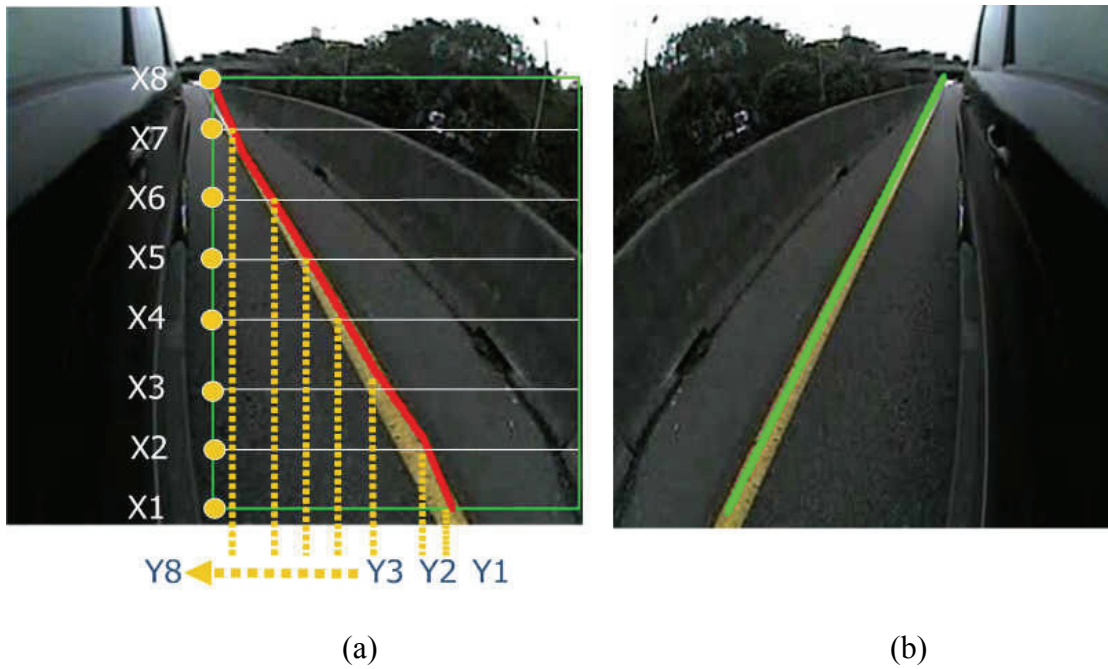


Fig. 55: LSR approximation.

According to the parameter information showed in Fig. 55(a), the linear model can be constructed by the equations (39), (40). The approximating straight lane boundary is displayed in Fig. 55(b), which is directly reflected since the image contents acquired by the camera mounted on the opposite side of the vehicle are

almost the same except for the reflective property.

### 5.3 Lane Departure Warning

Some algorithm has been developed to predict when the driver is in danger of departing the road but not annoy the driver sensitively. In other words, extending the interval of warning time can receive the more correct driving maneuver, but the number of nuisance alarms will increase apparently. Lee [63] and Ruder [64] considered that LDW does not necessarily need the precise offset and position information from each frame to add the computing load since it only assists the human driver and passively responds to the circumstance such as when the lane-departure occurs. In order to balance the systematic efficiency and acceptable detection rate in our LDW system, only two representative measures are selected to trigger the warning message. The two judging conditions are discussed as follows:

#### (1) Lateral displacement:

If the lane boundary is excessively close to the vertical borders of ROI, the driver will be in danger with higher possibility. We will regard this as a dangerous departing behavior even if it may be only someone's habit of driving. There, the safe region which contains the normal lateral offset of lanes is defined as follows.

$$\text{Safe Region} : \left\{ \frac{1}{4} ROI, \frac{4}{5} ROI \right\}$$

#### (2) TLC (time to lane crossing):

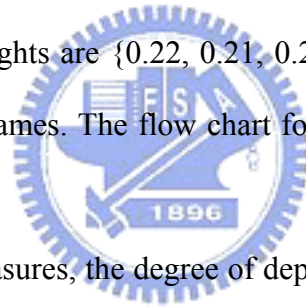
TLC which was first proposed by Godthelp [65], is a measure of the time remaining before a vehicle on a given trajectory will depart the road. It can provide



more reliable information than the lateral position merely due to the factor for lateral velocity can be considered. In our system, the definition of TLC is a ratio of lateral offset smaller than the width of ROI to the lateral velocity at the moment.

The classification for the dangerous degree of warning alarms and the deducing process of TLC are explained in details in the next section.

To prevent the noisy effect such as high frequency variances of the lateral offset of lane markers in each frame from measuring error, we take five frames processed by lane detection to estimate only one weighted average result for departure judgment such like a causal temporal filter. (In practice, there is always one frame only for Gaussian smoothing between the two frames used for lane detection in our system. In other words, consecutive five numbers of lateral positions occupy about 0.33 seconds for 30fps.) The values of weights are {0.22, 0.21, 0.20, 0.19, 0.18} from the present and the last four processed frames. The flow chart for TLC computation is shown in Fig. 56.



By the two obvious measures, the degree of departure warning can be classified with the color of alarms as the following:

if the current lateral offset is inside the safe region :  $\left\{ \frac{1}{4} ROI, \frac{4}{5} ROI \right\}$   
     if  $TLC \geq 2.5 \text{ sec} \ \& \ Vel \neq 0$   
         Alarm type : green light  
     else  
         Alarm type : yellow light  
   else  
     Alarm type : red light

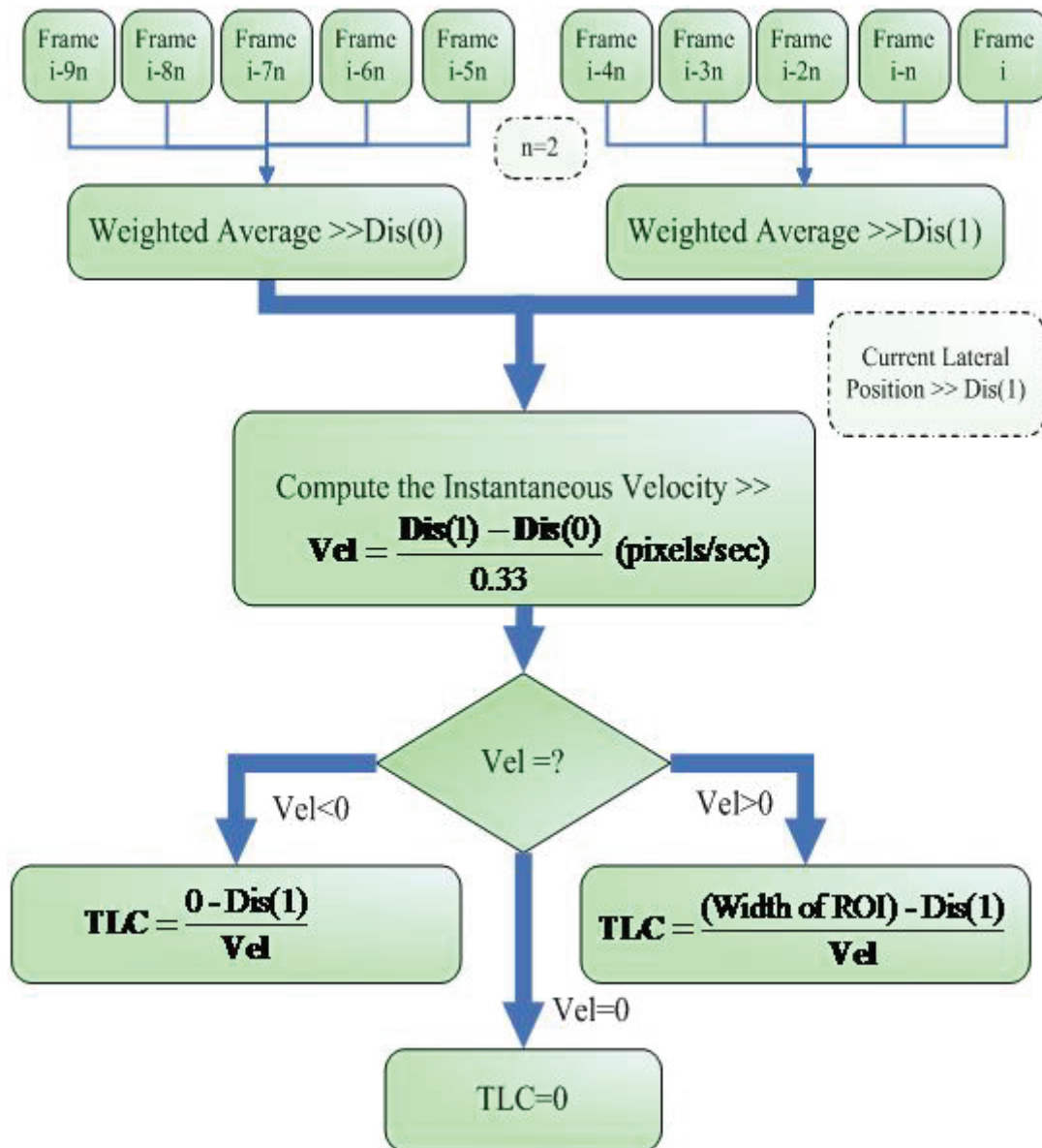


Fig. 56: The flow chart for TLC estimation.

## 5.4 Experimental Results

Fig. 57 shows that a fish-eye camera is mounted under the rear-view mirror on the side of the vehicle to acquire blind-spot view image sequences. In addition, the driver can immediately obtain the sideward information of road surface by the CRT which displays the real-time image sequences from the outside camera.



Fig. 57: The experimental architecture.

Table 11: Specification of platform information

CPU	Intel T5600 1.83GHz
Memory	1GB DDR2 RAM
Compiler	Borland C++ Builder 6.0
OS	Microsoft Windows XP
Resolution	320x240
Frame rate	30 FPS

Fig. 58 shows the realistic programming interface in the PC platform. Block (A) contains the input frame which is added the approximating straight lane boundary by LSR, as explained in Chapter 3, in the left part; the center part of (A) shows the result of lane detection method with ROI extraction; the right part of (A) which shows the

binarizing lane boundary only includes the image contents within ROI.

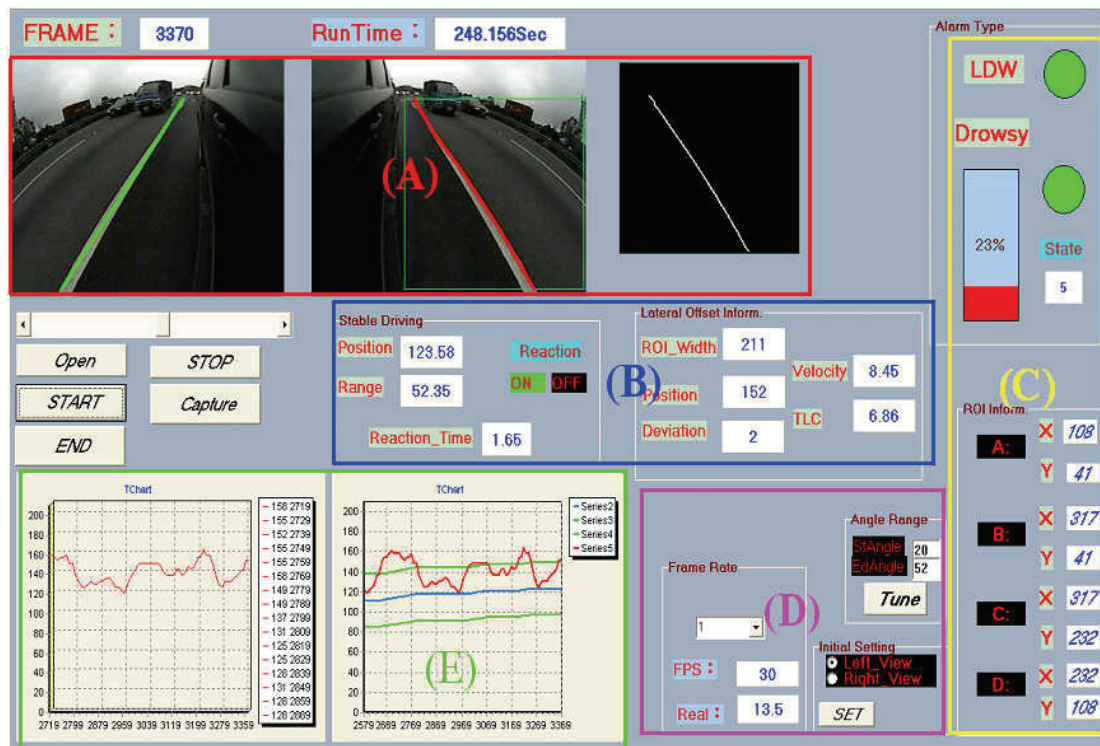


Fig. 58: The programming interface in the PC platform.

Block (B) contains the display of the related lateral information computed by LDW system. The warning alarms with different colors of lane of LDW and drowsiness estimation systems is contained by Block (C), where the coordinate values about the border of ROI are also included. Block (D) shows the searching range of angles about the piece-wise edge linking model, and the output frame rate which responds to the systematic performance. At last, Block (E) records the lateral offset and the maximum and minimum range of the reconstructed stable-driving distribution with real-time update.

- **Explanation of Experimental Conditions**

The driving environment is focused on highway with different light conditions.

The image sequences captured by the camera with unknown two pan- or tilt-angles are tested with the same lane detection algorithm in Fig. 59. At the same time, in order to observe if the lane-based warning system can maintain robust performance and tolerate the light variation, we select the video segments with three different periods, daytime, evening, and night of one day for experiment in the next section.



Fig. 59: The testing image with different mounting angles.

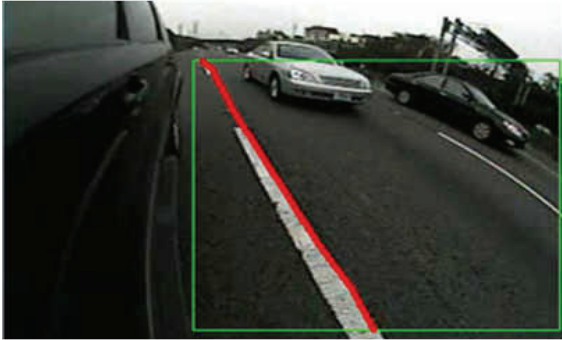
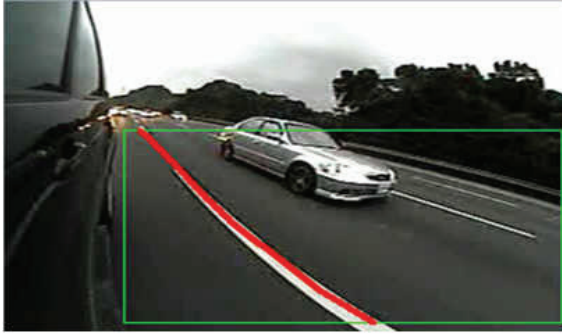
- Results of Lane Detection

In Fig. 60, the testing environment considers the two properties with respect to the view-angles and light conditions simultaneously. The detection results of daytime (a), evening (b), and night (c) are processed by the same programming setting.

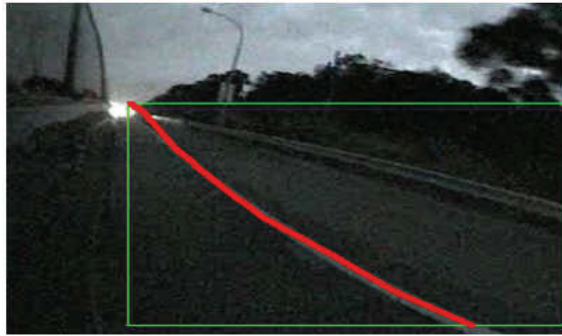
In Fig. 60 (c), the lane boundary can be clearly extracted in the nighttime driving environment even if the side-view of vehicle usually has more chances to subject to the perturbation from the exterior light-sources.

- Results of Lane Departure Warning

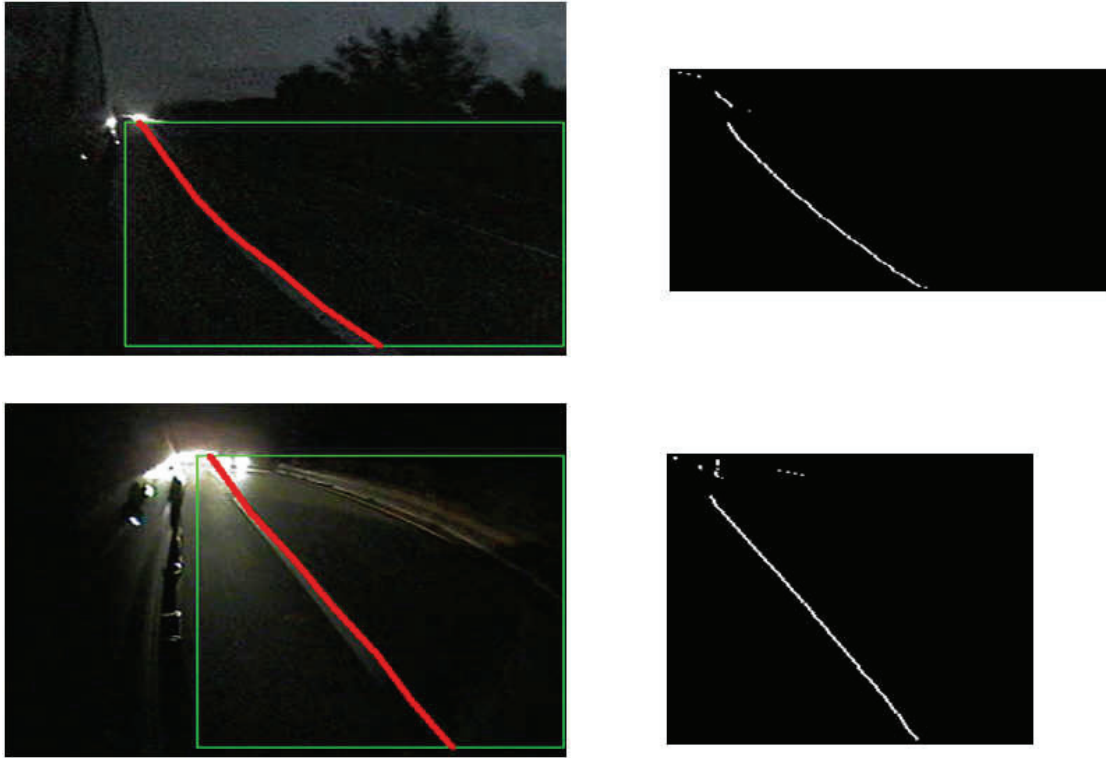
If the lane boundary is locked precisely by the lane detection mechanism, the lane departing maneuver can be tracked and recorded its position whether the lateral speed is faster or not. Fig. 61, Fig. 62, and Fig. 63 show the tracking results of the lane departure with different variations of light and moving direction of the vehicle.



(a)



(b)



(c)

Fig. 60: The results of lane detection.



# Frame 3293

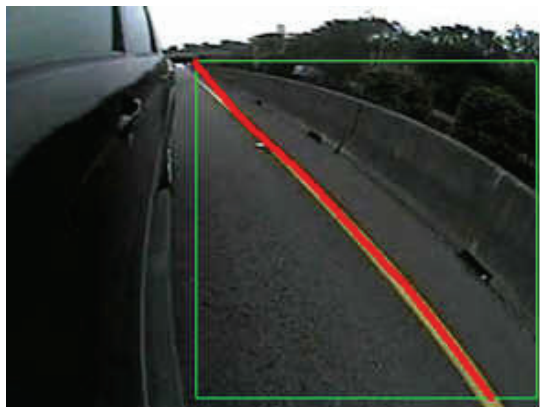
# Frame 3299



# Frame 3305



# Frame 3310



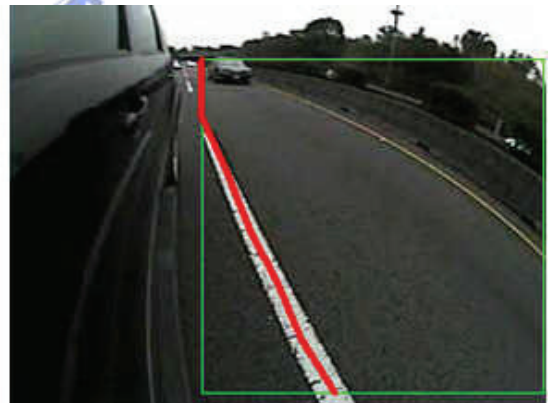
# Frame 3316



# Frame 3334



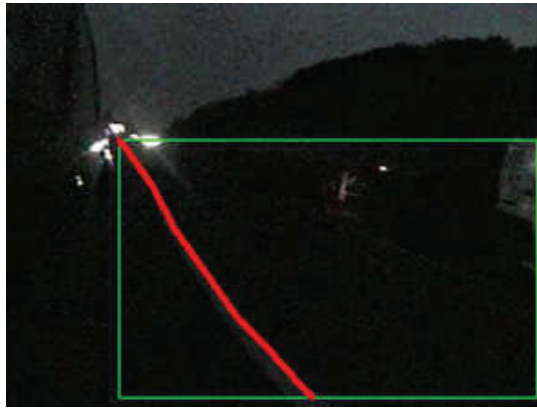
# Frame 3385



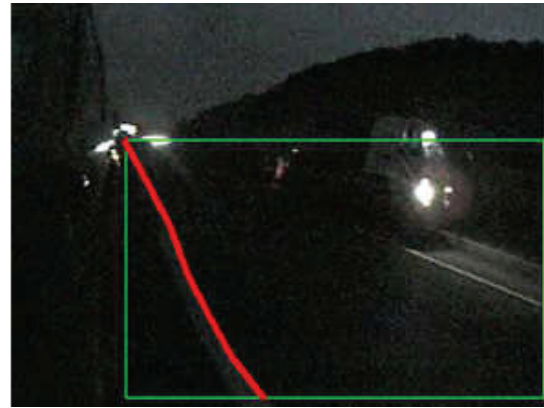
# Frame 3388

Fig. 61: The results of lane departure caused by cutting into the inside lane.

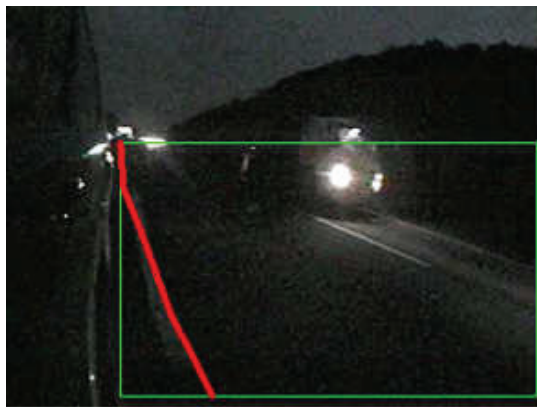




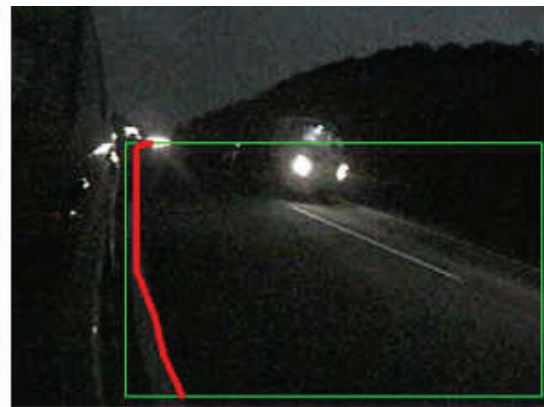
# Frame 693



# Frame 718



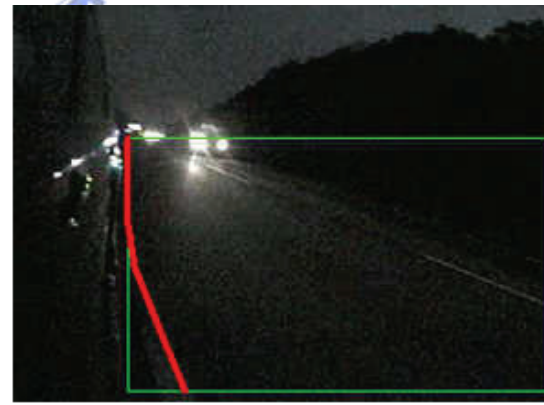
# Frame 733



# Frame 746



# Frame 787



# Frame 818

Fig. 62: The results of lane departure in the night time.

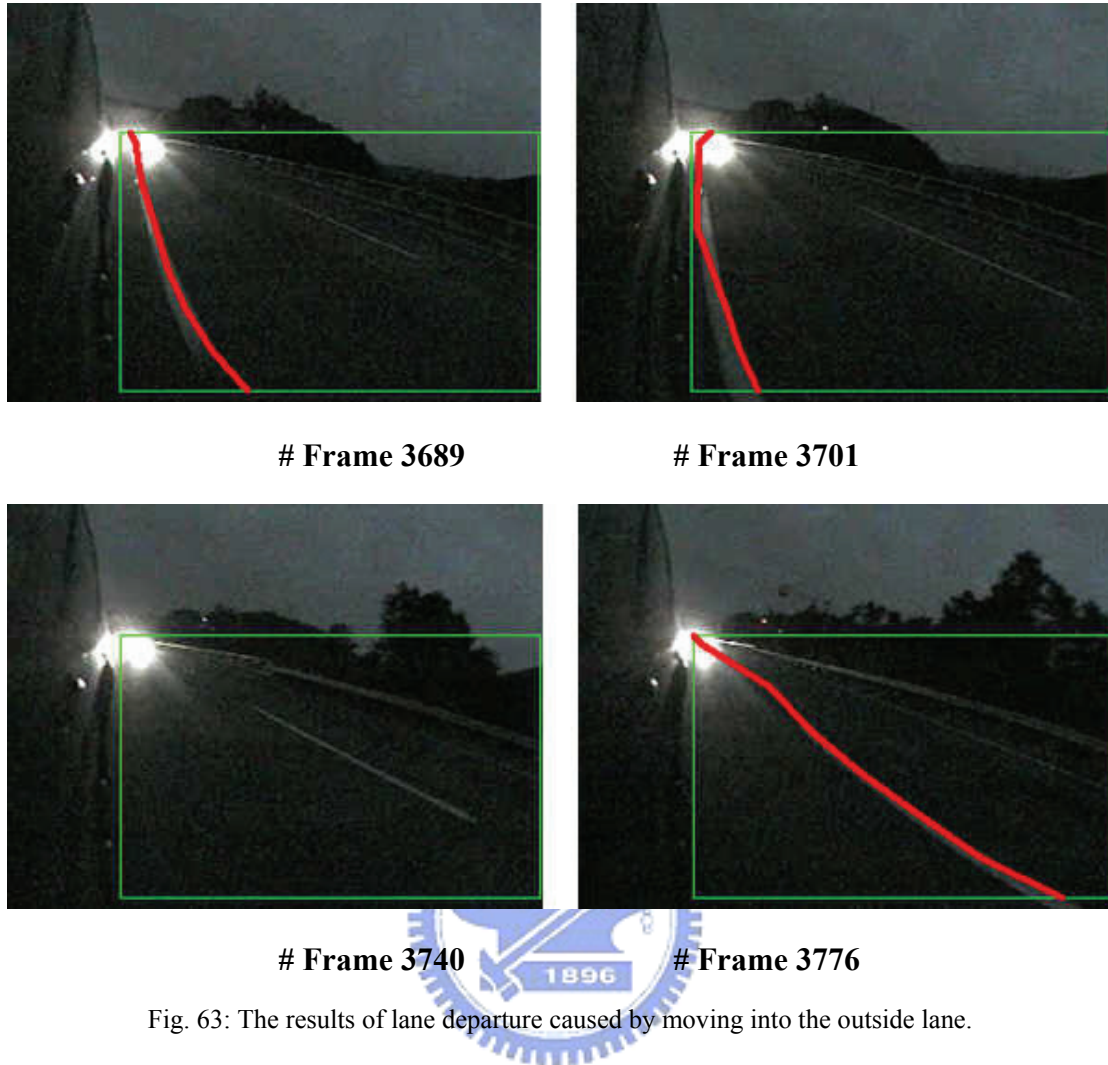


Fig. 63: The results of lane departure caused by moving into the outside lane.

## 5.5 Summary

In order to increase detection rate of LDW and drowsiness estimation system, the lane detecting error must be low as much as possible even if this algorithm is always subjected to the disturbance resulted from external factors. In Fig. 64, the lane markers can be still extracted by our developing method although they are unclear. However, the lane detection method we proposed in this thesis can not resolved some cases such as driving in a tunnel so that the contrast between lane markers and road surface is not enough, as shown in Fig. 65(a).



Fig. 64: Results of lane detection for the unclear lane markers.



(a)

(b)



(c)

Fig. 65: Some examples of detecting error in our lane detection system.

In addition, as explained in section 5.2.1, the range of ROI can be detected by the boundary information of the car window and that of the horizon in the image. But this property may be not suited to the environment which does not only contain the above clues for ROI extraction but be affected by the light conditions, such as the example shown in Fig. 65 (B). On the other hand, the external light in the nighttime has chance to produce a “light ring” effect on the camera lens which may cause the deviated parting position of the detected lane markers in the image instantaneously, as shown in Fig. 65(c).



## Chapter 6 Driver Assistance Alarm System

The lane departure warning system is to provide some triggers for caution with respect to the driving-off-road behavior through the lateral information of the lane extracted by the lane detection algorithm. After measuring the lateral velocity from the consecutive frames, the warning system will determine when the departure driving occurs based on the lateral displacement and TLC (time to lane crossing.)

On the other hand, the part for drowsiness prediction will try to combine the experimental results of BRC (Brain Research Center) from NCTU with the realistic driving video. In order to estimate the lateral location of lane where the driver gets used to navigate on the straight road, we construct the single Gaussian model to simulate the stable-state range about the lane position. Then, the additional updating mechanism will contribute to the systematic adaptation even if the driver changes his/her driving habits. At last, the proportional gauge of the drowsy degree we proposed will show if the driver has higher or lower probability in the drowsy state at that moment with the amount of reflection time measured by the lane position over the stable-state region.

### 6.1 Drowsiness Estimation

In recent years, preventing accidents caused by drowsiness has become a major focus of active safety driving. The major challenges in developing a real-time system for drowsiness prediction include: 1) the lack of significant index for detecting drowsiness and 2) complicated and pervasive noise interferences in a realistic driving environment. Therefore, the BRC (Brain Research Center) in National Chiao Tung University has developed a drowsiness-estimation system based on

electroencephalogram (EEG) to estimate a driver's cognitive state when he/she drives in a virtual reality (VR)-based dynamic simulator. The definition of the driving error in this experimental environment is the deviations between the center of the vehicle and the center of the cruising lane in the lane-keeping driving task.

In this section, the system architecture of BRC will be introduced in section 6.1.1. The relationship between the reaction time and driver's drowsiness will be explained in section 6.1.2. Before trying to reasonably and effectively integrate the measuring result from the VR-based driving environment into the lane detection system in this thesis, some changeable factors of the realistic image-based system must be discussed. In section 6.2.1, a stable-state range can be constructed to determine the lane's lateral position where someone gets used to driving in a straight road-path for a long time. Then, a gauge of the drowsy degree successfully combine the experimental result evaluated by the EEG-based analysis [66] with the realistic and dynamic LDW system successfully is proposed in this thesis, as described in section 6.2.2. Finally, in order to adaptively extend the experimental framework to the practical driving environment, we estimate the average velocity within the interval of reaction time by deducing the ratio of the lane-width on the realistic road plane to that in the video, as explained in section 6.2.2.

### **6.1.1 Experimental Architecture of BRC**

In general, measuring the precise data for human consciousness in dynamic driving environment is not easy. There may be some perturbations from the external noise or suddenly interference caused by the traffic variations affecting the data accuracy. In other words, strict training of human operators by the actual machines or vehicles in real sites not only has high demands in space, time, and money to perform such a training job, but also leads to another phase of the measuring problem. To

overcome the above dilemma, the worldwide trend is to use the virtual-reality (VR) technology to meet the requirements of public security in training and censoring of human operators. It can provide a realistic safety environment, which allows subjects to make on-line decisions by directly interacting with a virtual object rather than monotonic auditory and visual signals. Besides, VR is also an excellent candidate for brain research on real-time tasks because of its low cost, saving time, less space, and condition control to avoid the risk of operating on the actual machines, and thus extends the applications of possible brain computer interfaces to general populations.



Fig. 66: The VR-based dynamic driving simulation laboratory.

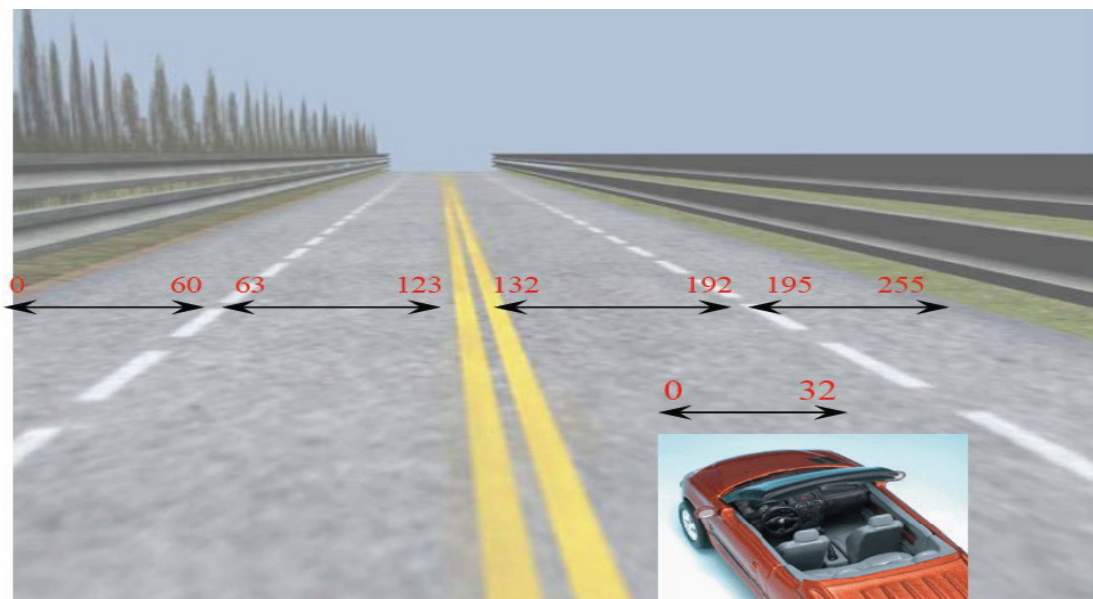


Fig. 67: The details about the width information of each lane, road, and car.

The experimental environment constructed by BRC is shown in Fig. 66. The

VR-based four lane highway scene is projected on a 120 degree-surround screen (304.1-cm wide and 228.1-cm high), which is 350 cm away from the driving cabin. The four lanes from left to right are separated by a median stripe. The distance from the left side to the right side of the road is equally divided into 256 points (digitized into values 0-255), where the width of each lane and the car is 60 and 32 units, respectively. The frame rate of highway scene is 60 fps. All the descriptions are depicted in Fig. 67.

### **6.1.2 Predictive Mechanism for Drowsiness Effect**

Before executing the experimental step, we have to find the relationship between the measured EEG signal and the subject's behavior performance. One point should be taken as a quantified index as the deviation between the center of the vehicle and that of the cruising lane [67]. By examining the video recordings, the pilot experimental studies show that when the subject is drowsy, the driving performance will decrease and vice versa. In this experiment, the subjects participated in the highway-driving simulation after lunch in the early afternoon when the alertness may easily diminish within one-hour monotonous working [68].

All the subjects were instructed to keep the car at the center of cruising lane by controlling a steering wheel. In all sessions, the subjects drive the car continuously for 60 minutes and are asked to try their best to stay alert. Participants then return on different days to complete a second 60-minute driving session or more if necessary. To mimic the consequences of a non-ideal road surface, the car is randomly drifted away from the center of the cruising lane every 5 or 10 minutes. So the driver must maintain high attention to immediately correct the direction of vehicle in the cruising lane due to the 60 pixels per second for the deviating velocity. When the driver is drowsy, the reaction time between the onset of deviation and steering wheel is



increased. This event can be used for ERP analysis of different drowsiness states using 30-channel EEG signals [66].

In general, the reaction behavior should be increasingly slower when people start to enter the drowsy state. In other words, the higher possibility for the measurement shows that the subject is drowsy when his/her average reaction time is gradually longer in a section of time interval. To avoid the fluctuation of drowsiness signal, the measured data for reaction time must be smoothed by a causal 90-second square moving average filter advancing at 2-seconds steps. The experimental trials are sorted according to the length of reaction time and equally divided into five groups as the index for drowsiness estimation in Fig. 68, where each group has 20 percentages of trials in order. This statistics evaluated by the EEG analysis [66] can be regarded as the reference implemented into our vision based lane departure warning system.

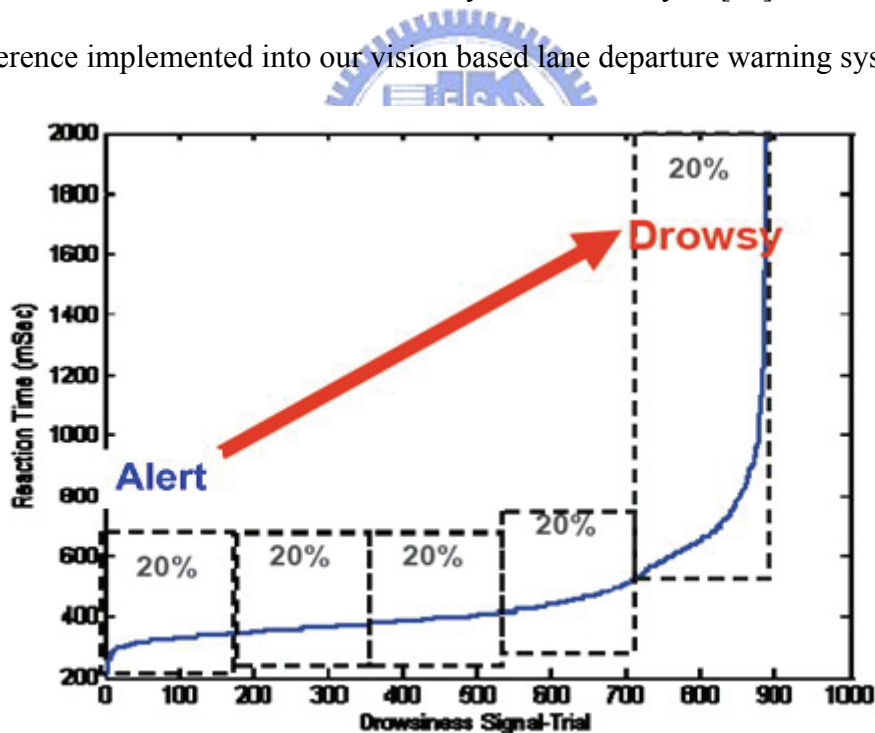


Fig. 68: The trials collected from the VR-based experiment are sorted according to the degree of reaction time.

## 6.2 Driving in Danger Analysis

### 6.2.1 Construct the Stable-Driving Region with Different Driver's Habit

According to the above experimental condition, the definition of reaction time is the duration between the onset of deviation and the occurrence for steering-wheel. Subjects have to move the vehicle's center back to the cruising lane to wait for the next testing deviation produced by the computer when they have been informed in advance. However, the restarting action is not easy to be determined due to the variation of different driving habits, especially the loose drivers which have a larger spread in lateral position so that the distance between the wheel and lane marker can not exactly fixed in the straight-road driving [69]. Therefore, the algorithm to extract the stable-state driving region must be developed before constructing the drowsiness estimation mechanism.

The standard for stable-state range determination is described as below: (1) the lateral position of lane markers within this region should be close to each other; (2) the TLC is larger; (3) The lateral offsets found by the LDW system in section 5.3 must be situated in this region for a long period.

According to the above properties, first of all, we take the lateral offsets with larger TLC about consecutive N frames processed by the LDW system. Second, by the previous statistics, the mean and standard deviation estimated by them with the clustering method are used to model the stable-state region as a normal distribution. At last, the updating method is developed to adjust the size and location of the range to the changed driving habit for a driver. The flow chart for stable-state region determination is demonstrated in Fig. 69.

To rapidly and precisely find out the optimal parameters of each normal distribution, we choose k-means to initially classify the statistics of N lateral offsets.

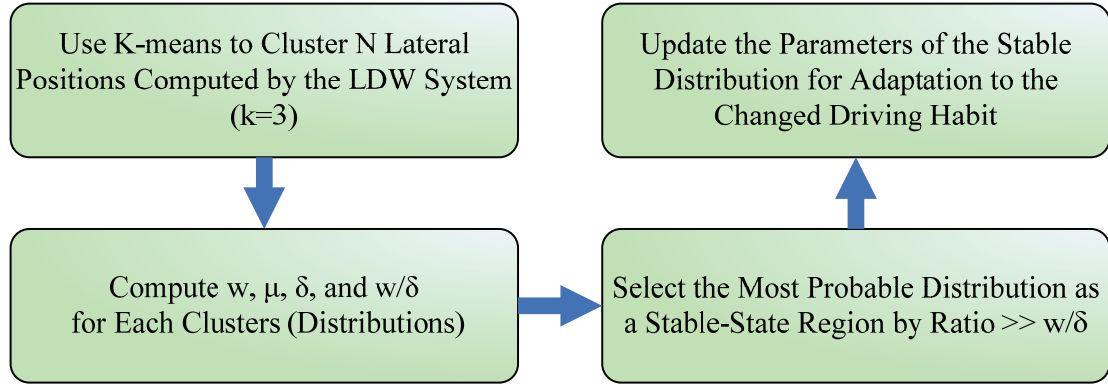


Fig. 69: The flow chart for stable-state region determination.

The error function which determines the clustering center point of each group is shown as follows:

$$d_i = \sum_{j=1}^k \sum_{x_j \in P_i} (x_j - \mu_i)^2 \quad (41)$$

where  $\mu_i$  is the centroid or mean point of all the points  $x_j \in P_i$   
 $P_i$  is  $i$ -th of  $k$  clusters,  $i=1,2,\dots,k$

In Fig. 69,  $\mu$  is the mean value of each distribution;  $\delta$  is the standard deviation of each distribution;  $w$  is the weight determined by the probability of each group. After initializing for each distribution model, we find that the  $N$  lateral offsets can be approximately modeled by only three normal distributions, which are respectively located on the points nearby the mean value and 1.5 standard deviations with high probably, as shown in Fig. 70. Therefore, we choose  $K=3$  as the initial clustering numbers.

Not the same as the adaptive background model [70], the human habit can last within a steady behavior style for a long time. Based on this psychological property, we only use a single normal distribution with some update mechanism to model the adaptive stable-state driving region to avoid its unreasonable fluctuation. Updating

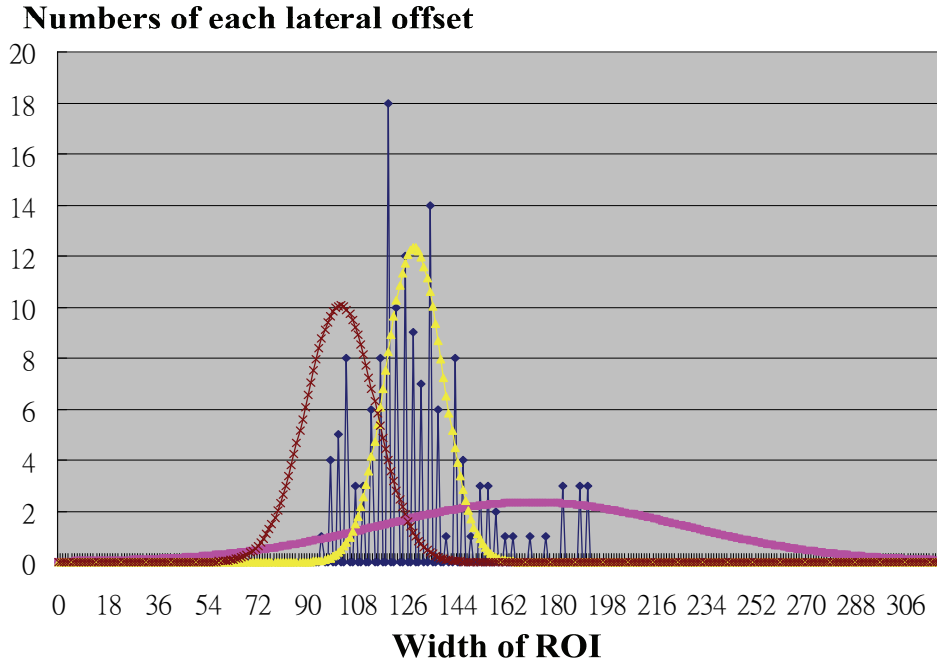


Fig. 70: The distribution of N lateral offsets and three approximately Gaussian model (N=200 in this Figure.)

the parameters of the stable-state model can adapt to the changed driving habit if the lateral offset is within 2.25 standard deviations of this distribution. The parameters of the distribution which matches the new observation for human habit are updated as follows:

$$\mu_t = (1 - \beta) \cdot \mu_{t-1} + \beta \cdot x_t \quad (42)$$

$$\sigma_t^2 = (1 - \beta) \cdot \sigma_{t-1}^2 + \beta \cdot (x_t - \mu_t)^2 \quad (43)$$

where

$$\beta = \alpha \cdot \eta(x_t | \mu_k, \sigma_t), \alpha \text{ is the learning rate} \quad (44)$$

$$\eta(x_t, \mu_t, \sigma_t) = \frac{1}{(2\pi)^{1/2} \cdot \sigma_t} \cdot e^{-\frac{1}{2}(x_t - \mu_t)^2 \cdot \sigma_t^{-1}} \quad (45)$$

By observing equation (49), the influence for this stable-driving distribution will

be unapparent when the distance between the current lateral offset and the mean value of the model is so far. This property can effectively maintain the stability of this region.

## 6.2.2 Data Collection and Adjustment for the Realistic Environment

After selecting the suitable driving region for the driver, the experimental statistics evaluated by EEG analysis from BRC can be integrated into our lane departure system. Not the same as experimental condition which stipulated that the reaction behavior can be increasingly slower when the subject starts to enter the drowsy state by observing the trend of reaction time for a long period (about 90 sec), the demand for drowsy estimation mechanism in our system should provide a real-time prediction if the driver is still on the alert. Therefore, we design a gauge chart to estimate and display the current driver's drowsy degree as much as possible, as shown in Fig. 71 (b).

In Fig. 71 (a), the difference in lateral offset between (B) and (C) is 52.45 pixels, the mean value (A) of stable-driving region is located at pixel value of 123.23, and the reaction time counted from (D) and (E) is 1.65sec, as shown in Fig. 71 (c).

As described in section 6.1.2, the definition of reaction time is the time interval of deviation between the center of the vehicle and that of the cruising lane in the VR-based experimental environment. In other words, the value of deviation can be the same as the lateral offset between the car-body and the lane marker in our vision-based system. By the known stable-driving region determined in section 6.2.1, the drowsiness estimation system can apply to drivers with different driving habits without directly selecting the unchanged center part of ROI, such as the restarting mechanism of BRC. Therefore, the count of reaction time starts when the lateral offset of lane marker deviates outside the stable region, and stops when the driver turns back

the steering wheel exactly in our system. However, since we judge the reactive behavior only by the image contents, the backward motion must be confirmed by the criterion that the direction of the lateral velocity keeps identical until the lateral offset is within the stable region again, as the points (D) and (E) in Fig. 71 (d) separately.

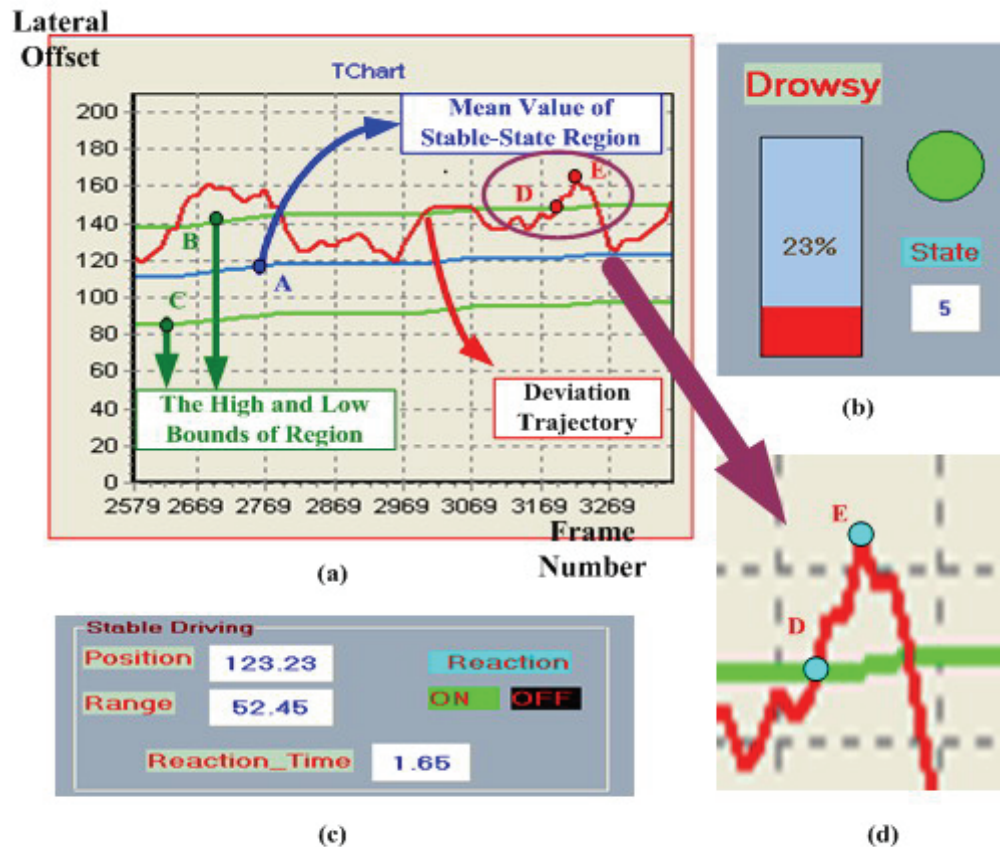


Fig. 71: The mechanism for drowsiness estimation in our LDW system. (a) The relationship between the stable-state region and the lateral deviations. (b) A drowsy-degree gauge chart. (c) A stable-driving group box, (d) The start and stop points of reaction time.

The flow chart for drowsy degree estimation by the reaction time is shown in Fig. 72.

The discussions about Fig. 72 are described as follows:

(1) The drowsy degree may be subtracted by 10% if the reaction time is never up to 1.5sec for 10sec. This automatic mechanism is based on the VR-based experiment of BRC that the computer will automatically produce the deviation behavior about 5~10sec. After all, the reactive behavior in drowsy state must be

increasingly slower without reducing the alert abruptly.

(2) The variation of drowsy degree displayed in the gauge chart, as demonstrated in Fig. 71 (b), depends on the estimated reaction time of the driver in the realistic environment. To avoid the variances in drowsy degree violating the nature of human operation, the changeful region for each estimation result is limited within plus and minus 20%.

(3) Use the classified alert and drowsy state in Fig. 68 analyzed by EEG-based algorithm as the evidence to determine the cognitive property of the driver in realistic environment.

(4) If the drowsy degree is exceeded 70%, the alarm light with red color will be displayed in our system. On the other words, the alarm light with yellow color will be turned on if the drowsy degree is exceeded 35% but not up to 70%. Otherwise, the green light is showed that the driver is still situated in the safety-state with higher alert.

(5) In general, the lane change maneuver can be not certainly judged as an intentional action for driving or an unintentional behavior with the drowsy consciousness only by the information of deviations. Therefore, the warning mechanism focused on this departing behavior is described as below:

```
if Pos(t) - Pos(t - k) > 0.8(width of ROI)
    ///This departing motion is recognized as the lane change maneuver
    if Drowsy Degree ≥ 70% (red light)
        Not change // Cause by the drowsy consciousness
    else
        Drowsy Degree = 0 // caused by intentional brhavior for normal driving
where
Pos(t) : The currently measured lateral offset.
Pos(t - k) : The previously measured lateral offset, k is dependent on the frame rate of video
```

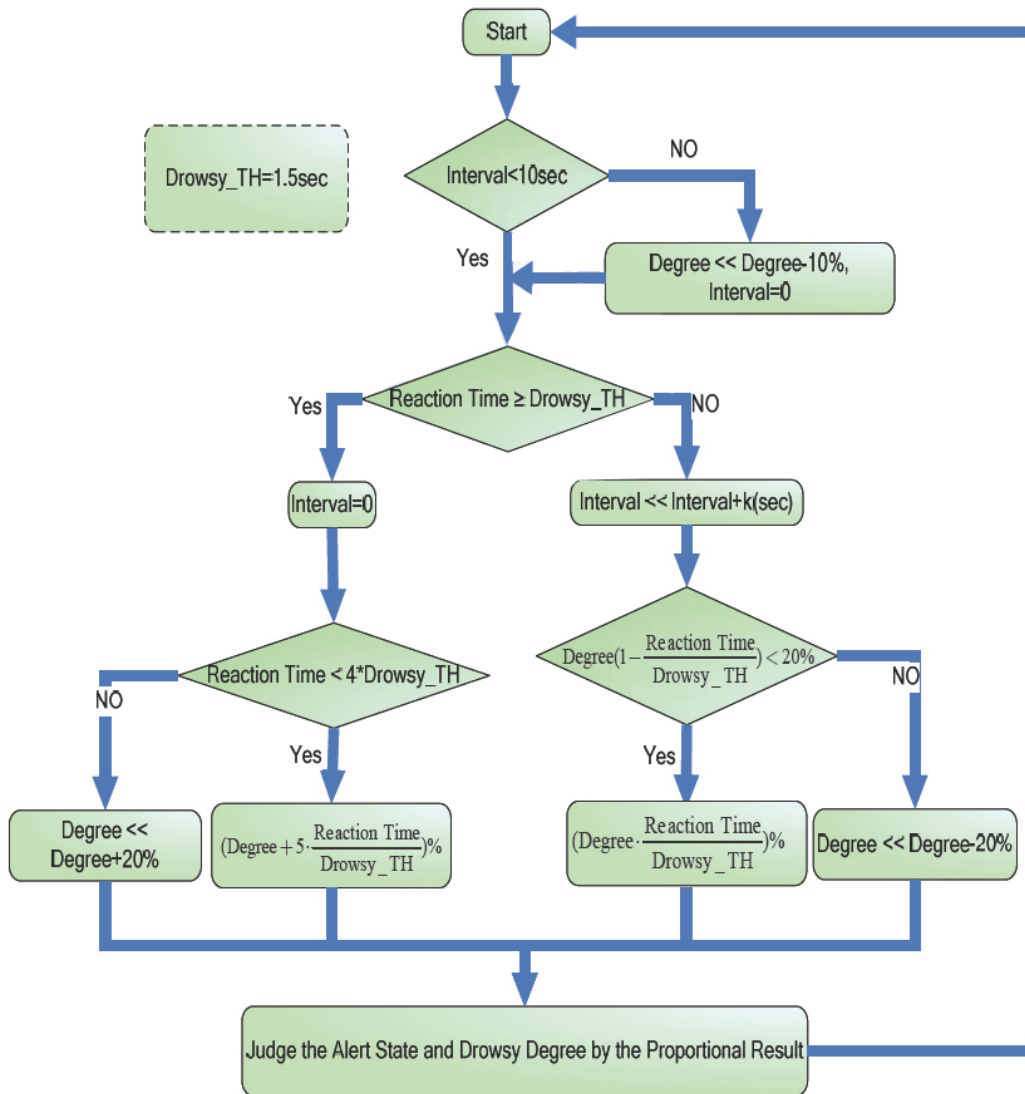


Fig. 72 : The flow chart of drowsy degree estimation by the average reaction time evaluated from BRC.

### 6.3 Summary

As described in section 6.2.1, the straight-road driving distance between the lane marker and wheels can be modeled by the clustered distribution with higher weight and smaller standard deviation. For further adaptation, we develop an update mechanism to make the stable region adaptive to the changeful driving habits of people. Fig. 73 shows the updating process of stable-region described as a statistical chart which contains the information of lateral offsets at the same time. From Fig. 73



(a) to (d), the mean value of the stable-region will increase obviously due to the accumulated lateral offsets which are almost situated over the region and can be regarded as the new driving habit of the driver adequately.

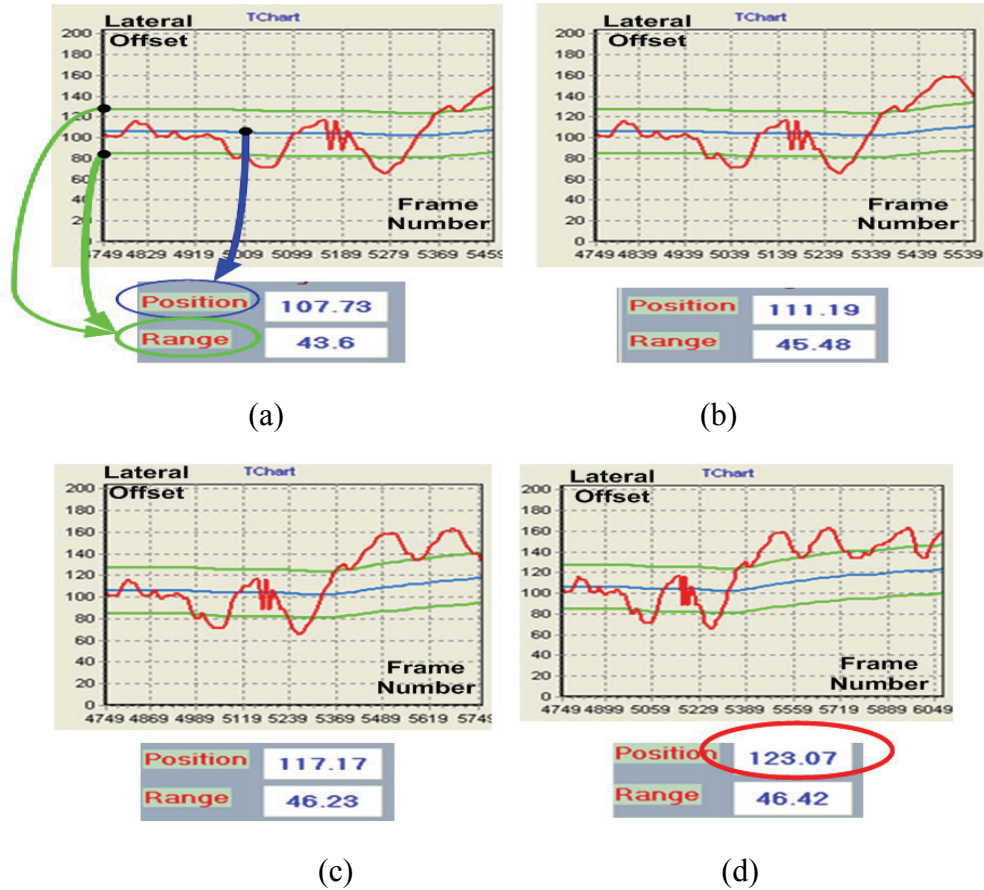
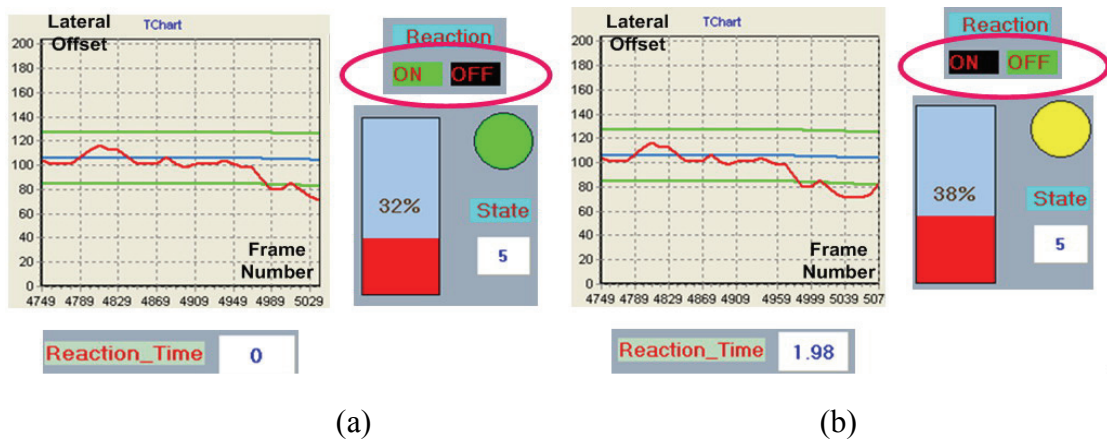


Fig. 73: Results of update for the stable-driving region.



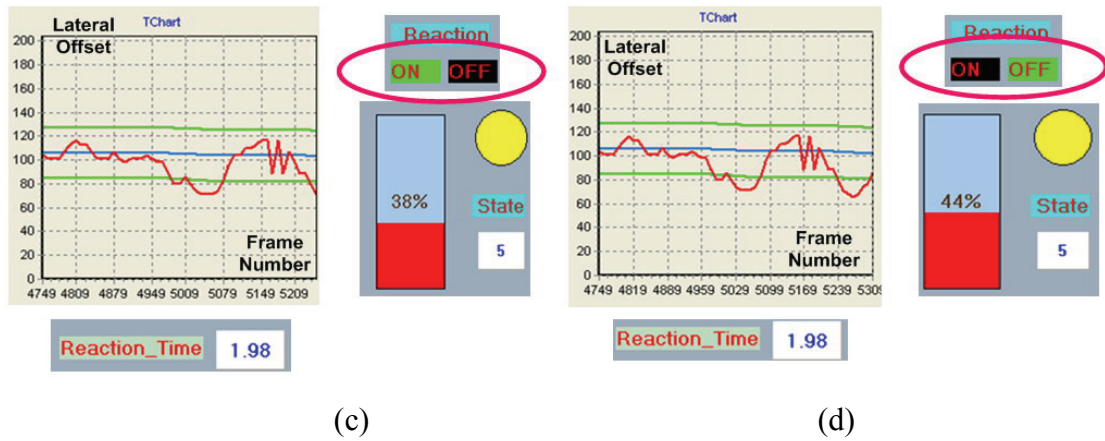


Fig. 74: Results of the variation of drivers' drowsy degree by the reaction time.

The relationship between the gauge chart of drowsy degree and the reaction time of drivers is demonstrated in Fig. 74. From Fig. 74 (a) to (b), the reaction time will start to be counted since the lateral offset is outside the stable-region at that moment. Therefore, the drowsy degree can be raised with a specific ratio of the measured reaction time to the threshold which has been evaluated by the EGG-based analysis from BRC. On the other hand, from Fig. 74 (c) to (d), the drowsy degree keeps increasing because the time interval between the current and previous reaction time which are both greater than the threshold is not for 10 sec.

# Chapter 7 Realization on Embedded Real-Time System

## 7.1 Introduction

In the early years of computers, computers were always dedicated to specific single function, and it was hard to call computers “embedded” due to the size of computers, cost of computers, performance of computers, and power consumption of computers. For the ideal to perform high performance, low cost, portability, and long battery life with a single function computer, the computer structure of embedded systems are designed differently from general-purpose computers. Hence, cross-platform development and programming techniques are used for developing embedded applications. The cross-platform development framework is shown as Fig. 75.

In this chapter, the development environment is divided into three parts. First of all, the overall development framework which is cross-platform development technique will be described in section 7.2. Second, the hardware specification will be described in section 7.3. Finally, the software optimization will be described in section 7.4.

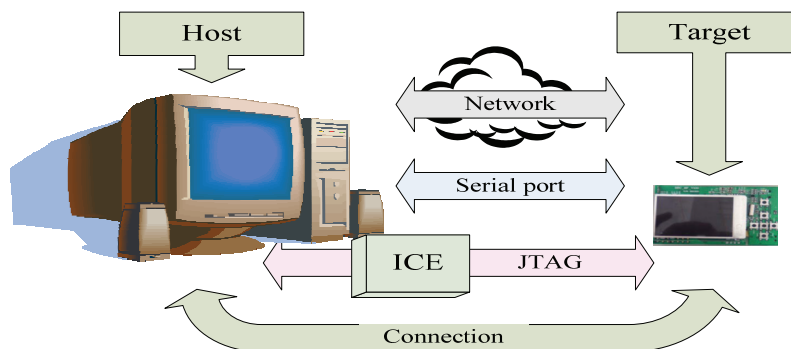


Fig. 75: Cross-platform development framework

## 7.2 Cross-Platform Development Framework

Owing to the lack of available resources on embedded systems, the cross-compilation, code editing, code linking, and source debugging are performed on powerful host PC. The system software, operating system, and application programs are first compiled as object codes. Then the linker on the host links up object codes and forms an executable image. Thus we have to understand thoroughly how executable images are downloaded to the target embedded systems. Executable image can be downloaded via internet, UART (Universal Asynchronous Receiver Transmitter), and ICE (In-Circuit Emulator).

## 7.3 Hardware Environment

In this thesis, the selected core processor is ADSP-BF561. The evaluation board is developed by Analog Devices Inc. The detailed hardware structure will be described below.

### 7.3.1 Introduction to Black-Fin 561 Processor

The Blackfin Processor family pushes the performance envelope with the ADSP-BF561. With two high performance Blackfin Processor cores, flexible cache architecture, enhanced DMA subsystem, and Dynamic Power Management (DPM) functionality, the ADSP-BF561 can support complex control and signal processing tasks while maintaining extremely high data throughput. The ADSP-BF561 is a functional extension of the popular Blackfin Processor family and is ideally suited for a broad range of industrial, instrumentation, medical, and consumer appliance applications—allowing for scalability based upon the required data bandwidth and

mix of control, plus signal processing needed in the end product.

The ADSP-BF561 has two identical Blackfin cores and each core contains two 16-bit multipliers, two 40-bit accumulators, two 40-bit arithmetic logic units (ALUs), four 8-bit video ALUs, and a 40-bit shifter, along with the functional units of each core as shown in Fig. 76. The computational units process 8-, 16-, or 32-bit data from the register file. All the functional units of each core are described below.

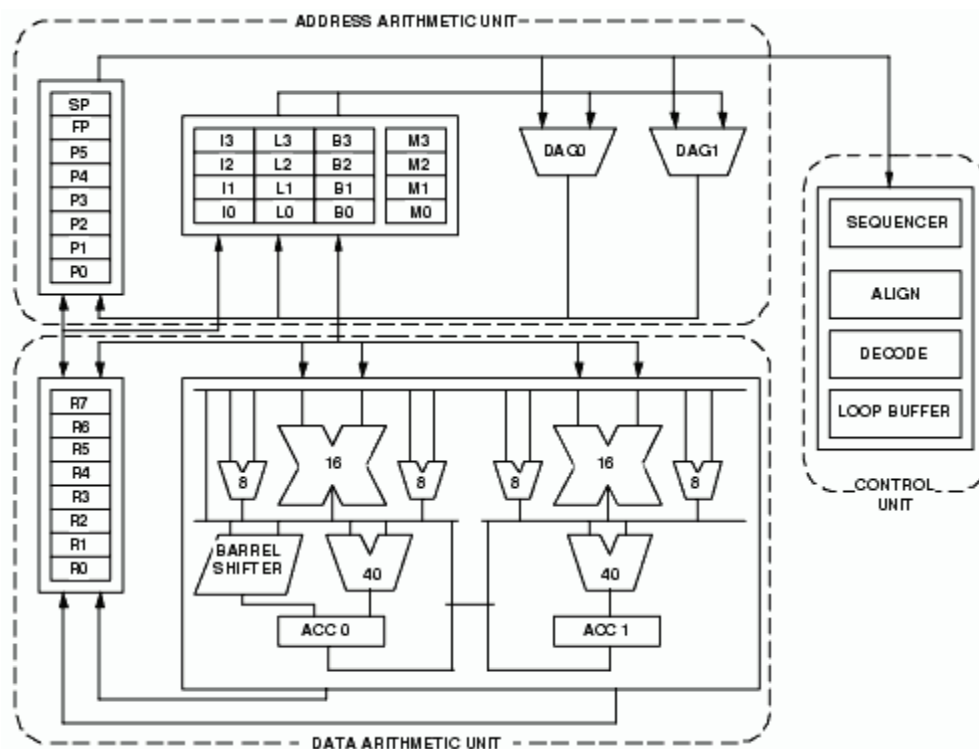


Fig. 76: Core Architecture of each ADSP-BF561 Core

The compute register file contains eight 32-bit registers. When performing compute operations on 16-bit operand data, the register file operates as 16 independent 16-bit registers. All operands for compute operations come from the multi-ported register file and instruction constant fields.

Each MAC can perform a 16- by 16-bit multiply per cycle, with accumulation to a 40-bit result. Signed and unsigned formats, rounding, and saturation are supported.

The ALUs perform a traditional set of arithmetic and logical operations on 16-bit or 32-bit data. Many special instructions are included to accelerate various signal processing tasks. These include bit operations such as field extract and population count, modulo 232 multiply, divide primitives, saturation and rounding, and sign/exponent detection. The set of video instructions includes byte alignment and packing operations, 16-bit and 8-bit adds with clipping, 8-bit average operations, and 8-bit subtract/absolute value/accumulate (SAA) operations. Also provided are the compare/select and vector search instructions. For some instructions, two 16-bit ALU operations can be performed simultaneously on register pairs (a 16-bit high half and 16-bit low half of a compute register). By also using the second ALU, quad 16-bit operations are possible.

The 40-bit shifter can deposit data and perform shifting, rotating, normalization, and extraction operations.

A program sequencer controls the instruction execution flow, including instruction alignment and decoding. For the program flow control, the sequencer supports PC-relative and indirect conditional jumps (with static branch prediction), and subroutine calls. Hardware is provided to support zero-overhead looping. The architecture is fully interlocked, meaning that there are no visible pipeline effects when executing instructions with data dependencies.

The address arithmetic unit provides two addresses for simultaneous dual fetches from memory. It contains a multi-ported register file consisting of four sets of 32-bit Index, Modify, Length, and Base registers (for circular buffering), and eight additional 32-bit pointer registers (for C-style indexed stack manipulation).

Blackfin products support a modified Harvard architecture in combination with a hierarchical memory structure. Level 1 (L1) memories typically operate at the full processor speed with little or no latency. At the L1 level, the instruction memory

holds instructions, the data memories hold data, and a dedicated scratchpad data memory stores stack and local variable information.

Multiple L1 memory blocks are provided, which may be configured as a mix of SRAM and cache. The Memory Management Unit (MMU) provides memory protection for individual tasks that may be operating on the core and can protect system registers from unintended access.

The ADSP-BF561 dual cores share an on-chip L2 memory system, which provides high speed SRAM access with somewhat longer latency than the L1 memory banks. The L2 memory is a unified instruction and data memory and can hold any mixture of code and data required by the system design.

The architecture provides three modes of operation: User, Supervisor, and Emulation. The User mode has restricted access to a subset of system resources, thus providing a protected software environment. The Supervisor and the Emulation modes have unrestricted access to the system and core resources.

The Blackfin instruction set is optimized so that 16-bit op-codes represent the most frequently used instructions. Complex DSP instructions are encoded into 32-bit op-codes as multifunction instructions. Blackfin products support a limited multi-issue capability, where a 32-bit instruction can be issued in parallel with two 16-bit instructions. This allows the programmer to use many of the core resources in a single instruction cycle.

The ADSP-BF561 assembly language uses an algebraic syntax. The architecture is also optimized for use with a C compiler.

### **7.3.2 Black-Fin 561 Hardware Structure**

The ADSP-BF561 processor integrates two high performance parallel peripheral interfaces (PPIs) and powerful DMA subsystems to stream data directly to

and from video encoders/decoders, display drivers, and general-purpose converters.

The DMA controllers support one- and two-dimensional DMA transfers between on-chip memory, off-chip memory, and system peripherals with a programmable number of data elements and array stride values.

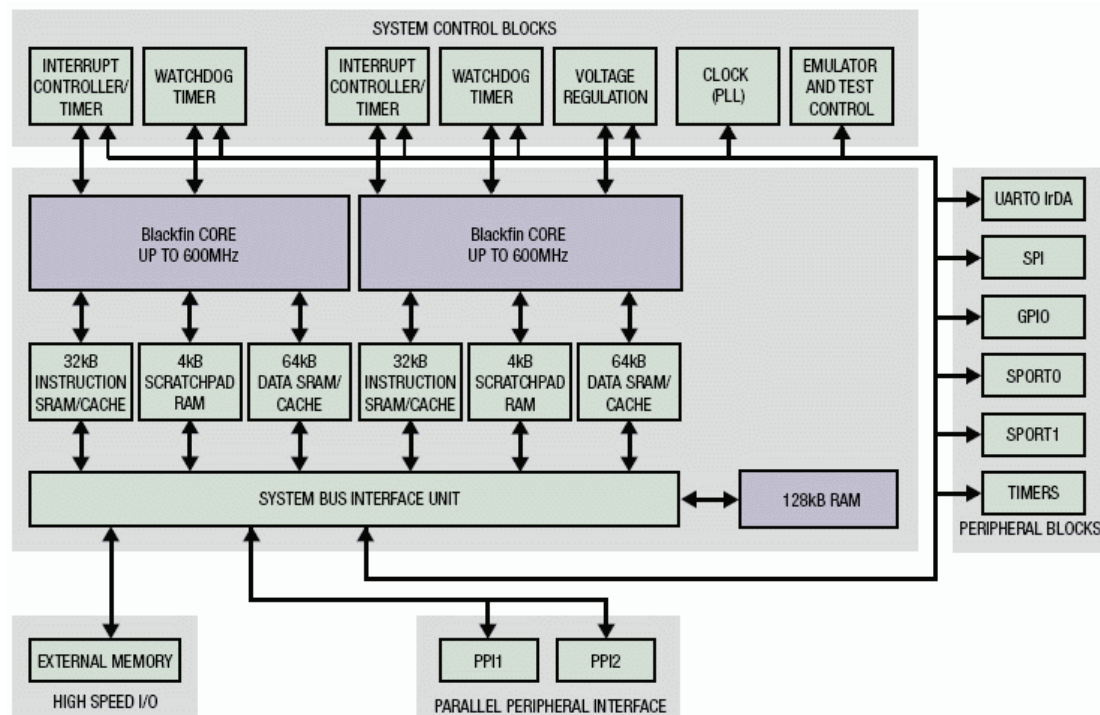


Fig. 77: ADSP-BF561 Block Diagram

### 7.3.3 Black-Fin 561 Evaluation Board

The ADSP-BF561 EZ-KIT Lite provides developers with a cost-effective method for initial evaluation of the ADSP-BF561 Blackfin Processor for audio and video applications via a USB-based PC-hosted tool set. Evaluation of analog audio applications is achieved through the use of the AD1836 multichannel 96 kHz audio codec. By utilizing the ADV7183A advanced 10-bit video decoder and ADV7179 chip scale NTSC/PAL video encode, the user is able to evaluate video applications such as simultaneous input and output video processing enabled by the dual core



architecture of the ADSP-BF561 Processor. With this EZ-KIT Lite, users can learn more about Analog Devices' ADSP-BF561 hardware and software development and quickly prototype applications.

The EZ-KIT Lite includes an ADSP-BF561 Processor desktop evaluation board along with an evaluation suite of the VisualDSP++ development and debugging environment with the C/C++ compiler, assembler, and linker. It also includes sample processor application programs, CE-approved power supply, and a USB cable.

The VisualDSP++ development and debugging environment, along with the USB-based debugger interface that operates up to 12 Mbits/second, enables users to perform standard debugging functions (such as read and write memory, read and write registers, load and execute executables, set and clear breakpoints, and single-step assembly, C, and C++ source code). The evaluation versions of the included software tools are limited to use with the EZ-KIT Lite. For faster and unrestricted debugging, a family of JTAG emulators and full versions of VisualDSP++ are available separately from Analog Devices. [71]

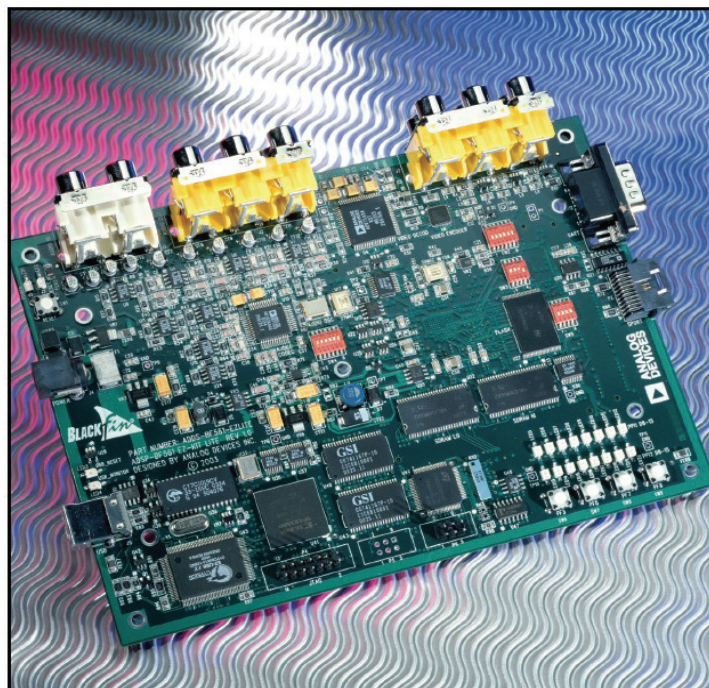


Fig. 78: Black-Fin 561 Evaluation Board

## 7.4 Optimization

In order to achieve high performance processing capability, we must understand the core processor structures that can help optimize performance. In this section, we will discuss the optimization, and it can be separated into two parts: system and coding. The system optimization is described in section 7.4.1. Section 7.4.2 discusses how to tune the C code for BG-561.

### 7.4.1 System Optimization

- **Memory**

Efficient system resource utilization is critical for developing applications that demand high bandwidth on an embedded platform. Systems can often run out of bandwidth, even if the throughput requirements are within the limits of the system. The critical factors that result in lower than expected throughput, more often than not, are external memory access latencies and inefficient utilization of system resources. In order to fully exploit the capabilities of an embedded processor, it is important to understand its system architecture and the available system optimization techniques. This EE-Note serves as a quick reference to Blackfin processor memory hierarchy and its system architecture. It also provides guidelines for using several optimization techniques to efficiently utilize the available system resources and discusses benchmark studies to evaluate and quantify the suggested optimization techniques.

The Blackfin processor's memory hierarchy is shown in Fig. 79 and the relative tradeoffs between on-chip (L1 and L2) memory and off-chip (external) memory. Guidelines are also provided to efficiently map code and data into the memory hierarchy to achieve minimal memory access latencies.

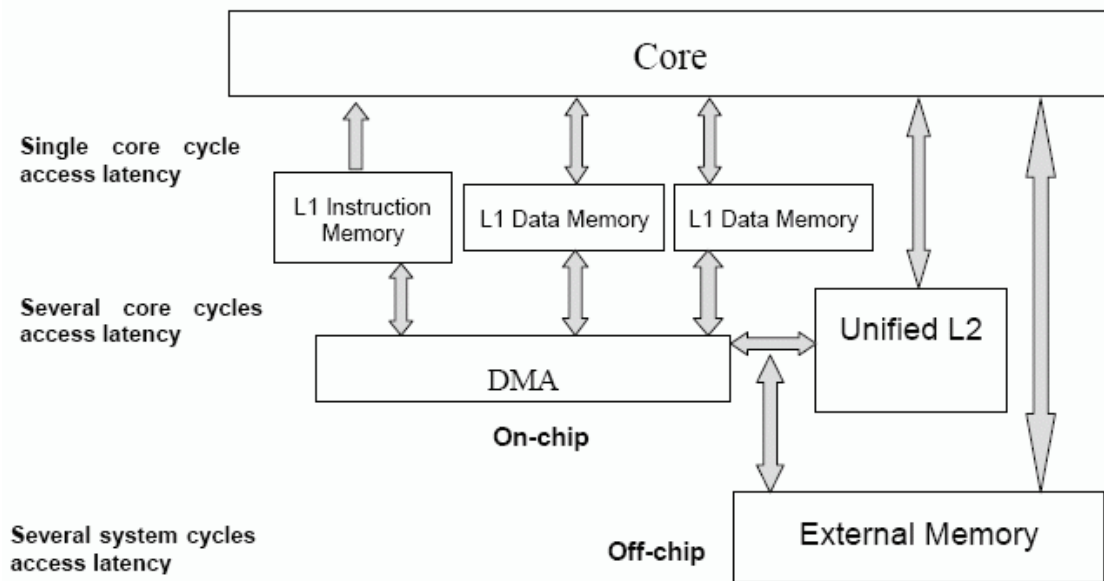


Fig. 79: Blackfin processor memory hierarchy

Cached memory can provide significant benefits for execution of code and data mapped to L2 or external memory. Cache performance depends on the temporal and spatial characteristics of the application. The disadvantage of cache memory is that it suffers from cache miss penalties, which increases memory access latencies, thus increasing external memory bandwidth requirements. Also, for streaming data, cache lines must be invalidated when new data is transferred in external memory. Invalidating cache lines is expensive and can significantly decrease performance.

- **System Architecture**

The Blackfin processor's system architecture includes the system buses, DMA controllers, peripherals, and external bus arbiter.

The system throughput can be greatly increased by using the maximum bus width for every transfer. Using 32-bit DMA access for ADSP-BF561 processors combined with packing can free up the system buses for other activities, thereby greatly increasing the throughput of the system. For example, the PPI provides 32-bit packing for ADSP-BF561 processors.

Blackfin processors provide traffic control on all the system buses. If the traffic on the bus is switching directions too often, the result will be increased latencies due to bank turnaround times. Using the traffic control registers is one of the best ways to optimize the system bus traffic, consequently improving bandwidth utilization. The traffic period for each of the DMA buses can be specified to group transfers in one direction, thereby minimizing bank turnaround times. Fig. 80 illustrates an optimized traffic pattern over the DAB bus. [71]

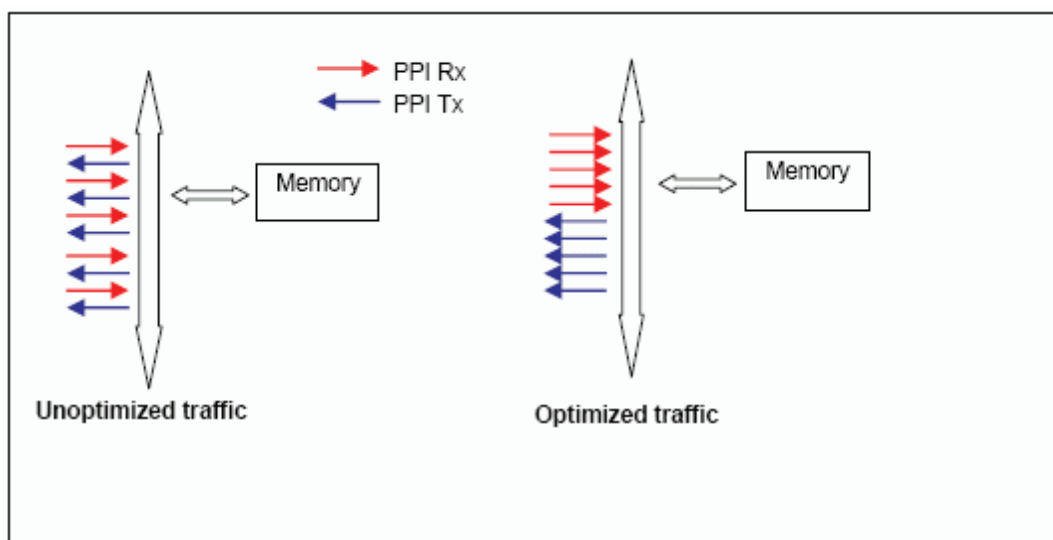


Fig. 80: Optimizing DMA traffic over the system buses

#### 7.4.2 Tuning C Code for Black-Fin 561

There is a vast difference in the performance of C code that has been compiled optimized and non-optimized. In some cases optimized code can run ten or twenty times faster. Note that the default setting is for non-optimized compilation, the non-optimized default being there to assist programmers in diagnosing problems with their initial coding.

- Avoid Float/Double Arithmetic

Floating-point arithmetic operations are implemented by library routines and,

consequently, are far slower than integer operations. An arithmetic floating-point operation inside a loop will prevent the optimizer from using a hardware loop.

- **Avoid Integer Division in Loops**

The hardware does not provide direct support for 32-bit integer division, so the division and modulus operations on int variables are multi-cycle operations. The compiler will convert an integer division by a power of two to a right-shift operation if the value of the divisor is known. If the compiler has to issue a full division operation, it will issue a call to a library function. In addition to being a multi-cycle operation, this will prevent the optimizer from using a hardware loop for any loops around the division. Whenever possible, do not use divide or modulus operators inside a loop.



- **Indexed Arrays versus Pointers**

C language allows you to program data accesses from an array in two ways: either by indexing from an invariant base pointer or by incrementing a pointer. The pointer style introduces additional variables that compete with the surrounding code for resources during the optimizer's analysis. Array accesses, on the other hand, must be transformed to pointers by the compiler, and sometimes it does not do the job as well as you could do by hand.

The best strategy is to start with array notation. If this looks unsatisfactory try using pointers. Outside the important loops use the indexed style because it is easier to understand.

- **Initialize Constants Statically**

Inter-procedural analysis will also identify variables that only have one value

and replace them with constants, which can enable better optimization.

- **Word-align Your Data**

To make most efficient use of the hardware, it must be kept fed with data. In many algorithms, the balance of data accesses to computations is such that, to keep the hardware fully utilized, data must be fetched with 32-bit loads.

Although the Blackfin architecture supports byte addressing, the hardware requires that references to memory be naturally aligned. Thus, 16-bit references must be at even address locations, and 32-bit at word-aligned addresses. So, for the most efficient code to be generated, we should ensure that data are word-aligned.

## **7.5 Summary**



The memory and system optimization techniques discussed in this chapter will help produce efficient code/data layouts and optimize system performance. Tuning C code gets maximal code performance from the compiler. All content in this chapter are our precious experiments for coding on BF-561.

## Chapter 8 Conclusions and Future Work

### 8.1 Conclusions

We propose an integrated system for lane departure warning and lateral collision warning. Driver's drowsiness was estimated by integrating the vehicle statistics evaluated by the EEG-based analysis approach developed from BRC into our lane departure warning system and lateral collision warning system. The lateral collision warning system aims at analyzing the image of the driver's blind spot region and exporting warning signal to remind the driver in the realistic driving environment.

The robust in-car DIS technique offers all major algorithms a stable image source. It requires a minor pre-processing, but following processing can be simplified massively.

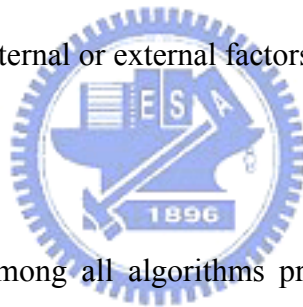
For the lane detection, we develop a method for automatic ROI extraction only by analyzing the image contents captured by the fish-eye camera mounted under the rear-view mirror without knowing the related camera parameters in advance. To overcome the light variations, the de-noising architecture which considers the spatial and temporal domain at the same time can restrain the noise effectively. Focusing on the geometric property of the blind-spot view, the adaptive edge operator and threshold selection can exactly detect the lane boundary. At last, an improved edge linking model proposed in this thesis not only increases the searching speed for lane trajectory but resolves the effect of fish-eye lens distortion.

In the topics of lane departure warning and drowsiness estimation, we construct a warning mechanism with lateral offsets and TLC computed by the lateral velocity and the border of ROI. Because of the different driving habits of people, we construct a stable-driving region for modeling by the information of previous lateral positions

of lane markers with an updating mechanism. Then, we use the deviation as the index for drowsiness estimation which has been analyzed and evaluated by EEG-analysis approach. By considering the human's behavioral style, the reactive behavior will be slower when the subjects enter the drowsy state gradually. We design a gauge of drowsy degree to estimate the driver's psychological state according to the reaction time of the driver.

The lane-based stable system is integrated into the blind-spot lateral collision warning system to increase the better detection rate and provide more robust performance. Besides, by constructing mechanism for drowsiness estimation in the dynamic driving environments, we can collect more data to further analyze other inattentive behavior of the driver so that the safety driving system can consider all possible risks caused by the internal or external factors of drivers as much as possible.

## 8.2 Future Work



First of all, although among all algorithms proposed in this thesis, only the lateral collision warning system has been coded on the embedded system, the whole algorithm is still designed under the consideration of being transplantable on embedded system. In addition, except the algorithm of lateral collision algorithm, 70% of the computing power is still free. Transplanting the whole system on embedded system is the next step.

Second, the lateral collision algorithm in this thesis uses different methods when working in the daytime and evening. It works well in normal situation, but it may make mistakes at the moment of entering and exiting the tunnel. This problem is due to the switching process of two methods used in the algorithm. This problem would be solved in the future.



## References

- [1] G. Jacobs, A. Aeron-Thomas, and A. Astrop, “Estimating global road fatalities,” *Australian National University, Transport Research Laboratory, Technical Report TRL 445*, 1999.
- [2] <http://www.motc.gov.tw/hypage.cgi?HYPAGE=index.htm>
- [3] -, “Traffic safety facts 2004.” *Technical report, National Center for Statistics and Analysis, U.S. Department of Transportation*, 2004.
- [4] Fei-Yue Wang, “Agent-based control for networked traffic management systems”, *IEEE Intell. Syst.*, vol. 20, no. 5, pp. 92–96, Sep./Oct. 2005.
- [5] Fei-Yue Wang, “Agent-based control for fuzzy behavior programming in robotic excavation” *IEEE Trans. Fuzzy Syst.*, vol. 12, no. 4, pp. 540–548, Aug. 2004.
- [6] I. Masaki, “Machine-vision systems for intelligent transportation systems”, *IEEE, Intell. Syst.*, vol. 13, no. 6, pp. 24–31, Nov.–Dec 1998.
- [7] Oshima, M. Hayashi, T. Fujioka, S. Inaji, T. Mitani, H. Kajino, J. Ikeda, K. Komoda, K. Matsushita Elec. Ind. Co. Ltd., Osaka., “VHS camcorder with electronic image stabilizer”, *IEEE Trans. Consum. Electron.*, vol. 35, no. 4, pp. 749–758, Nov. 1989.
- [8] Sato, K. Ishizuka, S. Nikami, A. Sato, M. Sony Corp., Tokyo, “Control techniques for optical image stabilizing system”, *IEEE Trans. Consum. Electron.*, vol. 39, no. 3, pp. 461–466, Aug. 1993.
- [9] K. Uomori, A. Morimura, H. Ishii, T. Sakaguchi, and Y. Kitamura, “Automatic image stabilizing system by full-digital signal processing”, *IEEE Trans. Consumer Electronics*, vol. 36, no. 3, pp. 510-519, Aug. 1990.
- [10] Sheng-Che Hsu, Sheng-Fu Liang, Chin-Teng Lin, “A robust digital image stabilization technique based on inverse triangle method and background detection”, *IEEE Trans. Consumer Electron.*, vol. 51, no. 2, pp.335-345, May, 2005.
- [11] <http://delphi.com/manufacturers/auto/safety/active/>
- [12] [http://www.siemensvdo.com/products\\_solutions/cars/propilot](http://www.siemensvdo.com/products_solutions/cars/propilot).
- [13] Sung-Hee Lee, Kyung-Hoon Lee, Sung-Jea, “Digital image stabilizing algorithms based on bit-plane matching”, *IEEE Trans. Consum. Electron.*, vol. 44, no. 3, pp. 617–622, Aug. 1998.
- [14] <http://newwww.itri.org.tw/tech-transfer/04.asp?RootNodeId=040&NodeId=041&id=3258>

- [15] Y. Egusa, H. Akahori, A. Morimura, and N. Wakami, “An application of fuzzy set theory for an electronic video camera image stabilizer”, *IEEE Trans. Fuzzy Syst.*, vol. 3, no. 3, pp. 351–356, Aug. 1995.
- [16] J.K. Paik, Y.C. Park, and D.W. Kim, “An adaptive motion decision system for digital image stabilizer based on edge pattern matching”, *IEEE Trans. Consum. Electron.*, vol. 38, no. 3, pp. 607–616, Aug. 1992.
- [17] J. K. Paik, Y. C. Park, and S. W. Park, “An edge detection approach to digital image stabilization based on tri-state adaptive linear neurons”, *IEEE Trans. Consum. Electron.*, vol. 37, no. 3, pp. 521–530, Aug. 1991.
- [18] Sung-Jea. KO., Sung-Hee. Lee, and Seung-Won. Jeon, “Fast digital image stabilizer based on Gray-coded bit-plane matching”, *IEEE Trans. Consum. Electron.*, vol. 45, no. 3, pp. 598–603, Aug. 1999.
- [19] F. Vella, and A. Castorina, “Digital image stabilization by adaptive block motion vectors filtering”, *IEEE Trans. Consum. Electron.*, vol. 48, no. 3, pp. 796–801, Aug. 2002.
- [20] S. Erturk, “Digital image stabilization with sub-image phase correlation based global motion estimation”, *IEEE Trans. Consum. Electron.*, vol. 49, no. 4, pp. 1320–1325, Nov. 2003.
- [21] Jyh-Yeong Chang, Wen-Feng Hu, Mu-Huo Cheng, Bo-Sen Chang, “Digital image translational and rotational motion stabilization using optical flow technique”, *IEEE Trans. Consum. Electron.*, vol. 48, no. 1, pp. 108–115, Feb. 2002.
- [22] J. S. Jin, Z. Zhu, and G. Xu, “A stable vision system for moving vehicles”, *IEEE Trans. Intell. Transport. Syst.*, vol. 1, no. 1, pp. 32–39, Mar. 2000.
- [23] Guan-Rong Chen, Yeou-Min Yeh, Sheng-Jyh Wang, Huang-Cheng Chiang, “A novel structure for digital image stabilizer”, *Proc. 2000 IEEE Asia-Pac. Conf. Circuits Syst.*, Tianjin, China, Dec. 2000, pp. 101–104.
- [24] Engelsberg, A.; Schmidt, G., “A comparative review of digital image stabilising algorithms for mobile video communications”, *IEEE Trans. Consum. Electron.*, vol. 45, no. 3, pp. 591–597, Aug. 1999.
- [25] M.B. van Leeuwen, “Motion estimation and interpretation for in-car systems” *Ph.D. dissertation*, Informatics Inst., Univ. Amsterdam, Amsterdam, The Netherlands, May 2002.
- [26] S. Erturk, “Image sequence stabilisation: Motion vector integration (MVI) versus frame position smoothing (FPS)”, *Proc. 2nd Int. Symp. Image Signal Process. Anal.*, 2001, pp. 266–271.
- [27] M. K. Gullu and S. Erturk, “Fuzzy image sequence stabilization”, *Electron. Lett.*, vol. 39, no. 16, pp. 1170–1172, Aug. 7, 2003.

- [28] M. K. Gullu, E. Yaman, and S. Erturk, “Image sequence stabilization using fuzzy adaptive Kalman filtering”, *Electron. Lett.*, vol. 39, no. 5, pp. 429–431, Mar. 6, 2003.
- [29] L. Chen and N. Tokuda, “A general stability analysis on regional and national voting schemes against noise —Why is an electoral college more stable than a direct popular election?”, *Artif. Intell.*, 163, no. 1, pp. 47–66, 2005.
- [30] S. Erturk, “Image sequence stabilisation: motion vector integration (MVI) versus frame position smoothing (FPS)”, *Proc. of the 2<sup>nd</sup> International Symposium on Image and Signal Processing and Analysis*, pp. 266-271, 2001.
- [31] S. Ertürk, “Real-time digital image stabilization using Kalman filters”, *Real-Time Imaging*, vol. 8, pp. 317-328, 2002.
- [32] Haruhisa Okuda, Manabu Hashimoto, Kazuhiko Sumi, and Shun’ichi Kaneko, ”Optimum Motion Estimation Algorithm for Fast and Robust Digital Image Stabilization.”, *IEEE Transactions on Consumer Electronics*, Vol. 52, No. 1, Feb. 2006
- [33] Gene F. Franklin, J.David Powell & Abbas Emami-Naeini, “Feedback Control of Dynamic Systems, 4th Ed.”, *Upper Saddle River, N. J. :Prentice Hall/Pearson Education, 2002.*
- [34] 林亨杰,“高速公路速限提昇前後之交通事故探討”, *道路交通安全與執法國際研討會*, Sep. 2004.
- [35] M. J. Flannagan, “Current status and future prospects for non-planar rearview mirrors”, *SAE Technical Paper Series No. 2000-01-0324*
- [36] 席世民,“學校交通安全教育工作推動現況與基本安全觀念介紹”, *交通部道路交通安全督導委員會*, Aug. 2004
- [37] M. Beauvaisand and S. Lakshmanan, “CLARK : a heterogeneous sensor fusion method for finding lanes and obstacles”, *invited paper, Image and Vision Computing, Special Issue on Intelligent Vehicles*, Vol. 18, pp. 397-413, 2000.
- [38] W. Enkelmann, “Vedio-based driver assistance – from basic function to applications”, *International Journal of Computer Vision* 45(3), pp. 201-221, 2001.
- [39] M. Ruder, W. Enkelmann, and R. Garnitz, “Highway lane change assist”, *IEEE Intelligent Vehicle Symposium*, pp. 240-241, Vol. 1, Jun. 2002
- [40] M. Bertozzi, A. Broggi, M. Cellario, A. Fasioli, P. Lombardi, and M. Porta, “Artificial vision in road vehicles”, *Proceedings of the IEEE*, Vol 90, No. 7, Jul. 2002.
- [41] 簡能俊, 王銘亨, 兵界力, ”高速公路隧道群(區)車流及行車事故分析”, *88 年道路安全與執法研討會*, 1999.

- [42] M. Betke, E. haritaoglu, and L. S. Davis, “Real-time multiple vehicle detection and tracking from a moving vehicle”, *Machine Vision and Applications*, pp.69-83, Dec. 2000.
- [43] 梅庭偉, “以智慧型視覺為基礎之快速公路車輛防擦撞資訊警示系統,” 國立交通大學電機與控制工程學系, 碩士論文, 2005.
- [44] A. Giachrtti, M. Campani, and V. Torre, “The use of optical flow for road navigation”, *IEEE Trans. on Robotics and Automation*, Vol 14, No. 1, Feb. 1998.
- [45] P. H. Batavia, D. A. Pomerleau and C. E. Thorpe, “Overtaking vehicle detection using implicit optical flow”, *Proc. of IEEE Transportation System Conf.*, pp. 729-734, 1997.
- [46] A. Techmer, “Real-time motion based vehicle segmentation in traffic lanes”, *23<sup>rd</sup> DAGM Symposium 2001, Munich(Germany)*, pp. 202-207, 2001.
- [47] A. Techmer, “Contour-based motion estimation and object tracking for real-time applications”, *IEEE Proc. of International Conference on Image Processing*, pp.648-651, 2001.
- [48] A. Techmer, “Real-time motion analysis for monitoring the rear and lateral road”, *2004 IEEE Intelligent Vehicles Symposium*, pp. 704-709, Jun. 2004.
- [49] A. Broggi, M. Betozzi, A. Fascioli, C. Guarino, L. Bianco, and A. Piazzzi, “The argo autonomous vehicle’s vision and control systems”, *Int’l Journal Intelligent Control and Systems*, vol. 3, no. 4, pp. 409-441, 1999.
- [50] M. Bertozzi and A. Broggi, “GOLD: a parallel real-time stereo vision system for generic obstacle and lane detection”, *IEEE Trans. Image Processing*, vol. 7, no. 1, Jan. 1998.
- [51] G. Y. Jiang, T. Y. Choi, S. K. Hong, J. W. Bae, and B. S. Song, “Lane and obstacle detection based on fast inverse perspective mapping algorithm”, *IEEE Conf. Systems, Man, and Cybernetics*, vol. 4, pp. 2969-2974, Oct. 2000.
- [52] Y. Wang, D. Shen, and E. K. Teoh, “Lane detection using Catmull-Rom Spline”, *Proc. IEEE Intelligent Vehicles Symp.*, Stuttgart, Germany, pp. 51-57, 1998.
- [53] Y. Wang, E. K. Teoh, and D. Shen, “Lane detection and tracking using B-Snake”, *Image and Vision Computing*, vol. 22, pp. 269-280, 2004.
- [54] C. R. Jung and C. R. Kelber, “A robust linear-parabolic model for lane following”, *Proc. SIBGRAOI, Curitiba, PR*, pp. 72-79, Oct. 2004
- [55] C. Che Wang, S. S. Huang, and L. C. Fu, “Driver assistance system for lane detection and vehicle recognition with night vision”, *Proc. IEEE Intelligent Robots and Systems*, pp. 3530-3535, Aug. 2005.
- [56] C. Kreucher and S. Lakshmanan, “LANA: A lane extraction algorithm that uses frequency domain features”, *IEEE Trans. Robotics and Automation*, vol. 15, no. 2, Apr. 1999.

- [57] Younguk Yim, Se-Young Oh, "Three-feature based automatic lane detection algorithm (TFALDA) for autonomous driving", *IEEE Trans. Intelligent Transportation Systems*, Vol. 4, NO. 4, Dec. 2003.
- [58] R. Chapuis, R. Aufrere, F. Chausse, "Accurate road following and reconstruction by computer vision", *IEEE Trans. Intelligent Transportation Systems*, vol. 3, no. 4, Dec. 2002.
- [59] A. Lopez, C. Canero, J. Serrat, J. Saludes, F. Lumbreras, T. Graf, "Detection of lane markings based on ridgeness and RANSAC", *Proc. IEEE Conf. on Intelligent Transportation Systems*, pp.254-259, Sep. 13-16, 2005.
- [60] D. J. Kang, J. W. Choi, I. S. kweon, "Finding and tracking road lanes using line-snakes", *Proc. IEEE Conf. on Intelligent Vehicles Symposium*, pp. 189-194, Sep. 1996.
- [61] Q. Li, N. Zheng, H. Cheng, "Springrobot: a prototype autonomous vehicle and its algorithms for lane detection", *IEEE Trans. On Intelligent Transportation Systems*, Vol. 5, NO. 4, Dec. 2004.
- [62] Chih-Hsien Yeh, Yung-Hsin Chen, "Development of vision-based lane and vehicle detecting systems via the implementation with a dual-core DSP", *Proc. IEEE Intelligent Transportation Systems Conf.*, Sep. 17-20, 2006.
- [63] J. W. Lee, "A machine vision system for lane-departure detection", *Proc. Computer Vision and Image Understanding*, vol. 86, pp. 52-78, Apr. 2002.
- [64] M. Ruder, W. Enkelmann, R. Garnitz, "Highway lane change assistant", *Proc. IEEE Conf. on Intelligent Vehicles Symposium*, Vol.1, pp.240-244, Jun. 2002.
- [65] H. Godthel, P. Milgram, and G. J. Blaauw, "The development of a time-related measure to describe driver strategy", *Human Factors*, 26(3): 257-268, 1984.
- [66] Chin-Teng Lin, Ruei-Cheng Wu, Sheng-Fu Liang, Wen-Hung Chao, Yu-Jie Chen, Tzyy-Ping Jung, "EGG-based drowsiness estimation for safety driving using independent component analysis", *IEEE Trans. Circuits and Systems*, vol.52, Dec. 2005.
- [67] P. Philip, J. Taillard, "Effect of fatigue on performance measured by a driving simulator in automobile drivers", *Journal Psychosomatic Research* 55, pp. 197-200, 2003.
- [68] J. Hendrix, "Fatal crash rates for tractor-trailers by time of day", *Proc. Int'l Truck and Bus Safety Research and Policy Symp.*, pp. 237-250, 2002.
- [69] P. H. Batavia, "Driver-adaptive lane departure warning systems", *doctoral dissertation*, Robotics Institute, Carnegie Mellon University, Sep. 1999.
- [70] C. Stauffer, W.E.L Grimson, "Adaptive background mixture models for real-time tracking", *Proc. IEEE Computer Society Conference on Computer Vision and Pattern Recognition*, " Vol.2, 1999.

[71] <http://www.analog.com>



# Vita

姓名： 范剛維

性別： 男

生日： 民國 65 年 6 月 1 日

籍貫： 台灣省新竹縣

學歷：

1. 民國 83 年 6 月桃園縣國立楊梅高級中學畢業
2. 民國 88 年 6 月私立中華大學資訊工程系學士畢業
3. 民國 91 年 6 月私立中華大學資訊工程系碩士畢業
4. 民國 91 年 9 月國立交通大學電機與控制工程學系博士畢業

## PUBLICATION LISTS

期刊部分：

- 
- [1] Chin-Teng Lin, Kan-Wei Fan, Chang-Mao Yeh, Her-Chang Pu, and Fang-Yi Wu ,  
“High-Accuracy Skew Estimation of Document Images”, accepted paper for  
publication, *International Journal of Fuzzy Systems*.
  - [2] Chun-Lung Chang, Kan-Wei Fan, I-Fang Chung, and Chin-Teng Lin, Fellow,  
IEEE , “A Recurrent Fuzzy Coupled Cellular Neural Network System with  
Automatic Structure and Template Learning”, *IEEE Trans. on Circuits and  
Systems—II: Express Briefs*, vol. 53, no.8, August 2006.
  - [3] Sheng-Che Hsu, Sheng-Fu Liang, Kang-Wei Fan, and Chin-Teng Lin, *Fellow*,  
IEEE, “A Robust In-Car Digital Image Stabilization Technique”, *IEEE Trans. on  
Systems, Man, and Cybernetics-Part C: Applications and Reviews*, vol. 37, no. 2,  
March 2007.
  - [4] Chin-Teng Lin, *Fellow*, IEEE, Kang-Wei Fan, Her-Chang Pu, Shih-Mao Lu and

Sheng-Fu Liang, “A HVS-Directed Neural-Network-Based Image Resolution Enhancement Scheme for Image Resizing”, accepted paper for publication, *IEEE Trans. on Fuzzy System*.

會議論文部分：

- [1] Chin-Teng Lin; Sheng-Fu Liang; Chang-Moun Yeh; Kang-Wei Fan , ”Fuzzy neural network design using support vector regression for function approximation with outliers”, *IEEE International Conference on Systems, Man and Cybernetics*, 2005, vol.3, 10-12 Oct. 2005 Page(s):2763 – 2768.
- [2] Chin-Teng Lin; Kan-Wei Fan; Wen-Chang Cheng , “An illumination estimation scheme for color constancy based on chromaticity histogram and neural network”, *IEEE International Conference* , vol. 3, 10-12 Oct. 2005 Page(s):2488 – 2494.
- [3] Chin-Tung Lin; Chiun-Li Chin; Kan-Wei Fan; Chun-Yeon Lin , “A novel architecture for converting single 2D image into 3D effect image”, *9th International Workshop on Cellular Neural Networks and Their Applications*, 2005, 28-30 May 2005 Page(s):52 – 55.
- [4] Chin-Teng Lin, Chun-Yeon Lin, Kan-Wei Fan, Her-Chang Pu, and Sheng-Fu Liang , “A Novel 2D to 3D Image Technique Based On Object-Oriented Conversion”, CVGIP 2005



